

Review of ultrasonic methods for monitoring, damage detection, and processing of lithium-ion batteries throughout their life-cycle

Simón Montoya-Bedoya,^{1, a} Tyler M. McGee,^{1, b} Joong Seok Lee,^{2, c} Sasha Litvinov,^{1, d} Ofodike A. Ezekoye,^{1, e} Donal P. Finegan,^{3, f} and Michael R. Haberman^{1, g}

¹ Walker Department of Mechanical Engineering, The University of Texas at Austin, Austin, TX 78712-1591, USA

² School of Mechanical Engineering, Chungnam National University, Daejeon 34134, South Korea

³ National Laboratory of the Rockies, 15013 Denver W Parkway, Golden, CO 80401, USA

(Dated: 14 January 2026)

Lithium-ion batteries (LIBs) are the leading technology used in consumer electronics, electric vehicles, and grid-level electrochemical energy storage applications. The ever-increasing use of LIBs has highlighted a gap in understanding of their behavior throughout their life-cycle. Current monitoring systems rely on electrical and sometimes temperature measurements to assess the internal state which limits information about complex electrochemical processes. In response, ultrasonic testing (UT) has shown promise for non-invasive assessment due to its ease of use and sensitivity to mechanical changes which are correlated with electrochemical changes within the battery. We summarize the research in UT methods applied to LIBs throughout their life-cycle and the relevant techniques at each stage. We also discuss physics-based and data-driven modeling approaches used to interpret ultrasonic signals in the context of LIBs, with an emphasis on the existing challenge of establishing rigorous links between electrochemical behavior and elastic and poroelastic wave physics to gain insight regarding physical changes in the LIB that can be directly measured using UT. Finally, we discuss the challenges of implementing UT across the LIB life-cycle and identify opportunities for further research. This review aims to provide helpful guidance to researchers and practitioners of UT in the growing field of UT for electrochemical battery systems.

Pages: 1–43

I. INTRODUCTION

Lithium-ion batteries (LIBs) have been used to power consumer electronics devices such as cellular phones and laptops since their first commercialization by Sony in 1991. With few widely-publicized exceptions¹, LIBs have achieved a long history of success in these applications. Due to recent advances in energy density², battery management systems (BMS) for safe operation³, and cost⁴, LIBs have become viable power sources for high-power and high-capacity applications such as electric vehicles (EVs) and renewable energy storage systems (ESS). Their viability in these applications, coupled with their role in transitioning to zero tailpipe emissions, has resulted in rapid growth in EV sales. From 2020 to 2024, the worldwide EV stock grew from 10.2 million

to 58 million and is expected to grow to 525 million by 2035⁵ (see Fig. 1.A). The primary drivers of this growth have been the approximately 720 % increase in pack-level energy density between 2008 and 2020 and an accompanying battery-pack price decrease of nearly 87 % between 2013 and 2025 (see Fig. 1.B-C).

This growth is projected to continue as governments, companies, and international organizations pledge to transition away from fossil-fuel-powered vehicles. The 2021 United Nations Climate Change Conference of the Parties launched the Zero Emission Vehicles (ZEV) Declaration with over 100 countries, businesses, and organizations committing to the “sales of new cars and vans being zero-emission globally by 2040”⁶. Indeed, auto manufacturers such as Ford Motor Corporation and General Motors have separately pledged 100 % EV sales by 2035^{9,10}. The People’s Republic of China is aggressively adopting Battery Electric Vehicles (BEV) by setting ambitious sales targets and efficiency mandates and making policies requiring the creation of more widespread EV infrastructure and battery recycling¹¹.

The rapid growth of the adoption of BEVs has strained conventional battery management approaches and placed LIBs in more challenging operating environ-

^asimonmontoyabedoya@utexas.edu

^btm34485@utexas.edu

^cjsleecnu@cnu.ac.kr

^dalitvinov@utexas.edu

^edezekoye@mail.utexas.edu

^fdonal.finegan@nrel.gov

^ghaberman@utexas.edu

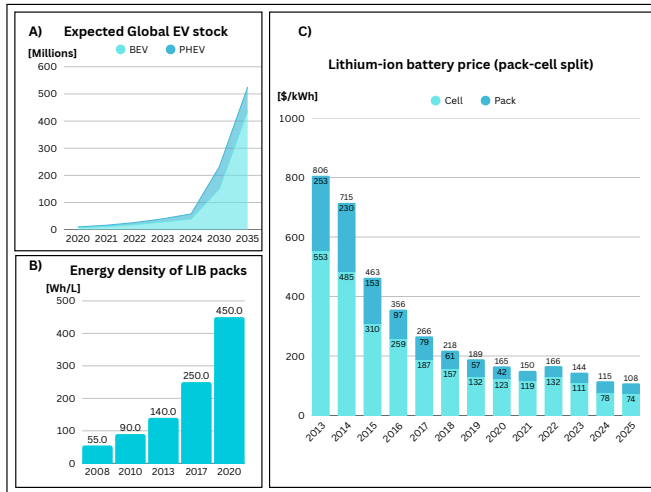


FIG. 1. Some of the main drivers for the increased adoption of LIBs in EV applications: **A)** forecasted global EV stock (BEV: Battery electric vehicle and PHEV: Plug-in hybrid electric vehicle), **B)** energy density of LIB packs in EVs, and **C)** price reduction of LIBs at pack and cell level. Data used to generate figures sourced from Refs. ^{5–7}

ments where thermal, electrical, and mechanical abuse are much more likely to be encountered¹². The impacts of battery system failure in EVs are costly in terms of monetary value and occupant safety. To that end, multi-billion dollar product recalls have been enacted to prevent occupant injury and other losses from battery system failures. Safety risk of battery fires is acute because they differ from conventional fires in key ways, namely they release flammable and toxic gases and may even reignite after being transported from the original failure location¹². Battery fires therefore spread easily and conventional methods to combat vehicle fires are often ineffective against battery fires. Additionally, battery systems can fail very suddenly. For instance, Maleki et al. showed that up to 70 % of a cell's electrical energy can be released in less than 60 s during an internal short circuit, which can cause internal heating that triggers thermal runaway¹³. More recent studies have reported that short circuits can range in magnitude; from 100 % energy release in less than 1 s due to rapid failure¹⁴, to the existence of slow-developing internal short circuits that occur over weeks due to slight overcharge throughout long-term cycling¹⁵. Early detection and identification of failure, as well as latent defects, are therefore of central importance for the adoption and safe operation of LIB systems. As a result, non-destructive testing (NDT) methods adapted for this purpose have been the focus of recent research¹⁶ and growth in battery management system (BMS) development³. Among the NDT methods, X-ray-, neutron-, and acoustic-based methods, infrared thermography, magnetic resonance, and advanced electrochemical techniques such as electrochemical impedance spec-

troscopy have been used to study LIBs' performance and safety, each with its own advantages and challenges^{16–18}.

Conventional BMS systems rely on electrical measurements to understand state of charge (SOC) and state of health (SOH). However, since the mechanical properties of LIBs are known to change as a function of charge level and temperature, mechanical methods of inspection have been explored as part of an updated approach to battery management¹⁹. Of those approaches, ultrasonic testing (UT) is particularly promising as different features of ultrasonic waves have been shown to correlate with SOC, SOH, thermal abuse, overcharge, and other cell conditions^{16,20–22}. Since ultrasonic wave propagation depends on the structure and mechanical properties of the media through which they propagate, and changes in the battery state lead to mechanical and structural changes on the internal materials of the LIBs, there is strong potential that ultrasonic sensors and methods can be developed to detect all of the relevant cell states under all operating conditions, which is likely to reduce the weight and complexity of the BMS. UT methods also show promise for enhancing predictive capabilities of cell cycle-lives and diverging behaviors of cells within battery packs, given the intrinsic link between ultrasonic signals and degradation of the material properties within a cell, and defect detection like gas generation. Furthermore, UT can be performed with very low-footprint sensors that do not need to be placed near the active electrical terminals of the cells to be effective. If UT can be performed with waves propagating through multiple cells, modules, or even full battery packs, the number of sensors in the BMS could be further reduced, which would further reduce BMS weight and cost.

An additional market for UT methods is in the evaluation of cells for second-life applications. The SOH of EV batteries diverge considerably throughout their cycle-lives²³ such that by the time a battery pack reaches its end-of-life, many cells within the pack may still have many more useful cycles in a second-life application. Assessing cell quality for risks using high-throughput approaches presents a tremendous challenge. Ultrasonic techniques have potential to rapidly provide information regarding the internal structural integrity and condition of the constituent materials of cells, which can be used to assess suitability for second-life applications. However, for all of the aforementioned applications of ultrasound-based diagnostics, high confidence does not yet exist in the relationship between ultrasonic signals and relevant physical phenomena within the cell, which limits widespread use of ultrasonic methods for BMS systems and screening for second-life applications^{24,25}.

In order to fully understand the propagation of waves through LIBs, one needs a high level of understanding of many different scientific fields, namely: solid mechanics, electrochemistry, materials science, heat transfer, and acoustics. The combination of these scientific domains has made the interpretation of experimental results and the creation of accurate models difficult in this rapidly developing field. In addition, although the

use of UT to detect changes in LIBs is a relatively new area of research, there has been a substantial number of studies over the last decade. Despite this research, the complexity and various form factors of LIBs (primarily prismatic, pouch, and cylindrical) and the complex electrochemical-mechanical coupling effects arising during operation, loading, and aging pose significant challenges to up-to-date and accurate ultrasonic state estimation. While these form factors can span a wide range of physical scales, from small pouch cells in consumer electronics to, in some cases, larger format prismatic cells in EVs, this review focuses on UT methods for characterizing individual cells. The fundamental principles of UT remain consistent across scales. Nevertheless, practical implementation details, such as transducer location and frequency ranges, must be customized to cell dimensions and the specific application. This review synthesizes recent advances in ultrasonic techniques and evaluates the experimental UT approaches that have been applied to inspect LIBs for state estimation and damage detection. It also provides a summary and background to modeling approaches that can be exploited to improve the use of UT for LIB monitoring. Finally, it aims to clarify common challenges of ultrasonic measurements and modeling in this rapidly growing area of research, offering valuable insights for researchers new to the field.

We divide the discussion about ultrasonic methods to characterize and monitor LIBs into three main sections: Section II presents an overview of the fundamentals of ultrasonic wave propagation in lithium-ion batteries and provides a detailed description of the relevant structure and function of LIBs. The latter information is essential for understanding the new and unique challenges of employing UT to inspect and monitor LIBs. Section III provides a comprehensive summary of the use of ultrasonic testing for different use cases. Section IV discusses challenges and opportunities regarding the eventual implementation of UT in the LIB life-cycle. We provide a summary and outlook in Section V. Finally, we provide Supplementary Material with an additional discussion about the mathematics and physics behind wave phenomena in LIBs.

II. FUNDAMENTALS: WAVE PHENOMENA IN LIBS

A. Wave phenomena in layered structured media

Lithium-ion batteries are heterogeneous media constructed with multiple layers of metals, polymers, and slurries filled with a liquid electrolyte. To understand ultrasonic wave propagation in LIBs, we must consider the layered heterogeneity of the cell, including the properties and geometry of each layer (as illustrated in Fig. 2.A for a pouch cell). One must understand the wave physics of single layers, which can be modeled as equivalent homogeneous elastic media under the long-wavelength assumption, i.e., when the length-scales of the LIB structure are much smaller than the shortest wavelength of US waves used for the measurement²⁶. In this sense, re-

searchers have primarily employed high-frequency transducers (1–5 MHz) due to their shorter wavelength and associated enhanced sensitivity to internal features²⁷. Conversely, other works have used low-frequency waves (below 250 kHz) for their ability to travel further distances inside the battery due to reduced attenuation²⁸.

Each layer of the battery is different with distinct electrochemical and mechanical properties. The current collectors (Cu, Al) are solid elastic layers, while the positive electrodes (the cathodes) and the negative electrodes (the anodes), and separators have interstitial pores filled with a liquid electrolyte. Although the microstructure of LIBs is very complex, ultrasonic waves in LIBs have been successfully described using well-known models for elastic/viscoelastic media (see Supplementary Material for a detailed mathematical description). The coupled dynamics of waves propagating in the two-phase solid-fluid structure of anodes, cathodes, and separators can be described using poroelasticity models, namely Biot's theory^{29,30}. Recent research has applied Biot theory to model and understand ultrasonic characterization of LIBs, including the layered structure^{31–40}.

Most UT of LIBs have employed bulk waves, which are longitudinal or shear waves that travel in the material without the influence of boundaries. However, researchers have also employed guided wave methods, which are a well-known and powerful tool in UT^{41,42}, to detect changes in LIBs^{28,33,43}. In contrast to bulk waves whose wave speed is not a function of frequency if the material is lossless, guided waves are dispersive, meaning their phase and group velocities are functions of frequency. The frequency dependence is determined by the dispersion relations, which are functions of the waveguide geometry and material properties. For the case of LIB cells, the most relevant geometry is usually the cell thickness. Dispersive wave propagation occurs in bounded elastic media because the wave-field must satisfy boundary conditions at all points along the waveguide. For elastic plate waveguides, this means that one observes standing wave modes in the thickness direction that propagate in the plane of the plate. This can be envisioned as the coherent interference of multiple reflections from top and bottom boundaries of a plate to yield a propagating standing wave pattern as indicated by Fig. 2.B. Guided waves in elastic plates, commonly known as Lamb waves, are an infinite set of symmetric and antisymmetric modes, each corresponding to specific frequency-wavenumber pairs. These modes can propagate when excited by a source or scatterer within the waveguide or at its boundaries. Each guided wave mode has its unique deformation pattern and sensitivity to material changes. Thus, Lamb waves may be able to detect variations in the properties of layers and conditions at interfaces within a LIB. It is important to note that the layered structure of LIBs can be represented as a homogeneous anisotropic material on the macroscale when the wavelength of propagating modes is much larger than the thickness of individual layers. In that case, guided wave modes are more complex than Lamb waves in isotropic

plates⁴¹. To advance research in ultrasonic diagnostics of batteries, it will be critical to understand guided wave modes in battery materials, as they may provide more refined information on the evolution of constituent material properties.

Biot's theory^{29,30} describes wave propagating in poroelastic media as consisting of three types of propagating bulk waves: a fast longitudinal wave (mainly transported by the solid skeleton), a slow longitudinal wave (caused by the relative movement between fluid and solid phases), and a shear wave. These waves are illustrated in Fig. 2.A. Despite being strongly attenuated and dispersive, the slow wave offers unique sensitivity to changes in porosity, fluid content, and structural integrity. A more detailed development of the governing equations for wave propagation in poroelastic media is discussed in the Supplementary Material.

Several works have employed poroelastic material modeling of wave propagation in LIBs, the most notable of which is the work by Gold et al.³¹. Although Biot's poroelastic model was only used in their work to estimate the propagation velocities of the three kinds of waves in the graphite electrodes of a LIB, they were the first to observe and discuss the existence and significance of the slow wave propagating in poroelastic materials in LIBs. Gold et al. suggested that the slow wave is a key parameter to evaluate SOC, because signal amplitude (SA) and time of flight (TOF) of the slow wave were observed to be linearly correlated with SOC. Namely, they observed that the SA increased linearly and TOF decreased linearly with respect to increases in SOC, while the SA and TOF of the fast wave did not change notably with SOC in their work. In contrast, Chang et al.³² reported different results on the sensitivity of fast and slow wave characteristics to SOC. By measuring a directly transmitted signal through a LIB (NiMnCoO_2) using two air-coupled transducers, the transmitted amplitudes of the fast and slow waves increased for higher SOC, although the time of arrival of the slow wave decreased as a function of increasing SOC, similar to the observations of Ref.³¹. Zhang et al.³⁷ later measured slow wave propagation through a LIB (LiCoO_2) pouch and showed that SA of both the fast and slow waves increased with increasing SOC. While TOF of the slow wave decreased with increasing SOC, they did not observe changes in the TOF of the fast wave.

The conflicting research highlighted above illustrates that although the existence and properties of Biot's slow wave may be a useful ultrasonic feature for characterizing LIBs, there is currently no consensus on the functional dependence of slow wave properties on LIB SOC. This is likely due to the well-known difficulty in measurement of the slow wave in poroelastic media^{44,45}. This wave type is strongly dissipative, making it challenging to observe in real-world scenarios. Furthermore, when compared with the fast and shear waves, which are primarily affected by the material properties of the solid phase in the electrodes, the relatively low amplitude of the slow wave originates from the coupling effect of solid/fluid phases,

which is highly dispersive and leads to strong distortion of the signal. Nevertheless, the concept of the use of the slow wave in UT of LIBs is still valid, as reported in the previous works^{31,32,37}.

The key challenge, however, is poroelastic effects as applied to ultrasonic wave propagation within LIB electrodes. Such relative motion introduces complex wave behaviors — including additional modes and increased attenuation — that must be considered in order to interpret ultrasonic data correctly. Thus, ultrasonic studies of LIBs should consider both elastic and poroelastic wave propagation mechanisms in modeling wave phenomena to extract insights from experimentation and increase understanding. The Supplementary Material provides a detailed mathematical description of the bulk waves for elastic and poroelastic media, guided waves, and modeling implementations.

B. Structure and function of LIB

It is essential to understand the structure of LIBs and how changes in electrochemical state during operation, aging, and damage can affect ultrasonic wave motion. Additionally, the wide variety of LIBs, specifically different chemistries and form factors, should be highlighted since they introduce numerous variables that must be considered when interpreting ultrasonic data under the different external loading conditions applied to the battery.

Commercial lithium-ion cells are manufactured with tens to hundreds of individual component layers in planar or cylindrical arrangements. The simplest representation of an electrochemical system consists of the anode, cathode, separator, and current collectors, as illustrated in Fig. 2A. Each layer has varying thicknesses: current collectors typically range from $10 - 20 \mu\text{m}$ ⁴⁶, electrodes from $40 - 150 \mu\text{m}$ ⁴⁷, and separators from $20 - 25 \mu\text{m}$ ⁴⁸. In these systems, design choices such as the chemical composition, thickness of layers, and porosity of electrode coatings and separators, dictate the electrochemical behavior of the cell such as cell voltage, cycle life, and chemical and thermal stability⁴⁹. This section provides a detailed description of the mechanical structure and electrochemical function of each cell component, with an emphasis on how the mechanical properties of each component are affected by the state of the cell.

The electrodes are the active components in the cell, and it is the difference in the redox energies between the cathode and anode that dictates the cell's operating voltage. This redox energy is associated with the tendency of the electrodes to be oxidized or reduced to allow the movement of the lithium-ions between both electrodes during the battery operation⁵⁰. Notably, this process of lithiation/delithiation leads to changes in mechanical properties, and therefore can be detected with ultrasonic elastic waves. Commercial lithium-ion cells are constructed with metal oxide cathodes, which can be divided into classes based on their chemical structure and operating principle: the layered oxides, the spinel oxides,

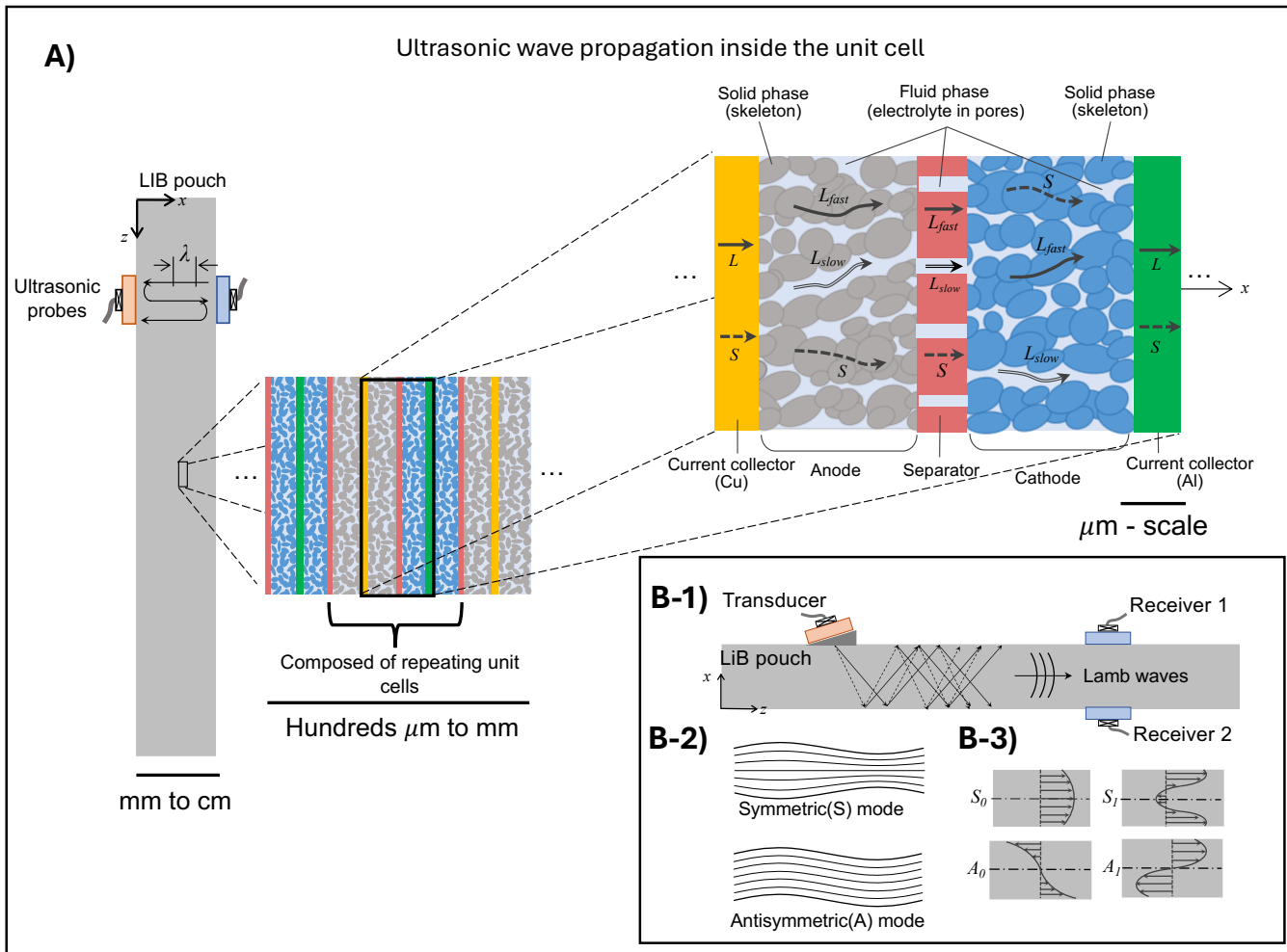


FIG. 2. (A) Schematic of ultrasonic wave propagation through a LIB pouch cell, highlighting the layered structure composed of repeating unit cells, which include current collectors (Cu and Al), anode, separator, and cathode. For the porous materials, each layer consists of a solid skeleton and fluid-filled pores (electrolyte). Longitudinal (L) and shear (S) waves propagate through the solids, while only longitudinal waves propagate through the fluid phase. Scale bars are not exact. They are provided as a generic reference scale for microscale (0.5–100 μm) and macroscale ($> 0.1 \text{ mm}$) features. (B) Scheme of guided wave generation and detection using ultrasonic probes: (B-1) Experimental setup showing guided wave propagation along the z-direction. (B-2) Illustration of symmetric (S) and antisymmetric (A) Lamb wave modes in the LIB pouch. (B-3) Various modes of Lamb waves (S_0 , S_1 , A_0 , A_1) and their relative particle displacement profiles across the thickness of the pouch.

and the polyanion oxides⁵¹. When performing mechanical inspection of LIBs, it is critical to state the cathode chemistry, as the choice of cathode chemistry affects not only the electrochemical performance, but also the mechanical properties during charge-discharge cycling, aging, and damage mechanisms. When charging under normal operating conditions, lithium ions are removed from the cathode, migrate through the electrolyte and separator, and are either inserted into or deposited on the anode. Lithium ions follow the same path, but in reverse during discharging. The ionic charge imbalance caused by this electrochemical process initiates the movement of electrons through an external circuit, creating the flow of charge required for electronic devices to work.

The active material of the anode in most commercial LIBs is graphite, although lithium-metal anodes and other anode materials such as silicon are currently being heavily investigated and nearing commercial viability⁵². Some commercial cells have small quantities of SiO_x and Si mixed into their graphite anodes⁵³, but since graphite is presently the most common commercially available anode material, the present discussion is restricted to the structure and function of anode materials with graphite as the active material to illustrate how charging and discharging affect ultrasonic wave propagation. During charging, lithium ions are inserted into the layered structure of graphite, which causes a strain in the crystal lattice with concomitant changes to the unit cell volume

and elastic moduli. The observed changes in the overall mechanical properties of the cell are most often attributed to the changes in the mechanical properties of the graphite anode, as the volume of graphite has been found to increase by approximately 13 % and the Young's modulus has been found to increase by three times at full lithiation^{54,55}. Lithium ion intercalation in graphite anodes occurs in multiple different stages: stage 4, where lithium ions are sparsely intercalated (ratio of carbon to lithium is 72 : 1), stage 3, intermediate lithium insertion (ratio of carbon to lithium is 36 : 1), stage 2, where every second graphite layer is replaced by denser lithium layers (ratio of carbon to lithium is 18 : 1) and stage 1, where all layers are fully lithiated with lithium ions (ratio of carbon to lithium is 6 : 1). Each stage of lithiation can be identified by specific structural arrangements and voltage plateaus in the negative electrode potential during cycling^{56,57}. Conversely, cathodes experience an opposite behavior, a decrease in both volume and Young's modulus during charging due to delithiation, but to a lesser extent compared to the graphite anode^{58,59}, see Fig. 3. Critically, both electrodes contain active materials and conductive additives (typically some form of carbon), and binder materials (most commonly polyvinylidene fluoride (PVDF), styrene butadiene rubber, or carboxymethyl cellulose). In order to create an ionically conductive medium to aid the diffusion of lithium ions between the electrodes, the cell is soaked with a liquid electrolyte. In most commercial LIBs, the electrolyte is a solution of lithium salts dissolved in a carbonate-based solvent, such as ethylene carbonate (EC) or diethyl carbonate (DEC). Thus, the structure of the electrodes has been described as a slurry, which itself retains some level of porosity to allow for electrolyte saturation. This structure leads to poroelastic wave motion in the electrodes as mentioned in Section II A. A discussion of the impact of this complex porous structure on the coupled acoustic and elastic wave motion equations is provided in the Supplementary Material.

For LIBs to operate, the cathode and anode must be electrically isolated while retaining lithium ion conductivity. This functionality is achieved with the separator. In most commercial LIBs, the separator is a thin and porous polyolefin material, such as polyethylene (PE), polypropylene (PP), or a PP-PE blend. The electrically insulating properties of the separator mitigate the risk of internal short circuits between the electrodes while its porosity allows lithium ion transport. Because the separator is polymeric, it represents a highly compliant, porous, viscoelastic component of LIBs whose properties depend on loading history. Polymeric separators also have the lowest melting temperature of the cell components, and they are known to shrink at elevated temperatures, which can reduce their porosity or lead to internal short circuits. Reductions in separator porosity may be indirectly measured as increases in the internal resistance of a cell or as changes to the effective material properties of the cell, which affect its ultrasonic response²⁶.

As previously noted, commercial cells consist of hundreds of more basic repeating units consisting of two electrodes in contact with metallic current collectors separated by a polymeric separator, permeated by a liquid electrolyte that fills the pores of the electrodes and the rest of the cell (Fig. 2). In addition, LIB cells have different form factors as illustrated in Fig. 4 depending on the arrangement and packaging of the basic small-scale structure shown in Fig. 2. Cylindrical cells, such as the common 18650 cell, are constructed by winding these components around a central core. The outside casing of these cells is typically a rigid steel shell. A separate manufacturing approach is to lay the layers on top of each other to produce a planar layered structure. A common approach to this design is the Z-fold, where the separator is folded on top of itself with electrode sheets and conductors are placed in between separator layers. Cells with this arrangement are referred to as pouch cells when the outer casing is a flexible polymer-coated metal. A third common form factor are prismatic cells, which can have both approaches, wound or Z-folded, in a rectangular rigid steel case. Most commercial prismatic cells are wound^{60–62}.

The cell structure can have a large impact on its evolving mechanical properties and therefore ultrasonic measurements. For example when the anode expands with lithiation, the rigid constraint of prismatic and cylindrical cells will resist expansion and cause an increase in the internal cell pressure leading to compression of the porous separator. In the case of thermal abuse, for example, internal cell pressure may increase the boiling temperature of the electrolyte, which may change the point at which gas generation is mechanically detectable^{63–65}.

As the electrolyte saturates the porous anode, cathode, and separator, the macroscale effective mechanical properties of the cell change significantly. Given this structure, the electrode materials have been described as slurries³⁴, crushable foams^{64,66}, or porous media^{38,67}, and each approximation has different approaches to defining effective material properties. Each of these modeling paradigms presents challenges in terms of modeling the physical behavior of LIBs as it pertains to US wave propagation.

One of the key difficulties in modeling wave phenomena in LIBs is accurately estimating the influence of electrode and separator porosity on the propagation of ultrasonic waves in any given state. This is exacerbated by the fact that the porosity and constituent properties fluctuate over time due to cell wetting or unwetting or ongoing solid-electrolyte interface (SEI) growth. A reliable modeling approach that captures the microscale wave physics and provides insight into experimental data is to use poroelastic material models for these layers. These models include the so-called fast and slow compressional waves which arise when the compression of the fluid (electrolyte) and solid components in each layer are either in- or out-of-phase, respectively⁶⁸. These models also capture attenuation based on fluid viscosity and porosity

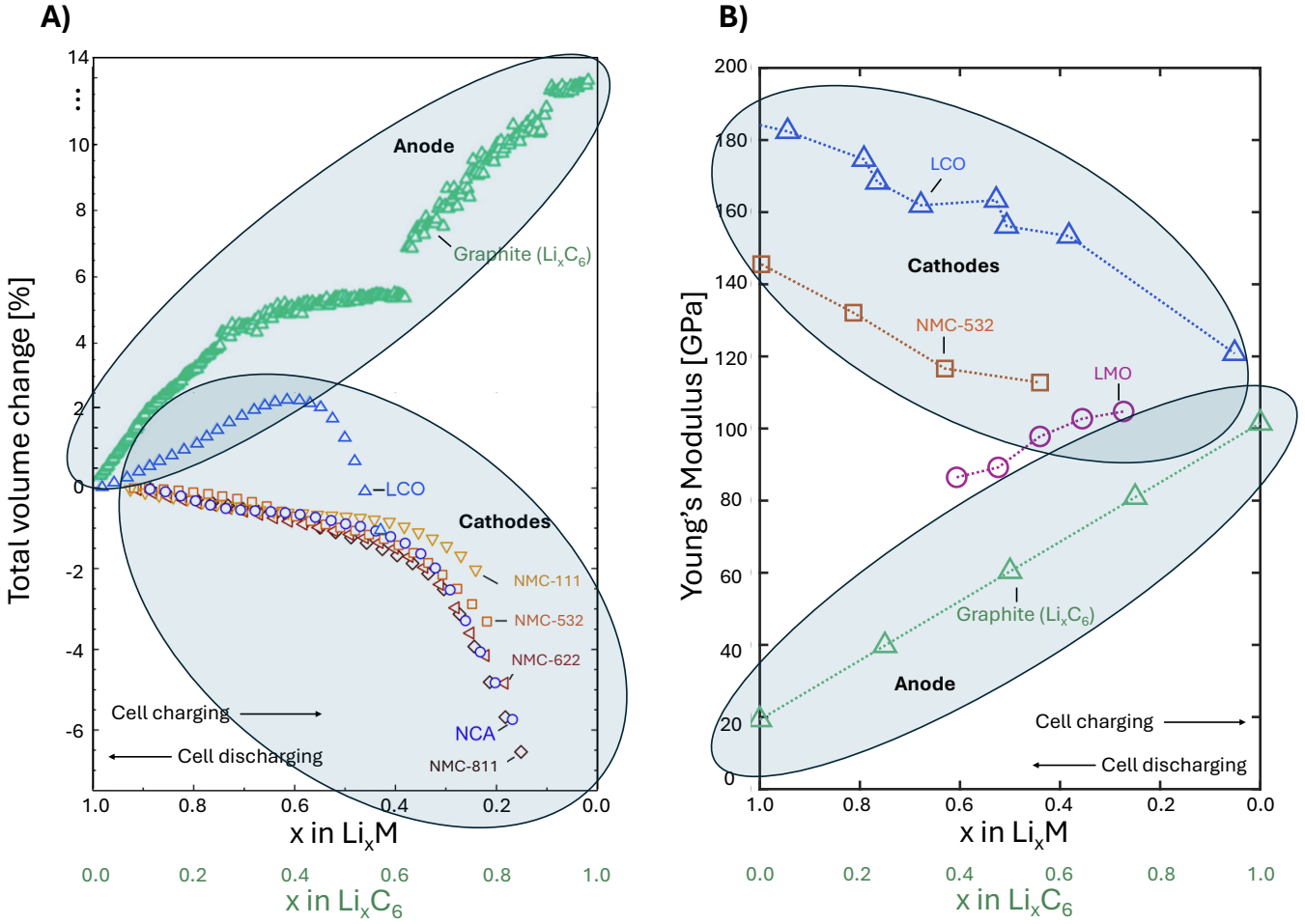


FIG. 3. Changes in volume and Young's modulus of common commercial LIB cathode and anode materials. During discharge, cathode materials generally exhibit an increase in volume and Young's modulus, while the graphite anode typically shows a decrease in volume and modulus. Some exceptions to this behavior are observed for LCO and LMO. This figure is based on raw data for the graphite anode^{54,55} Li_xC_6 , and various cathodes^{58,59}: Li_xCoO_2 (LCO), $\text{Li}_x\text{Ni}_y\text{Mn}_z\text{Co}_{(1-y-z)}\text{O}_2$ (NMC), $\text{Li}_x\text{Ni}_y\text{Co}_z\text{Al}_{(1-y-z)}\text{O}_2$ (NCA), $\text{Li}_x\text{Mn}_2\text{O}_4$ (LMO). The decrease in volume of cathode materials is generally much smaller than the volume increase of graphite under normal operating conditions.

which can be helpful in monitoring changes in LIB structure. The biggest obstacle in the poroelastic modeling for LIBs is the lack of clear information on the relevant material properties of the constituent solid and fluid phases in LIBs under various conditions. Since the direct measurement of wave-related properties is still a challenge for these LIBs, many mechanical properties used in poroelastic material modeling have been assumed with only minimal validation or have been adopted from a few previous literature in a duplicated manner.

Additionally, since the cells include hundreds of layers, one must either explicitly model each layer using techniques like the transfer matrix method^{26,34,36,38,69,70} or simplify the system using effective medium models, i.e. by assuming periodic boundary conditions²⁶ such as Floquet-Bloch approaches⁷⁰ (see Supplementary Mate-

rial for a discussion on modeling implementation through different matrix-based methods). In each of these cases, the microscale structure and properties (constituent material properties, pore size and volume fraction, fraction of active materials, layer thicknesses, etc.) and their evolution when subjected to electrochemical and thermomechanical loading must be considered as a starting point for any model that wishes to capture the complex wave mechanics in these systems. In many cases, the mechanical properties of cell components are not known, especially when considering effects such as degree of lithiation, electrode degradation, formation and growth of the SEI, and the influence of temperature. Without direct knowledge of cell mechanical properties under diverse operating conditions, accurately approximating or modeling cell components is imperative for constructing full cell

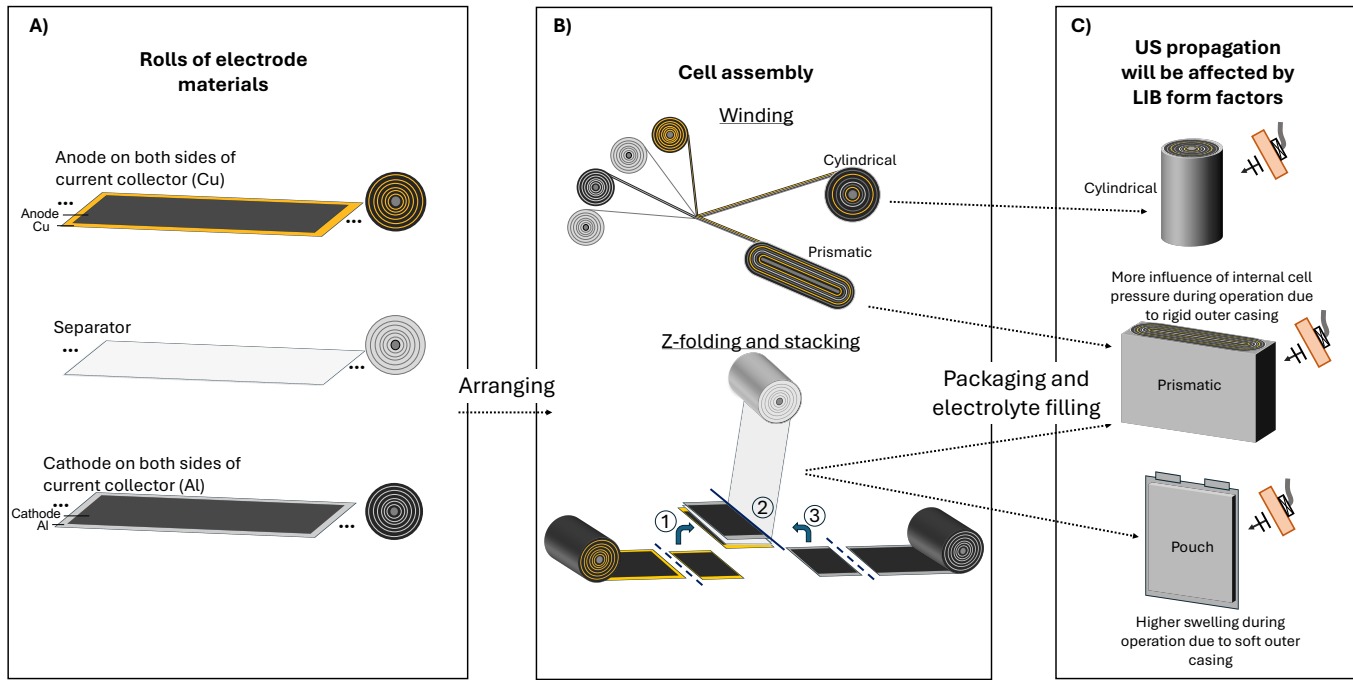


FIG. 4. Principle fabrication steps in the creation of LIB and comparison of LIB form factors, including cylindrical, prismatic, and pouch cells. **A)** Assembly process from electrode rolls through various packaging configurations. **B)** Winding for cylindrical cells, and stacking or Z-folding for prismatic and pouch cells. **C)** Differences in internal structure and mechanical response under operational pressure are highlighted. These structural differences influence swelling behavior and ultrasonic signal propagation within the cells.

models which accurately describe the wave phenomena occurring within cells.

Another layer of complexity in LIBs is that they can undergo multiple degradation mechanisms during battery operation, which depends on operating and abuse conditions. Each of these mechanisms can alter the structure of LIBs in different ways. Detailed descriptions of multiple degradation mechanisms with a comprehensive evaluation of their current understanding can be found in Refs. ⁷¹⁻⁷³. All of these degradation mechanisms have complex mechanical consequences that are still under study, but, more importantly, these degradation mechanisms lead to phenomena like particle expansion, interfacial debonding, loss of stiffness, crack generation and propagation, and porosity changes. All of these changes alter ultrasonic wave propagation through the cell and affecting characteristics of ultrasonic signals by altering propagation velocity, attenuation, and scattering. Table I reports key features on some of the degradation mechanisms that have been studied with UT, namely as SEI growth, lithium plating, particle cracking/electrode delamination, electrolyte dry-out, separator failure, and gas formation. The latter is not specifically a degradation mechanism but rather a consequence of multiple degradation mechanisms and because of its importance within the study of UT for LIBs, has been included as its own category. In some cases, the same stimulus can cause multiple types of degradation within a battery. However,

we have highlighted the most common degradation types investigated using UT and listed them separately for clarity, noting how they are reported in the existing literature. UT observables are similar for many of the battery degradation mechanisms, which can lead to some ambiguity of existing UT methods. Improved UT techniques or integration of UT data with other monitoring methods should be the subject of future work to specify them to known types of damage and degradation in order to make this approach more valuable for all aspects of LIBs life-cycle. This review provides an overview of recent research on UT of LIBs with the objective of providing researchers with sufficient understanding of the relevant electrochemistry and elastic wave phenomena to create representative models, design experiments, and interpret results for ultrasonic methods to be useful for research and application of LIBs.

III. UT METHODS FOR LIBS

Although previous UT research was conducted on other multilayer membrane systems, such as reverse osmosis membranes⁹⁰ and solid-state fuel cells⁹¹. The first publication involving ultrasonic testing of lithium-ion batteries was published in 2013 by Sood et al.⁹². Since then, interest in UT to detect changes structure and SOH as well as condition and process monitoring of LIBs has grown, as evidenced by the rapidly growing number of

TABLE I. Summary of LIB degradation mechanisms that can be detected using ultrasonic testing methods. The following definitions are used within this work. UT sensitivity is qualitatively defined as Low, High, or Very High based on the estimated resolution at common UT frequencies within 0.5–5 MHz. Length scales are defined as: Nanoscale (1–500 nm), Microscale (0.5–100 μ m) and Macroscale (> 0.1 mm).

Degradation	Stimulus	Electrochemical characteristic	Hypothesis for UT changes	UT observable	UT sensitivity	Length scale	Relevant refs.
SEI growth	High temperature (> 40°C)	Consumes lithium inventory and electrolyte solvent	Change of impedance at interfaces	Ultrasonic TOF increase due to overall thickness increase	Low	Nanoscale (10–200 nm) ^{74,75}	Bommier et al. (2020) ⁷⁶ , Chai et al. (2021) ⁷⁷
	High current rates (> 1C)	Irreversible capacity loss due to lithium confinement in SEI	Increased layer thickness Stiffness increase with growth of impedance at anode surface SEI changes wave speed	Slight change in reflection amplitude due to changes in acoustic			
Lithium plating	Low temperature (< 10°C)	Lithium plating may generates additional SEI formation through reaction with electrolyte	Reduced density and stiffness of lithium plating significantly reduces acoustic impedance	Significant decrease in SA (even after correction due to temperature)	High	Microscale (10–100 μ m lithium plating) ^{78,79}	Bommier et al. (2020) ⁸⁰ , Chang et al. (2020) ⁸¹ , Wasylowski et al. (2024) ⁸² , Meyer et al. (2025) ⁸³ , Xu et al. (2025) ⁸⁴
	High current rate (> 1C)		Lithium dendrites introduce scattering sites	TOF at max charge depends on C-rate. Promising indicator of degree of Li plating at low-temperature and fast charge			
	High SOC/Voltage	Lithium plating may cause dendrites growth that short circuit through separator	Dendrites increase surface roughness, which may increases incoherent scattering and causes mode conversion	Attenuation of transmitted signal through-thickness resonance frequency during low-temperature battery charging			
		Accelerated side reactions from reactive lithium plating correlate with gas generation					
Particle cracking/ Electrode delamination	High temperature (> 45°C) → Large thermal stress	Exposes pristine electrode surface to electrolyte may lead to more SEI growth and gas generation	Cracks are discontinuities that increase impedance contrast and scattering	Significant changes in the measured attenuation and shift in center frequency of waveform	Very high	Micro- to Macroscale (10–50 μ m cracks and 0.1–1 mm delamination) ⁸⁵	Pham et al. (2020) ⁸⁶
	Low temperature (< 0°C) → graphite embrittlement		Gas-induced delamination	Loss of transmitted signal due to delamination of the electrode layers			
	Volumetric expansion in cells with Si content		Delamination generates large impedance mismatch, significantly reducing transmission				
Scattering increases attenuation							
Electrolyte dry-out	Extended cycling	Gas encapsulation causes loss of ionic contact area	Void creation decreases density and stiffness, which significantly reduces acoustic impedance	Strong reduction of transmitted signals in unwetted regions	Very high	Micro- to Macroscale (Dry regions ranging from 10 μ m to 1 mm) ^{87,88}	Deng et al. (2020) ⁸⁷ , Elsosky et al. (2022) ⁸⁸
	SEI solvent consumption		Ionic transport limitation	Higher reflection in unwetted regions			
	High temperature (> 55°C)		Unwetting reduces coupling between layers, creating significant reductions in transmission amplitude	TOF increase due to reduced wave speed caused by voids			
Separator failure	High temperature (> 100°C)	Side electrochemical reactions at high temperature may lead to SEI decomposition and gas generation	High enough temperatures leads to softening and ultimately melting of polymer separator	Increase in TOF due to increase in compliance of polymer separator	High	Microscale (\approx 25 μ m polymer layer ⁸⁹ with < 1 μ m internal voids that grow with damage)	McGee et al. (2023) ⁹⁴ , McGee et al. (2024) ⁹⁶
	Abusive thermal cycling	Melting of polymer separator may lead to internal short circuit		An increase in temperature reduces the SA due to increase in internal viscoelastic losses at moderate temperatures			
				High temperature gas generation leads to loss of transmitted signal			
Gas formation	Thermal runaway	Side electrochemical reactions happening due to high interfacial reactivity	Gas pockets have low density and stiffness, which significantly reduces acoustic impedance	Strong reduction of transmitted signals due to acoustic impedance mismatch with gas generated	Very high	Micro- to Macroscale (0.1–2 mm gas regions and pouch swelling) ⁹⁰	Bommier et al. (2020) ⁷⁶ , Owen et al. (2024) ⁹⁵
	Overcharge		Strong wave scattering	Reduction of coherence in reflections coming from gas regions			
	Overdischarge	Electrolyte decomposition leading to gas generation					
		Particle cracking/Electrode delamination	Increase of internal pressure/stresses that might lead to reduced contact between layers in other regions	Ultrasonic imaging can be used to accurately visualize gas pockets			

research articles published on the subject through 2025, as shown in Fig. 5. To clearly communicate progress in this broad application area of ultrasonics, this review uses the following grouping of UT methods as applied to LIB research: (i) UT for state estimation (Sec. III A), (ii) UT for damage detection (Sec. III B), and (iii) UT to improve manufacturing, extend life cycle, and assess next generation batteries (Sec. III C).

Generally speaking, ultrasonic testing and monitoring can be used as a non-destructive characterization and monitoring technique for LIBs at the different stages of their life cycle²², which can be identified using a circular economy framework as manufacturing, use, reuse, and

recycling processes. Figure 6 illustrates different applications of UT along the cell life cycle to include cell manufacturing, cell conditioning, cell use, second-life use, and finally cell recycling.

A. State detection during normal operation: SOC and SOH

The first publication that employed UT techniques to evaluate LIBs by Sood et al. employed a pitch-catch configuration on an unconstrained lithium-ion pouch cell before and after undergoing a reduction in SOH to approximately 75 %. They found that the ultrasonic signal received through the aged cell was a “very weak,

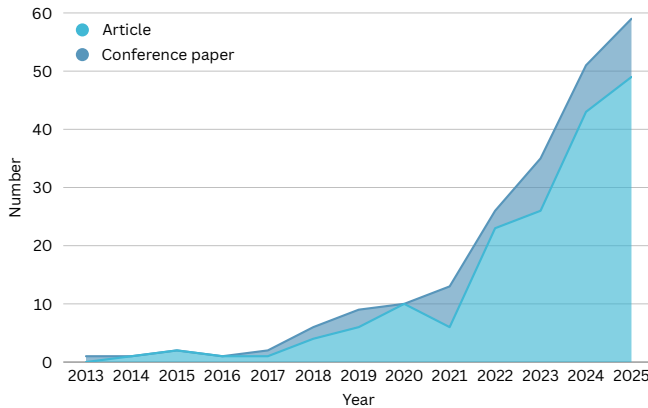


FIG. 5. Number of publications by year on the subject of UT of batteries since 2013, using the relevant papers from the following search criteria in Scopus: **TITLE-ABS-KEY ("Li-ion*" OR "Lithium-ion*") AND (ultrason* OR acoustic*) AND (diagnos* OR estimation OR "state of health" OR "state of charge" OR health OR characterization OR monitoring) AND NOT (welding) AND NOT ("acoustic emission")**.

delayed pulse⁹² and attributed the changes in signal characteristic to various aging mechanisms including gas formation, the formation and growth of SEI layers, and “electrode ruffling” where the layers within the cell are no longer flat due to the localized stresses associated with repeated cycling. Importantly, their observations of the ultrasonic signal point to two ultrasonic signal characteristics that have been reported in almost every other publication on the subject since: the signal amplitude (SA) and the change in propagation time compared to a pristine cell, which is also known as the time-of-flight shift (TOFS). These signal characteristics are chosen because they are both easy to calculate and indicative of numerous changes within the cell. Linking these metrics to specific internal processes is a challenge that is the subject of a large percentage of publications to date. For example, increases in TOF (positive TOFS) may indicate increased propagation length or decreased wave velocity^{93,94}. Decreases in SA can be related to increases in attenuation^{95,96}, reduced impedance matching between the transducer and cell^{97,98}, or the introduction of frequency-specific band gaps in layered systems^{69,70,96}. Following Sood et al.⁹², numerous authors have attempted to fully investigate the relationship between changes in ultrasonic signal characteristics and SOC and SOH. That research has been categorized in this review according to whether the work used bulk or guided waves to inspect the cells.

1. Bulk Waves for SOC and SOH Detection

The use of bulk waves for UT of lithium-ion cells is often employed because the configuration is simple, using either contact or non-contact methods, and the data is easily analyzed and interpreted since dispersion is only a result of material response and layering. As noted in Sec. II A, bulk waves can be classified as either longitudinal or shear waves, and their propagation speed is independent of boundary conditions. For transducers with large aperture, i.e. when $k_0a \gg 1$ where $k_0 = 2\pi f_0/c_0$ is the wavenumber at the center frequency, f_0 , of the generated pulse, c_0 is the phase speed in the cell at f_0 , and a is the descriptive length of the transducer, bulk waves travel as collimated beams from the transmitting transducer through the cell and back. The waveform is detected by a receiving transducer, either positioned at the other side of the cell (known as pitch-catch configuration) or using the same transducer to generate the pulse and receive echoes from inhomogeneities and boundaries (known as pulse-echo configuration). To ensure the beam-like propagation, most studies have employed pulses with $f_0 \geq 1$ MHz, although a small number of authors have chosen frequencies as low as 300 kHz³⁷ with the intent of using bulk wave methods. The investigation of SOC using ultrasonic propagation in LIBs has employed either ultrasonic measurements concurrent with cell cycling^{34,66,99–103} or at specific SOC levels with the cell at rest^{31,92,104–108}. Concurrent ultrasonic measurements and cell charging is more practical for real-time monitoring of battery SOC to avoid overcharging or over-discharging. Taking measurements after the cell has reached a certain SOC and rested may be more helpful for understanding SOC-specific structural changes, like the changing stages of graphite intercalation, which is easier to identify in an electrochemically static state. Regardless of the approach, most authors have used SA and TOFS as ultrasonic metrics of SOC. Other authors make use of related measurements like the calculation of wave velocity^{93,107}, time of the maximum pulse envelope, via the Hilbert transform¹⁰⁹, estimates of the signal energy using the square of the SA¹¹⁰, signal rise time¹¹¹, amplitude of the maximum frequency in the received spectrum¹⁰⁹, counts of the number of times that the ultrasonic signal exceeds a specified threshold¹¹². Moreover, due to the heterogeneous, multilayered, and dynamic nature of LIBs, some researchers have explored other more advanced signal metrics such as the attenuation of peak resonance frequencies^{69,113}, tracking shifts in the power spectral density of the ultrasonic signals^{114,115}, and combined metrics that employ time and frequency features such as the *S*-value proposed in Ref.¹¹⁶. Furthermore, some authors have argued that nonlinear stress-strain relationships may exist in LIB constituent materials due to their highly heterogeneous structure that includes localized damage and components that undergo phase transformations. It has therefore been suggested that UT techniques that exploit the effects of material nonlinearity, such as harmonic generation, may be more sensitive to changes in battery state^{117–120}. For exam-

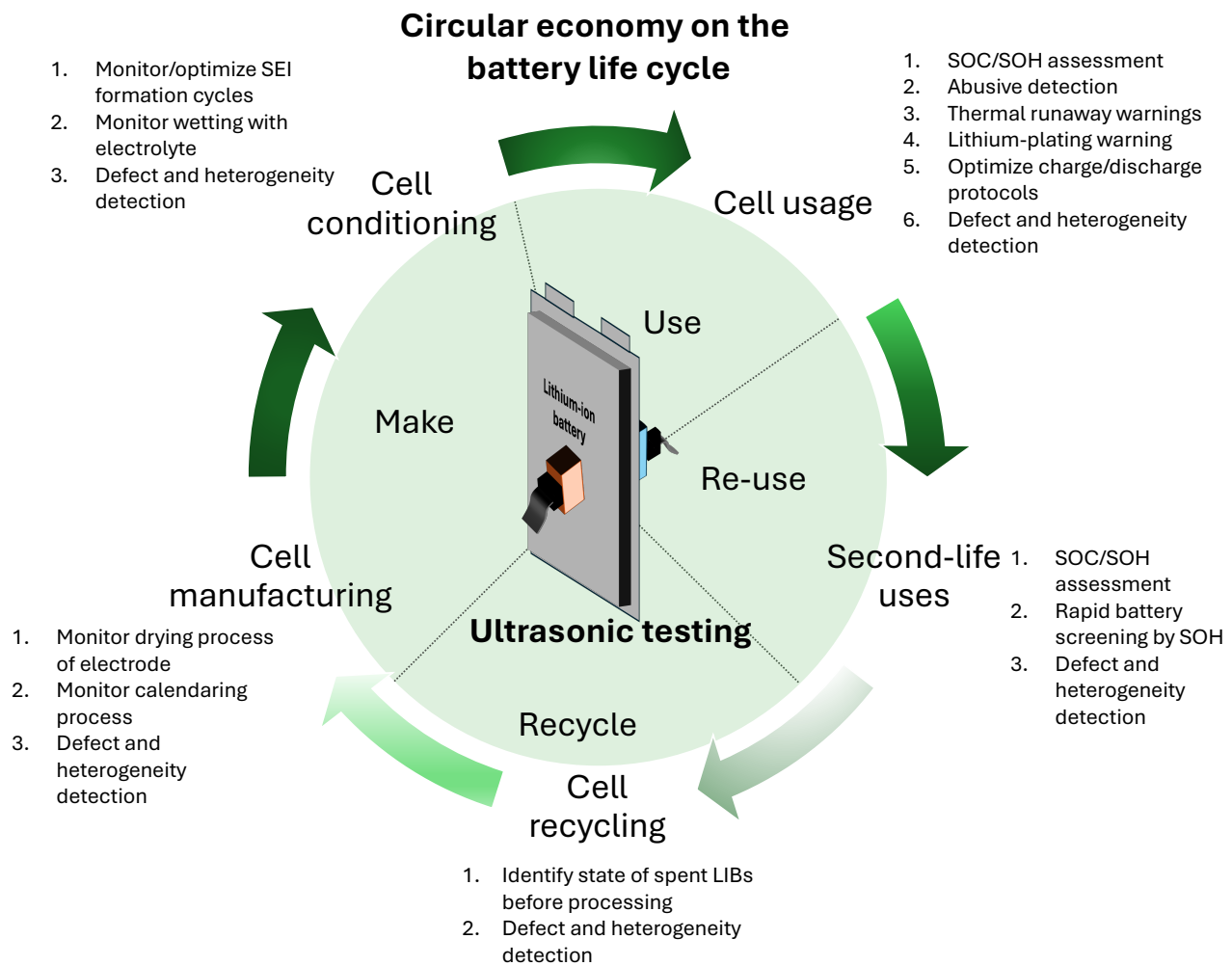


FIG. 6. Schematic of the battery life cycle showing applications of ultrasonic testing at different stages in a circular economy framework.

ple, Sun et al. estimated the nonlinearity parameter, β , which compares the amplitudes of the fundamental and second harmonic frequencies¹²⁰. In other work considering material nonlinearity, Yuan et al. measured “quasi-static” pulses (QSP) at 0.5 MHz that were generated by a 8.5 MHz bulk longitudinal wave¹¹⁹ and Lin and colleagues measured similar QSP at 0.25 MHz generated by a 5 MHz primary guided wave¹¹⁷.

In addition, since SA and TOFS measured using contact methods are highly sensitive to the contact pressure between the ultrasonic sensors and the cells, and researchers must be careful to ensure good coupling for reproducibility and accuracy, several researchers have employed non-contact ultrasonic techniques, such as air-coupled ultrasound^{32,107,108}, laser-generated ultrasound¹²¹, or using contactless electromagnetic acoustic transducers (EMATs)^{122,123}. However, these non-contact techniques present challenges that have been encountered in other applications of ultrasonic test-

ing, namely low transduction efficiency due to the high acoustic impedance mismatch between air and the transducers, and severe roadblocks in the eventual implementation in real-world applications^{42,124}. As a result, most ultrasonic measurements of LIB have employed contact methods, using conventional coupling agents such as liquid couplants (e.g., grease⁹³, canola oil¹¹³, acoustic gel¹²⁵), solid couplants (e.g., rexolite¹²⁶ or epoxy resin for fixed contact approaches⁶⁴), or immersion approaches, which employ liquid immersion (e.g., water⁹⁴, silicone oil¹²⁷) to enable mechanical scanning. Still, there is a growing niche for air-coupled and other contactless methods when handling or contamination is critical.

In contact methods, most authors have found that the TOF tends to decrease with increasing SOC, which allows TOFS to be an indicator of SOC^{26,31,32,37,66,80,93,95,99,100,104,106,107,109,128–135}. Conversely, the SA tends to increase with increasing SOC, as reported by most

studies^{26,31,32,37,66,93,95,96,99,106,110,136–139}. However, some authors have observed a decrease in SA with increasing SOC, which may indicate the presence of non-bulk modes or other factors that were not accounted for in the experimental apparatus^{93,109,132,140,141}. While these latter works were conducted on cells with different cathode chemistries, form factors, and capacities, it is noteworthy that despite these differences, one typically observes the same general trends in ultrasonic measurements, namely a decrease in TOF and an increase in SA with increasing SOC. Under normal operating conditions, this behavior may be ascribed to the graphite anode, which experiences larger changes in volume and Young's modulus than the cathode in LIBs, as shown in Fig. 3. These results suggest that the anode behavior drives the cell response that is measured when using bulk longitudinal wave propagation^{95,99}.

After the initial works described above, authors have tried to delineate the effects of different cell components or experimental variables on the observed ultrasonic signal trends in an effort to improve the specificity of ultrasonic testing methods for LIB monitoring. Liu et al. built custom half-cells with extra-thick separators (27 times larger than standard cells) in order to decouple the effects of the anode and cathode from the ultrasonic propagation. They found that the TOF decreased and the SA increased with SOC for the graphite anode, while the lithium iron phosphate (LFP) cathode showed opposite trends for both TOF and SA¹³⁴. Meng et al.⁹⁶ used a frequency sweep excitation from 0.5 MHz to 3.5 MHz, finding that the SA increased for the tested 0% to 80% SOC range for all tested frequencies, although to different extents. They also observed a cell thickness change from 4.50 mm to 4.60 mm for the same SOC range. Similarly, Sun et al.⁹³ performed experiments at 750 kHz, 1 MHz and 1.5 MHz excitation frequencies. They identified a direct correlation of SA with SOC for the 1.5 MHz frequency. However, they did not find clear correlations of SA with SOC at the 750 kHz and 1 MHz frequencies, which they attributed to the low sensitivity of the transducer used for those measurements. Nonetheless, they showed that the attenuation of the three frequencies were sensitive to battery SOC changes. The choice of input frequency deserves attention for its effect on wave propagation within the cell. Different input frequencies may excite guided types of wave propagation within cells, or may experience frequency-specific attenuation or wave speeds based on the layering structure and constituent properties. McGee et al. highlighted the importance of understanding the mode of propagation, as different input frequencies were shown to excite different propagating modes within the battery using the same transducers due to the response of the transmitting transducer. Additionally, they noted that through-thickness bulk modes and guided wave modes may have different SA and TOFS trends with cycling and heating⁶⁴. Regarding the relationship between ultrasonic metrics and SOC, some authors have explored extending this concept to map SOC as a function of the location

within the cell since ultrasonic reflection/transmission scanning allows localized estimation of mechanical property changes, thereby enabling spatially-varying estimates of the SOC^{94,106,142–144}. Understanding spatial heterogeneity in the SOC is crucial since it could indicate non-uniform utilization of the lithium inventory and active materials within the cells, which may influence cell degradation¹⁴⁵. For example, Xie et al.¹⁴⁶ explored inhomogeneous degradation resulting from low temperatures and fast charging operating conditions and used bulk ultrasonic waves to help identify localized changes in SOC.

For bulk wave propagation, the relationship between TOFS and reduced SOH is better understood than that between SA and SOH. The mechanisms that contribute to a change in TOFS are either changes in the propagation path length or changes in the effective stiffness or density of the cell. For example, cells expand as they age which increases the propagation distance and can cause an increase in the TOFS if the sound speed does not change appreciably. It is more difficult to explain how various aging mechanisms that may occur simultaneously can affect the SA. These mechanisms include microcracking of active particles⁷¹, continued growth of the SEI⁷³, or increasing internal cell pressure^{63,131}. Perhaps because it is easier to interpret changes in the TOFS of bulk longitudinal waves with aging, at present there is more agreement in the literature on this relationship than between SA and SOH. Many authors have found that the TOFS increases over the entire SOC range with decreasing SOH as shown in Fig. 7.A^{99,104,128,131,133}. This increase has been attributed to a combined effect of electrode thickening and mechanical softening with aging. Likewise, groups who only investigated TOFS at a specific SOC have found that TOF increases with decreasing SOH¹⁴⁷. A recent study by Williams et al.¹⁴⁸ has shown that tracking TOFS from different portions of a single reflected ultrasonic signal using pulse-echo configuration can have different trends with decreasing SOH. As shown in Fig. 7.B, the TOF trends of the earlier and later echo peaks from A-scans differed between the two tested NMC811 cells. In cell A, earlier peaks consistently shifted to longer TOFs, while long peaks shifted to shorter TOFs as SOH decreased. This behavior was not observed in cell B, where both peaks exhibited matching trends with decreasing SOH. Those authors did not provide a definitive explanation for these differences in the cell and attributed it to possible manufacturing discrepancies between the cells. More research should be conducted on a larger sample of cells and a greater number of cycles to identify the underlying causes of these results.

When investigating the effect of SOH on US propagation, it is important not to extrapolate trends from the first few cycles. Authors have begun to delineate early-life aging mechanisms that occur during the initial charge-discharge cycles from more long-term aging mechanisms that occur progressively as the cell is cycled further since it has been shown that different trends may occur during battery degradation due to SEI formation

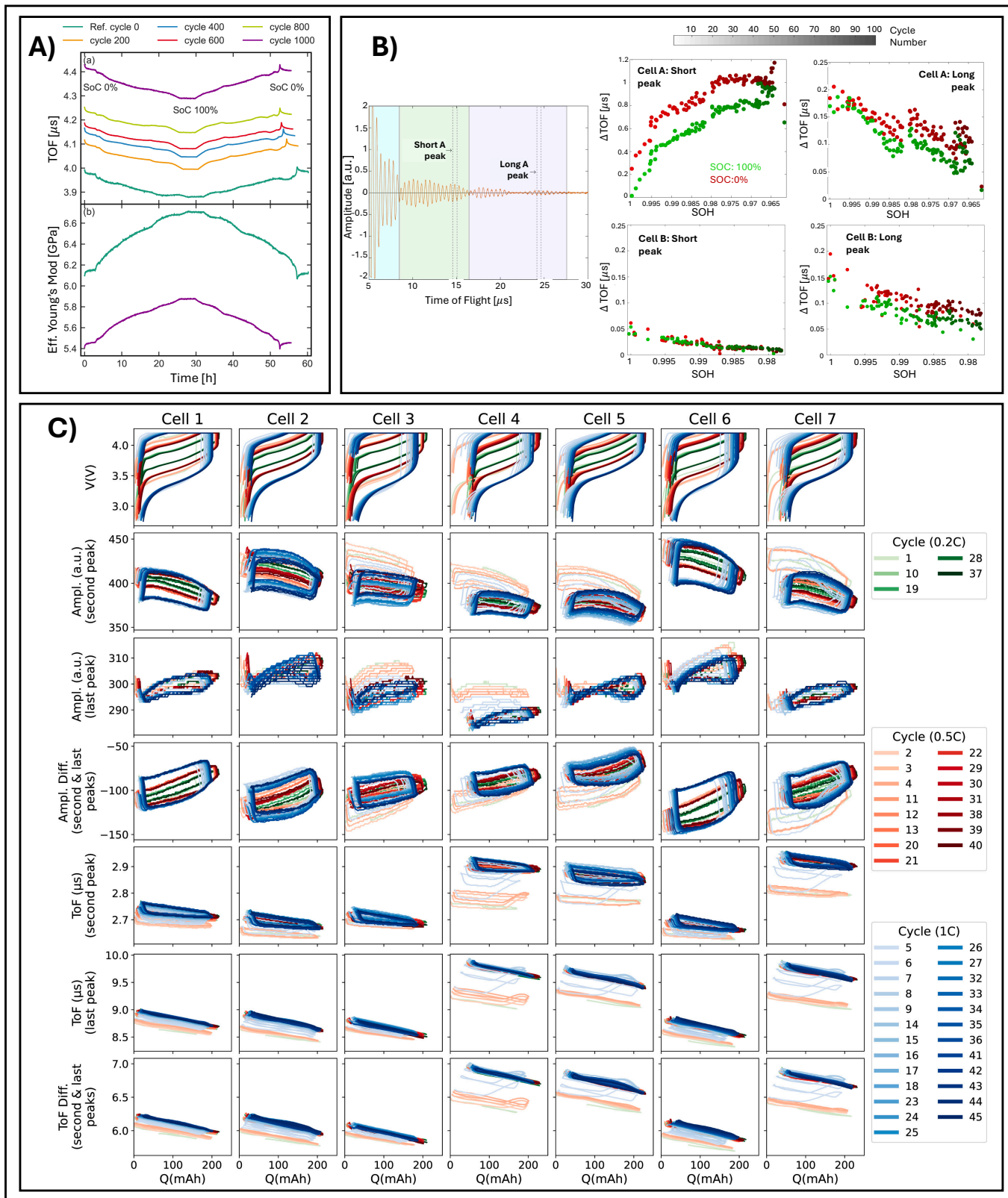


FIG. 7. Use of ultrasonic bulk waves for SOC/SOH assessment. **A)** Feiler et al. found that the TOFs of bulk longitudinal waves increased for all SOC with decreasing SOH. Reproduced with permission from Ref.¹³³ Copyright 2023 Wiley. **B)** Trends of earlier and later echo peaks TOF shifts (of about 1 μs) with decreasing SOH for two different NMC811 cells. Reproduced with permission from Ref.¹⁴⁸ Copyright 2025 Elsevier. **C)** Voltage and acoustic metrics measured during early aging at different C-rate conditions. Reproduced with permission from Ref.¹⁴⁹ Copyright 2025 Elsevier.

at a initial stage, followed by stabilization and saturation stages at a higher number of cycles⁷¹. Knehr et al. cycled a cell 100 times and found that the TOFS increased mostly in the first 12 cycles during what they call the “break-in” period¹³¹, with more modest increases in TOFS occurring in subsequent cycling. They observed that the cell thickness increased most rapidly during the “break-in” period, and hypothesized that the increasing internal pressure within the cell may be forcing the electrolyte to wet previously inactive regions of the cathode material, in a process they call “electrode crosstalk”¹³¹. Furat et al.¹⁵⁰ and Wade et al.¹⁵¹ have noted that particle cracking occurs in the first 10 cycles, which may be a contributing factor to the changes associated with the “break-in” period in some cases, although the SEM images provided by Knehr et al.¹³¹ do not suggest particle cracking occurs in their samples. Davies et al.⁹⁹ and Wu et al.¹⁰⁴ also found that the most rapid changes in TOFS occurred in the early cycles. It is also important to note when conducting aging studies that accelerated aging is not entirely representative of aging due solely to charge-discharge cycling. Accelerated aging is often preferred when conducting any experiment on LIBs exploring reductions in SOH due to the extremely long time-scales involved for SOH reduction, for example, Deng et al. cycled cells 2,500 times over the course of two years to monitor changes in battery properties and ultrasonic metrics⁸⁷. Although faster to perform, caution should be exercised when performing accelerated aging experiments, as the introduction of other variables, such as increased cell temperature or extended voltage ranges, can affect the mechanical properties of the cell over time. Some works have explored the influence of different charge/discharge current rates (C-rate, which is defined as the ratio of the current to the rated capacity, and refers to the speed of charging and discharging) and the temperatures generated for these different operating conditions on the propagation of bulk waves in LIBs^{130,139}. For instance, Fig. 7.C shows a summary of the experiments performed by Galiouunas et al.¹⁴⁹, where they cycled seven cells at three C-rates (0.2C, 0.5C and 1C). Other authors showed approaches to account for temperature correction^{65,152}, but this is still an open research question that is being investigated in terms of decoupling the C-rate and temperature conditions on the behavior of bulk ultrasonic waves for different battery states. In this sense, Galiouunas et al.¹⁰³ exposed the importance of careful consideration of temperature effects and thicknesses changes over degradation because they can mask degradation markers, generating misinterpretations of the ultrasonic insights.

As previously noted, the relationship between SA and SOH is less clear. Some authors have found that the SA increased globally with decreasing SOH^{104,109}, while others found the opposite trend^{81,87,99,102,116,141,147,153}. Wu et al. found that the SA increased consistently for the first 50 cycles, noting a potential leveling off after that point, perhaps indicating an early-life aging mechanism¹⁰⁴. Sun et al. found that SA decreases

with decreasing SOH¹¹⁶, which they attribute to loosening structure within the cell and the loss of contact between active particles. This hypothesis would also be consistent with the results from others that found an increasing TOFS with cell aging. There are many different aging mechanisms that occur in cells, both due to charge-discharge cycling and from calendar-aging, which may affect the mechanical properties of the cell. In order to improve the understanding of the effect of SOH on SA, we suggest that authors include the full history of cells when discussing UT results, including time from purchase to experiment. When possible, authors should additionally identify aging mechanisms either via advanced imaging techniques or through other analyses such as electrochemical impedance spectroscopy or incremental capacity analysis.

Regarding SA trends, Chang et al. charge-discharge cycled a cell for over 800 h at 60 °C noting that the TOFS and SA decreased with cycle number⁸¹. Cai et al. conducted an accelerated aging study using bulk wave ultrasonic inspection on a 10 A h pouch cell cycled 200 times at 40 °C. The authors calculated two measures of SA and one measure of TOFS. However, their TOFS measure appears to be susceptible to errors in the automated calculation, as indicated by un-physical jumps in the TOFS values. Such inconsistencies are common in automated TOFS calculations due to limitations in time resolution¹⁴⁷. Similarly, Feiler et al. cycled a cell 1000 times, taking ultrasonic measurements every 200 cycles and reported a decrease in SOH to 95 % after 1000 cycles and noting that the SA consistently decreased with aging¹³³ (see Fig. 7.B). During LIBs degradation, sometimes LIBs can exhibit a rapid nonlinear degradation drop commonly referred to as “knee” points, where the SOH will suddenly decrease due to various “knee” degradation mechanisms such as lithium plating, electrode saturation, resistance growth, electrolyte and additive depletion, percolation-limited connectivity, and mechanical deformation, as reviewed by Attia et al.¹⁵⁴. In this regard, Sun et al.¹¹⁶ used 5 MHz US bulk waves to detect this nonlinear degradation decay on NMC811 pouch cells. For this purpose, they calculated a joint time-frequency metric based on the SA that exhibits distinct characteristic peaks that change throughout the cycling process. The disappearance or shift of these peaks correlates strongly with the onset of nonlinear capacity decay that occurred at about the 70th cycle, providing a precursor signal to detect the “knee” point. They induced this behavior using high, uneven C-rates of 0.5C for charge and 1C for discharge, contrary to the 0.2C value recommended by the manufacturer of these cells.

2. Modeling Bulk Wave Propagation

We can define two broad categories of modeling approaches for UT of LIBs: wave physics models and data-driven models. Wave physics models draw from multi-scale wave mechanics to derive models that predict ultrasonic propagation, which enables inversion of ultrasonic signals to determine changes in constituent properties

and geometry. In contrast, data-driven models rely on statistical methods like machine learning to solve for empirical relationships between wave propagation and battery state.

Wave Physics Models: When constructing a physical model, researchers have many important questions to answer. For example, what is the best approach to accounting for the high number of layers within cells? Approaches taken to address this have included creating simplified models with reduced numbers of component layers^{34,116,155–157}, neglecting individual component layers^{34,64,116}, or creating a repeating unit-cell of specific component layers and invoking Bloch-Floquet periodicity^{26,34,116}. In general, the propagation of ultrasonic waves in this constantly changing, heterogeneous medium is heavily influenced by the impedance mismatches associated with the characteristic impedance of each layer within the cells, as indicated in Fig. 8.A. Other questions include how to model the dynamic mechanical response of electrode layers, which are composed of active materials, binders, conductive additives, and are soaked with liquid electrolyte. Researchers have approximated their dynamics by simply modeling them as being composed of only active materials¹¹⁶, or by using effective medium theory^{26,64,66}. For the latter case, the electrode materials have been modeled as either poroelastic^{31,32,34–36,38,40} or viscoelastic materials^{26,64}. The choice of assumed constitutive behavior dictates the equations of wave motion and required material properties. Finally, in terms of implementation, previous work has employed finite-elements^{37,38,64,129,155} or transfer matrix methods^{26,34,36,38,69,70,96,156,157} to simulate the wave propagation. The paragraphs that follow provide a summary of relevant physical modeling approaches for understanding and approximating ultrasonic wave phenomena in LIB.

Hsieh et al. simulated wave propagation through a stack of LIB constituent materials, including the outer pouch cell casing, the copper current collector, the anode electrode with graphite and PVDF, the separator, and the cathode containing LCO, PVDF, and carbon binder. They used 1D wave equations and modeled the battery components with their densities and elastic moduli. Those authors assumed that the densities of LCO and graphite varied with SOC. In addition, they modeled the electrodes as being composed of 80 wt% active material, 10 wt% conductive additive, and 10 wt% binder and used either mass-fraction or volume-fraction weighted sums of the density and modulus. That work acknowledged the difficulty in obtaining accurate material properties of cell components and that their model simplified the internal structure of the cell, so they refrained from drawing strict conclusions from their model.⁶⁶

Li and Zhou created a finite-element model of a cell to simulate wave propagation in the LIB generated via air-coupled excitation. They simplified the internal structure of the cell by creating a 21-layer representation where the thicknesses of the layers were added together. They additionally model the electrolyte as a dis-

crete layer on both sides of the separator. They used this model to detect void defects at differing layer depths, which they referred to as “stomata”¹⁵⁵.

In order to study variation within the cell, Copley et al.¹²⁹ introduced a finite-difference scheme for the 1D wave equation and assuming that variations in the local material properties could be captured by assigning different values of the sound speed as a function of the location in the cell. Since this work used material properties from Hsieh et al.⁶⁶, they only consider changes in the density of the graphite and LCO and neglect changes in the elastic modulus of those components or changes to any other cell component property. The resulting model accurately simulated received ultrasonic signals at different frequencies. However, they did not make any claims about simulated TOFS or SA with SOC.

The global matrix approach implemented by Meng et al. considered a cell comprised of 127 layers of battery components. Their model accurately modeled the ratio of the transmitted wave amplitude to the input wave amplitude, which they used to identify equally-spaced band gaps centered at 456 kHz, 1.37 MHz, 2.28 MHz, and 3.19 MHz associated with the layer periodicity⁹⁶. Using SOC-dependent material properties of cell components, they found that the band gaps shifted by 10 kHz when the cell SOC increased from 0 to 0.8 SOC.

Sun et al. used pseudo-two-dimensional (P2D) modeling within COMSOL. A unique feature of their model is the inclusion of the SEI. Their model provided approximations of the stress induced via lithium insertion or removal, which they then used to simulate changes in Young’s modulus and density. Their model considered a unit cell formed by the NMC811 cathode, the separator, and the graphite anode, which was repeated five times, resulting in a 15-layer model. They simulated longitudinal propagation through a fresh and an aged cell under high-rate discharging conditions, finding that the wave propagated through an aged cell arrived later in time and had a reduced amplitude, suggesting a reduction in the effective longitudinal modulus and increase in attenuation with cell aging due to SEI damage, which Sun et al. refer to as rupture¹¹⁶.

Finite elements were also employed by Song et al. to simulate lithium ion concentrations in the anode using the built-in isothermal lithium-ion battery module in COMSOL Multiphysics¹⁵⁷. Their approach employed a strain-energy approach to obtain elastic constants, which they used in conjunction with Ref.⁵⁵ to calculate the Young’s modulus of the graphite with SOC. Their model combined Legendre orthogonal polynomial and global matrix method¹⁵⁶ to simulate the reflection coefficient through a simplified 11-layered cell at specific angles, frequency, and SOC which they compared to 11-layered and 51-layered finite element models in COMSOL finding good agreement¹⁵⁷.

Another relevant finite element model was introduced by Zhang et al. who created a two-dimensional, 59-layer finite-element model in COMSOL, which accounts for the porosity of the electrodes and separator through

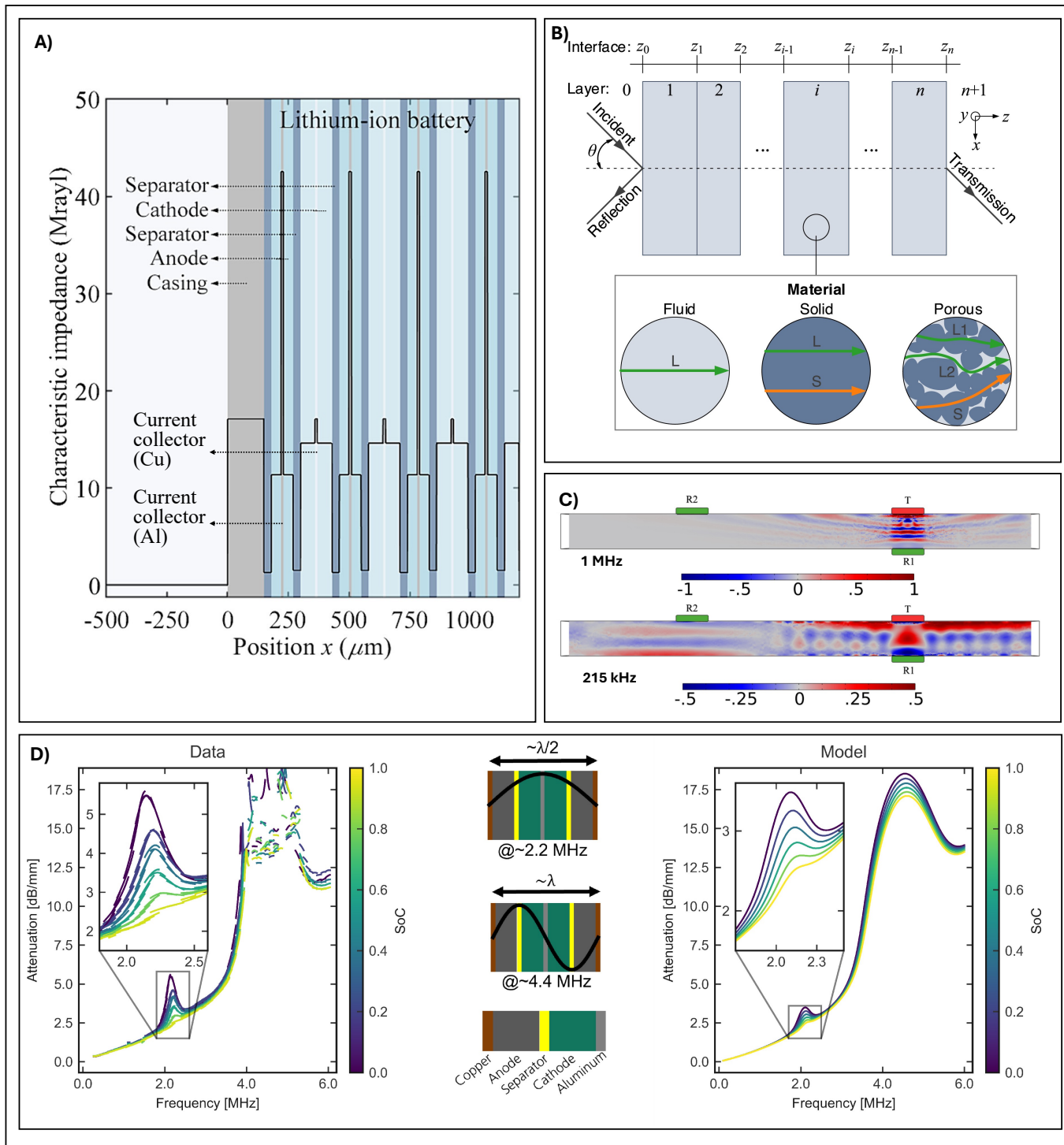


FIG. 8. Modeling as a key tool to understand ultrasonic bulk waves in LIBs. **A)** Representation of the acoustic impedance mismatches between different layers of LIBs. Reproduced with permission from Ref.⁷⁰ Copyright 2024 Elsevier. **B)** Each layer of the multilayered structure of LIBs can be modeled as a fluid, solid, or porous material, which will determine the number and type of propagating waves (L: longitudinal and S: shear). Electrodes and separators are modeled as porous materials consisting of elastic active particles in a fluid electrolyte, while the current collectors are assumed to be solid elastic materials. Reproduced with permission from Ref.³⁶ Copyright 2023 Elsevier. **C)** Simulation of US bulk waves (top) that are localized in space due to a beam-like field generated by transducers with a large aperture compared to the transmitted wavelength and guided waves (bottom) that can be used to interrogate larger cell volumes. The selected excitation frequency is a critical parameter that determines the type of ultrasonic propagating waves. Reproduced with permission from Ref.⁶⁴ Copyright 2023 Elsevier. **D)** Measured and modeled attenuation per length on multilayered LIBs. High attenuation near 2 MHz and 4 MHz is due to stop bands associated with the periodic structure of pouch cells, as indicated by the unit cell shown between data and model results. Reproduced with permission from Ref.⁶⁹ Copyright 2024 Wiley.

the use of Voronoi polygons. They found that the TOF increased and the SA decreased with decreasing SOC, which is consistent with most of the literature³⁷. The same group also used a global matrix method based on Biot's theory further employing their Legendre orthogonal polynomial method and their use of COMSOL to simulate material property values based on lithium ion concentrations³⁸. Using this model, those authors simulated reflection coefficients through the cell at different frequencies and identified passbands at frequencies around 650 kHz and 900 kHz, which shifted to higher frequencies with increasing SOC³⁸.

Huang et al. used both the transfer matrix method and the stiffness matrix method to construct a global matrix based on Biot's theory of poroelasticity to model the propagation of ultrasonic waves through the porous-solid-porous structure of porous active material adhered to solid current collectors³⁶, as represented on Fig. 8.B. The results of this model indicated that the slow longitudinal wave had a wavespeed multiple orders of magnitude slower than the fast longitudinal wave and had an attenuation six orders of magnitude larger than the fast longitudinal wave³⁶. These results indicate how difficult it would be to observe a slow longitudinal wave experimentally, even though it has been observed in other areas of wave physics^{44,45,68}.

Later, McGee et al. developed a homogenized material model of the cell by considering only the separator and the active material of the anode and cathode. These authors used this effective material in COMSOL to visualize the wave propagation in the cell and to identify the propagation mode for different frequency excitations⁶⁴, recognizing the importance of frequency selection on the wave propagation behavior as exemplified in Fig. 8.C. This last point was also addressed by Feiler et al.⁶⁹, who used a semi-empirical transfer matrix model to calculate the group velocity and attenuation of transmitted ultrasonic waves for a range of about 0.5 MHz to 6 MHz. They obtained a good agreement between model and experiment for different values of SOC, as shown in Fig. 8.D. Feiler et al. showed enhanced attenuation at the band gaps where the wavelengths match the periodicity of the battery layers. This phenomenon is caused by the constructive interference of reflected waves, which raises the total reflection, lowers transmission, and subsequently increases attenuation, as previously reported by Ma et al.⁷⁰. Ma et al. also used a transfer-matrix model with Floquet-Bloch periodicity to show that LIBs exhibit a band gap for longitudinal waves from 2 MHz to 3 MHz, which was validated with experiments. More recently, McGee et al. derived a periodic transfer-matrix model of the cell considering the separator, anode active material, copper current collector, cathode active material, and copper current collector to simulate longitudinal wave propagation through a cell with both SOC-dependent and temperature-dependent material properties²⁶. They found that the TOFS decreased with increasing SOC and that the TOFS increased while the SA decreased with

increasing cell temperature for longitudinal wave motion due to softening of the polypropylene separator.

Data-Driven Models: Many research groups have opted to use statistical or data-driven models including limited or no physical behaviors to find correlations between US signals and internal battery states including SOC, SOH, and moderate changes in operating temperature^{31,99,102,104,106,131,132,139,140,147,158–162}. These methods have generally been successful, but remain limited as the creation of a model is specific to its training data. A model created based on a specific training set of experimental data using given excitation frequencies, cell geometry, anode and cathode chemistry, etc, may not be adaptable enough to be applied to scenarios where the cells or experimental setups differ. Additionally, since these models do not consider the underlying physical behaviors, it is possible for them to draw unphysical conclusions¹⁶³. For example, some models claim that specific data points in a received signal carry more weight in correlating with cell state. However, any individual point in a received waveform does not correlate with any particular component or position in the cell. The point may be statistically correlated, but this signifies nothing of physical interest. This limitation is of particular importance, as it reduces the ability of a researcher to say with certainty which cell component or cell location is the cause of the perceived cell state. Despite this complication, data-driven methods are of significant interest to this area of research and a significant number of publications have shown promising results, which are summarized below.

Regarding the challenge of generalization for data-driven models, Galioumas et al.¹⁴⁹ examined six features extracted from reflected bulk ultrasonic waves from seven different cells tested over 40 cycles for three different C-rates (0.2C, 0.5C, and 1C), with the main goal of finding general patterns between acoustic features and SOC that can be used between different cells (Fig. 7.C). They found a lack of generalization for the ultrasonic features selected, suggesting the presence of cell-specific patterns rather than generalizable trends for the acoustic features. In this sense, the results call for caution in evaluating the efficacy of acoustic signals for battery diagnosis, as previous studies may have overlooked the difficulty of generalization in their claims. However, this is still an open research question that future experiments and modeling will address.

Notable initial work in this area includes that of Davies et al. who applied Support Vector Regression (SVR) to develop a model capable of estimating SOC and SOH based on various combinations of input data, including TOFS, SA, or the total waveform, in conjunction with cell voltage. Their model achieved an impressive accuracy, predicting SOC and SOH within approximately 1%⁹⁹. Building on the integration of multiple data sources, Wu et al. utilized the Mahalanobis distance data fusion method to combine cell temperature measurements with ultrasonic signals. When applying this approach to a cell overcharged to 5 V, they found

that their model provided an earlier indication of damage compared to relying on temperature data alone¹⁰⁴. Further exploring deep learning techniques, Galiounas et al. developed a feed-forward neural network that incorporated entire received waveforms, specific waveform data points exhibiting high Pearson correlation with SOC, and Fourier coefficient magnitudes obtained via fast Fourier transform (FFT). Their model achieved highly accurate SOC estimation, with an error as low as 0.75 % when analyzing C-rates between 0.2 and 1C¹³². Similarly, Huang et al. applied deep learning techniques, including a feed-forward neural network, a convolutional neural network, and a fully connected neural network, using the full received waveform as input for SOC estimation, achieving a root mean squared error (RMSE) of 3.02 %¹⁰⁶.

Additional notable data-driven methods include the work of Zhang et al. who explored a different neural network architecture, developing a backward propagating neural network that leveraged six time-domain features of the received waveforms: time-domain peak, envelope peak, energy integral, waveform index, Kurtosis coefficient, and shape coefficient—as inputs¹⁴⁰. Their model predicted SOC with an RMSE of 7.42 % and cell temperature with an RMSE of 0.4 °C. Taking a regression-based approach, Qin et al. employed nonlinear multivariable regression to model the relationship between two SA-based measures and the reduction in capacity of a single cell cycled 200 times. Their model achieved an RMSE of 0.89 %¹⁰². Expanding on this work, their research group incorporated machine learning techniques, integrating the Random Forest and extreme gradient boosting (XGBoost) algorithms to enhance SOH estimation based on ultrasonic characteristics similar to SA and TOFS. Their improved model achieved a mean squared error of 0.4 % when estimating capacity from the same cell's data¹⁴⁷.

Beyond conventional machine learning approaches, Copley and Dwyer-Jones developed a genetic algorithm based on a finite difference solution to the 1D wave equation. Unlike other studies that relied on ultrasonic signal characteristics such as SA and TOFS, their model directly processed raw received waveforms. Given material thicknesses, their algorithm predicted wave speed of individual layers with an error ranging from 3 to 29 %, while, given material properties, it estimated layer thickness with an error between 3 % and 13 %¹⁵⁸. Xu et al. introduced an adaptive Extended Kalman Filter and an adaptive H-infinity filter, using the ultrasonic signal feature they termed the “energy of the oscillatory wave,” which corresponds to the squared SA of the received signal before the first echo. These models accurately predicted SOC during discharge under varying temperature conditions (−5 °C, 25 °C, and 40 °C) with an RMSE of approximately 1 %¹³⁹.

Another work by Zhang et al. reported a strong correlation between the 1st and 2nd transmitted pulses parameters and battery state, where the amplitude of both of them increased with SOC, while the TOF of the 2nd transmitted pulse decreased for the same SOC

behavior⁶⁷, indicating an overall increase in stiffness and reduction in losses with increased SOC. Ultrasonic signals showed increasing attenuation and TOF shifts as aging progressed over 183 charge/discharge cycles. To accurately model these relationships, a hybrid sparrow search algorithm (SSA) and relevance vector machine (RVM) approach was developed, optimizing kernel width for precise state estimation. The model achieved a maximum relative error of 1.51 % for SOC and an absolute error of 0.79 % for SOH.

Despite these advances, questions remain regarding the direct correlation between AI-based battery state predictions and physical changes within the battery. Addressing this challenge, a recent study applied explainable AI techniques to analyze selected ultrasound signal features such as TOF, max-min values, peak-peak values, and the maximum amplitude of frequency spectra¹⁶². This research provided quantitative insights into the influence of these features on different regions of the predicted SOH, shedding light on the interpretability and physical relevance of AI-driven battery state estimations. However, it is still an open research question how different physical mechanisms (such as gas generation, electrode delamination, voiding, and electrode expansion) are related to these ultrasonic features during battery operation and aging.

3. UT for SOC/SOH Detection: Guided Waves

As discussed in Sec. II A, ultrasonic guided wave methods offer a unique approach to assess characteristics of LIBs. Guided ultrasonic waves can propagate longer distances and can be selected to probe specific regions within a battery⁴² and therefore may be more suited for detecting specific types of internal mechanical changes in LIB. Furthermore, the combination of bulk wave and guided wave ultrasonic testing may allow for more complete mechanical characterization of the cell and its components. Previous use of guided wave modes for UT has been achieved by placing the transmitting and receiving transducers on the same surface of the cell (see Fig. 9.A) and using frequencies below 1 MHz. The same ultrasonic signal characteristics, i.e., SA and TOFS, can be used to quantify changes in guided waves associated with changing cell conditions.

Many groups have used longitudinally polarized piezoelectric transducers as their actuators to excite guided wave propagation within LIBs^{43,64,114,164,168–170}. While these transducers are not specifically designed to maximize the energy of guided wave modes, they can still excite and detect guided wave propagation within LIBs, providing insight into physical changes within cells under different loading scenarios. When using these non-specialized transducers to excite guided waves, it becomes necessary to prove that the observed waveforms are indeed due to guided wave motion either through experiments together with signal processing techniques¹⁶⁶ or via simulation⁶⁴. Other groups have opted to design and/or operate transducers that have been optimized to transmit guided wave motion^{122,171,172}. While employing

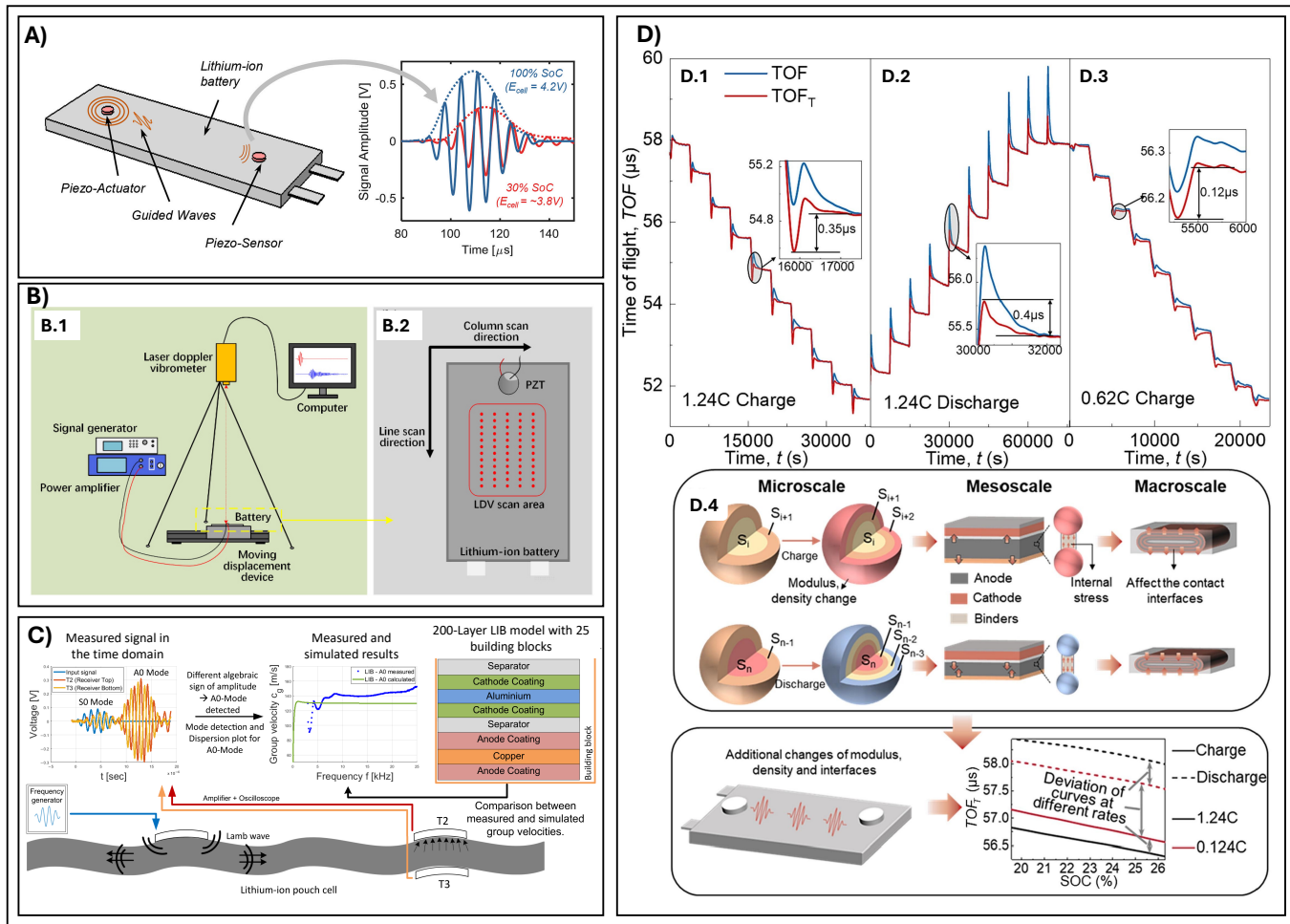


FIG. 9. Use of ultrasonic guided waves for SOC and/or SOH assessment. **A)** Transducer positioning for guided wave measurements using disk-shaped contact transducers. The receiving transducer is placed on the same surface of the cell as the transmitter. Reproduced with permission from Ref. ¹⁶⁴. Copyright 2018 Elsevier. **B.1-B.2)** Experimental setup using a scanning laser Doppler vibrometer to monitor out-of-plane displacement due to guided wave propagation. Reproduced with permission from Ref. ¹⁶⁵. Copyright 2022 MDPI, under the terms of the CC BY license [<https://creativecommons.org/licenses/by/4.0/>]. **C)** Schematic to determine Lamb wave modes generated in a multilayered LIB. Reproduced with permission from Ref. ¹⁶⁶. Copyright 2022 MDPI, under the terms of the CC BY license [<https://creativecommons.org/licenses/by/4.0/>]. **D.1-D.3)** TOF and TOF_T measurements during galvanostatic intermittent titration experiments for charge and discharge at various C-rates. **D.4)** Illustrations of possible factors affecting TOF changes with different C-rates. Reproduced with permission from Ref. ¹⁶⁷. Copyright 2024 Elsevier.

a receiving sensor on the cell face may be more appropriate for *in situ* applications, monitoring guided wave propagation via non-contact methods such as with a scanning laser Doppler vibrometer (SLDV)^{114,165,169} or a contactless electromagnetic acoustic transducers¹²³ could be useful for the laboratory setting.

While much less work has been done employing guided waves for UT of SOC compared to bulk waves, most authors find that the TOF tends to decrease with increasing SOC which allows TOF shift (TOFS) to be an indicator of SOC^{39,43,114,164,168,173}. However, Li et al.¹⁷⁰ found the opposite trend, suggesting that more work is required to understand this discrepancy. All authors who

measure SA find that this metric tends to increase with increasing SOC^{39,43,114,164,170}.

The first use of guided waves for UT of LIBs was presented by Ladpli et al.¹⁶⁴. A diagram of their experimental configuration is shown in Fig. 9.A. These authors used input frequencies between 100 and 200 kHz in a pitch-catch configuration and also used the ultrasonic signal characteristics of SA and TOFS¹⁶⁴. Popp et al. also used piezoelectric transducers mounted on the same cell surface for their guided wave study of LIBs. They used transducers with resonant frequencies of 9 kHz and a square wave excitation¹⁶⁸. Zhao et al. used guided waves with a piezoelectric transducer as the transmitter

and used laser vibrometry to measure the out-of-plane velocity at a single point associated with the passage of the guided wave¹¹⁴. Their work used a 5-cycle sinusoidal tone burst with a center frequency of 110 kHz as the excitation signal. Additionally, the power spectral density (PSD) was calculated as an additional indicator alongside the TOF and SA to assess changes in the battery state. The trends observed in the PSD were analogous to those of the SA. The authors showed that the sensitivity of the SA diminishes progressively with battery degradation, attributing this phenomenon to changes in the lattice structure of the battery electrodes. Such findings require further research to elucidate the underlying mechanisms contributing to this behavior. A modified experiment was performed by Li et al.¹⁶⁵, where instead of a single point measurement, they did a scan of the battery with a SLDV to get spatial information of the ultrasound guided wave propagation, as shown in Fig. 9.B.

Zheng et al. used guided wave UT on a very thin lithium-ion pouch cell, having a thickness of 3.5 mm¹⁶⁹. They used a 5-cycle Hanning-windowed sinusoid excitation similar to Refs.^{114,170} with a center frequency of 100 kHz. Similar to Li et al.¹⁶⁵, they used an SLDV to scan the cell surface for their receiving sensor and scanned a cell at 100 % SOC and claimed to find a relatively large defect of $22 \times 18 \text{ mm}^2$, although this was not confirmed with other methods¹⁶⁹.

Koller et al. used three piezoelectric transducers for guided wave UT in a configuration similar to Ref.¹⁷⁴, with one receiving transducer on the same face as the transmitter and the second receiving transducer opposing the top-mounted receiving transducer some distance away from the transmitting transducer¹⁶⁶. The use of this transducer configuration, enables comparison of the phase of the received waveform at the top and bottom cell surface, which they use to determine symmetric or anti-symmetric Lamb modes, as illustrated in Fig. 9.C. They measured the A0 group velocity in the range of 60 m s^{-1} to 170 m s^{-1} for different tested batteries up to 25 kHz. The same authors extended this work by conducting a separate experiment on 32 Ah NMC/graphite pouch cells and piezoelectric transducers as transmitters and receivers¹⁷⁵. Using this setup, they performed guided wave inspection at nine cell voltages between 3.59 V and 4.20 V and at temperatures between 5 °C, 25 °C, and 45 °C and found that group velocity of the A0 increased with increasing SOC and decreased with increasing temperature. They further demonstrated their technique in a BMS based on lookup tables that had a mean absolute error of 3.48 % to 5.32 % for SOC estimation¹⁷⁵.

Siegel et al. built and tested an EMAT specifically to excite the A0 mode in lithium-ion pouch cells, which was confirmed by monitoring the motion on the opposite cell faces with accelerometers¹²². Once this mode was identified, they recorded the TOF at different accelerometer distances from the EMAT to report and observed the A0 group velocity at 119 m s^{-1} . The same group later expanded on this work by creating a 2-D finite element model in COMSOL that included 264 layers of

the cell. Their experimental measurements indicated a group velocity of 69 m s^{-1} , which aligns with their previously reported range of 60 m s^{-1} to 170 m s^{-1} ¹¹⁶⁶. Notably, these experiments employed cells with ostensibly the same chemistry and form factor; however, they were conducted at different states of charge (SOC) — specifically, 40 % in Ref.¹⁶⁶ and 100 % in Ref.¹⁷¹. This discrepancy in SOC is significant, as it likely influences the A0 group velocity due to variations in the mechanical properties associated with these states. In addition, for results presented in Ref.¹⁷¹, they had to reduce the model inputs of Young's modulus for both the anode and cathode material by 30 %, to match the experimentally measured A0 group velocity of 69 m s^{-1} with the simulated value of 71 m s^{-1} . Their rationale for this change was attributed to using values of Young's Modulus of a dry stack of electrodes, which is not representative of the case within the batteries. This scenario illustrates the utility of modeling these phenomena for a comprehensive understanding of guided wave motion while concurrently highlighting the importance of being cautious in determining the parameters for these modeling approaches.

At about the same time, Li et al.¹⁷⁰ employed guided waves for ultrasonic testing using a 5-cycle Hanning-windowed sinusoid between 25 kHz to 200 kHz similar to the work of Zhao et al.¹¹⁴. Li et al. used seven features of the received signals for their analysis, including the peak amplitude and centroid of the waveform in time, which are metrics analogous to SA and TOF, respectively. Although their experiments employed stepped-sine excitation from 25 kHz to 200 kHz, it is notable that the transmitted energy between 20 kHz and 70 kHz is very low. Then they reported that the extent to SA variation with SOC depended on excitation frequency, which was not disambiguated from the transducer transmit and receive sensitivity¹⁷⁰. In an attempt to tie observations to battery performance, they built an “adaptive [fully connected neural network] FNN-XGBoost model for battery state estimation” using their seven chosen signal features and found a root mean square error of 2.24 % SOC. They found that the TOFS increased with increasing SOC, opposite to most bulk wave approaches, which may be due to the low frequencies used which are likely to create standing wave fields rather than bulk wave pulses. However, they did not present any reason for this different outcome.

Jie et al. also performed guided wave ultrasonic testing, with measurements on a 2.3 Ah LCO pouch cell using two PZT transducers on the same cell face³⁹ and reported the relationship between SA and TOFS with SOC at C-rates between 0.75C, 1.0C, and 1.25C and at temperatures of 20 °C, 25 °C, and 30 °C. They found that SA increased and TOFS decreased with increasing SOC³⁹. In a similar study, Liu et al.¹⁶⁷ investigated the effects of the charge/discharge rate on ultrasonic guided waves. They found a nearly linear decrease in TOF with increasing SOC at a constant charge/discharge rate. To decouple the influence of temperature and C-rate on TOF variations, they introduced a temperature-compensated

TOF metric, denoted as TOF_T . However, even after temperature compensation, TOF_T remained dependent on the C-rate. To analyze this dependency, they performed a galvanostatic intermittent titration technique (GITT) experiment, evaluating the stationary and dynamic responses of TOF_T with C-rate changes, as shown in Fig. 9.D.1-3. They found that sudden changes in C-rate cause instantaneous TOF_T , and made three key observations: (i) the TOF_T increased more after discharging stopped than it decreased after discharging stopped, indicating that discharging induces more pronounced electrode phase transitions under equivalent C-rates. (ii) After discharging stopped, the TOF_T suffered longer stabilization times compared to after charging stopped. (iii) Higher C-rates induced higher TOF_T changes after charge/discharge stops. They further suggested that electrochemical phenomena at the micro-, meso-, and macroscales contribute to these results (see Fig. 9.D.4).

The state of the literature on using guided wave US for SOH estimation is even less developed than that for guided wave UT for SOC estimation. To the author's knowledge, only experiments by Ladpli et al.¹⁶⁴ and Zhao et al.¹¹⁴ have been conducted to correlate decreasing SOH with guided wave ultrasonic signal characteristics. Ladpli et al. considered accelerated aging by cycling cells 200 times at a 0.8C with the cells at an elevated temperature of 45 °C in a laboratory oven¹⁶⁴. Through this cycling protocol, they achieved a reduction in SOH to 96.5 %. Zhao et al. aged a cell by cycling it 165 times, taking UT measurements every 30 cycles¹¹⁴, leading to a 5 % decrease in SOH. Presently, in electric vehicle or portable device applications (i.e., high power demand), LIBs are removed from service when their SOH reaches 80 %¹⁷⁶. Since both studies only achieved minor reductions in SOH, questions remain about ultrasonic guided wave signal trends with continued aging. Regardless, their results provide the only studies of this type and are therefore summarized below.

Both groups found that the TOFS decreased globally with decreasing SOH^{114,164}, but provide conflicting results regarding the SA trend with SOH. Ladpli et al. found that the SA increased globally with decreasing SOH¹⁶⁴, while Zhao et al. found a decreasing trend¹¹⁴. Zhao et al. found that the effect of SOH on SA was not the same for all SOC. Instead they found that the SA at 100 % SOC experienced a greater decrease with aging than the SA at 0 % SOC¹¹⁴. Notably, a separate study by Li et al. , which only cycled their cell 10 times, observed a decreasing SA at 100 % SOC with each cycle¹⁷⁰. There is much room for continued exploration of the effect of SOH on guided wave and bulk wave ultrasonic signal characteristics. Future work should be conducted on cells as they undergo isolated, individual aging mechanisms such as the aforementioned calendar-aging and cycle-aging. At the present, one can only extrapolate in order to assume the effect of more severe reductions in SOH on ultrasonic signal characteristics. We also stress that while Ladpli et al.¹⁶⁴ and Zhao et al.¹¹⁴ found different trends of SA with SOH, this does not automatically

suggest that their results are in disagreement. Without understanding the exact guided wave mode measured by their experimental apparatus and how the mode might change with reduced SOH, one cannot draw a conclusion regarding which trend is correct. Here, a topic that may arise is the apparent contradiction in some of the reported trends of ultrasonic signals from bulk and guided waves regarding their changes with SOH. In this sense, degradation has been reported to both increase¹³³ and decrease¹⁶⁴ the TOF (for experiments on the same NMC chemistry). Bulk wave experiments suggest a decrease in longitudinal stiffness in the thickness direction, while guided waves suggest an increase in the stiffness that is more related to shear wave propagation. This inconsistency may be due to the evolving behavior of the cell over aging and must be a topic of future research.

4. Guided wave modeling approaches

Guided wave propagation can be modeled using similar approaches as bulk wave propagation, namely matrix methods employing standard equations for Lamb waves^{164,168}, matrix methods employing modified equations considering poroelastic effects^{28,33,39}, finite element approaches^{39,171,177}, or data driven approaches^{170,178,179}.

Wave Physics models: Ladpli et al. created an analytical model that considered the layered structure of the cell and two-dimensional elastodynamic equations of motion of each layer. Those equations were solved using the global matrix method to find the dispersion curve of the cell¹⁶⁴. By using SOC-dependent material properties of electrodes, they used the dispersion curves to calculate the group velocity and then estimate the TOF as a function of SOC. They observed a good agreement between the simulated and measured TOF of the US guided waves. The difference in TOF between 0 % and 100 % measured was about 7 μs while the simulation predicted 11 μs , without aging considerations. Nonetheless, the 0 % SOC conditions showed higher mismatches between the simulation and experiments compared to the 100 % SOC condition. Additionally, the simulation failed to capture some nonlinearities exhibited by the measured TOF.

Jie et al. also employed a global matrix approach, but used Biot's theory of propagation in poroelastic media to model the wave propagation through a multi-layered structure of graphite/copper/graphite. Using this approach, they calculated dispersion curves for this structure and identified the lowest order symmetric and anti-symmetric Lamb modes. They assumed that the current collector had a porosity of 0.01 in order to use Biot's theory for all layers, thereby exactly satisfying boundary conditions between layers of otherwise dissimilar media.³³ The same group later expanded their approach to simulate the dispersion curves through a 19-layer model of a LIB including graphite, copper, LiCoO_2 , aluminum, separator, electrolyte, and outer cell casing³⁹. Using SOC-dependent material properties, those authors were able to extract the group velocity from the simulated dispersion curves as a function of SOC and found that the group velocity increased with SOC, in agreement

with the experimental results of Refs. ^{114,164,168}. Jie et al. additionally created a 2D finite-element simulation of this 19 layer model in COMSOL, solving for the dispersion curve using Biot's theory and found good agreement between this simulation and their global matrix model³⁹. The same research group also showed a preliminary theoretical model of longitudinal guided wave propagation in the axial direction for cylindrical cells showing some calculations for the influence of the SOC and circumferential order on the dispersion curves¹⁸⁰. A more recent study by the same group reported an analytical acoustic model based on state-vector formalism and Legendre polynomial method that also considered the coupling of the electrochemical behavior of the LIBs to the mechanics (see scheme on Fig. 10.A) through the mechanical stress that will be generated on the graphite electrode during charge/discharge, which they named the diffusion-induced stress (DIS)²⁸. That research used COMSOL to simulate the electrodes changes in the mechanical properties during charge/discharge and the distribution of the lithium concentration for different SOC to calculate the DIS and calculate the dispersion curves for different SOC, as shown in Fig. 10.B. This theoretical framework can be further used to analyze the propagation of guided waves in batteries with different SOH by including the simulation of battery degradation.

Koller et al. made use of The Dispersion Calculator, version 1.11.2 by Armin Huber to calculate the dispersion curves up to 15 kHz for a 200 layer model of the cell¹⁶⁶. Their model predicted a group velocity of the A0 mode of 76 m s^{-1} at the frequency of interest of 8 kHz¹⁶⁶, which lies between the experimental A0 mode group velocity of 60 m s^{-1} to 170 m s^{-1} . Siegel et al. later expanded on this work by creating a 2-D finite element model of a 264-layer cell in COMSOL. In order to match experimentally measured group velocity of 69 m s^{-1} they had to reduce the model inputs of Young's modulus for both the anode and cathode material by 30 %, which resulted in a simulated group velocity of 71 m s^{-1} ¹⁷¹. This research group extended their work to simulate the dispersion curves of a cell with SOC-dependent Young's modulus of the anode active material, finding that the group velocity should increase for the A0 Lamb mode with increasing SOC¹⁷⁵.

Most of the work on modeling ultrasonic wave propagation in LIBs has focused on elastic phenomena, leaving out thermoelastic and viscoelastic considerations that can also affect the ultrasonic signals, as has been shown in some of the reported research of this review. One of the only groups to consider thermoelastic effects was Lin et al.^{181,182} who proposed an approach to analyzing the properties of thermoelastic wave propagation in a multi-layered porous electrode. Further, most of the modeling approaches reported in the literature can be described as root-finding methods using a characteristic equation of frequency and wavenumber to find dispersion curves associated with unforced wave propagation. In this regard, approaches like the work of Zhang et al.¹⁸³, which employed spectral methods instead of root-finding techniques, might be interesting to extend to the

LIBs case. Spectral methods use spectral differentiation matrices and orthogonal polynomials to solve differential equations by numerical interpolation and have emerged as an alternative for root-finding techniques in recent years. Zhang et al.¹⁸³ used the spectral approach for the Lamb wave equation for multilayered porous media and demonstrated its application to well-known porous materials. Although they did not apply the method for solving guided wave dispersion curves in LIBs, the spectral methods have the potential for faster computation speed and a more straightforward encoding process compared to root-finding methods. However, their applicability and usability in modeling US waves remain to be proven.

Data-driven models: The number of data-driven approaches to model ultrasonic guided waves is fewer than for bulk waves. However, they are based on similar principles but usually employ different features from the ultrasonic signals for battery state estimation. Liu et al.¹⁷⁸ used an artificial neural network that relies on simple parameters like SA and TOF, demonstrating that these characteristics are related to SOC, yet are vulnerable to environmental noise and the complexity of propagating modes.

In contrast, Li et al. built an “adaptive fully connected neural network(FNN)-XGBoost model for battery state estimation” using seven signal features from a guided wave experiment and found a root mean square error of 2.24 % SOC¹⁷⁰. They found that the TOFS increased with increasing SOC, which is in contrast to the experimental results of Refs. ^{114,164,168}. Similar to this approach, Ji et al.¹⁷⁹ reported a multi-feature fusion technique that integrates both time and frequency domain features ranked using the XGBoost-SHAP (XGBoost - Shapley additive explanations) model. Their Particle Swarm Optimization Gaussian Process Regression (PSO-GPR) model achieved an accuracy of RMSE 3.65 % and demonstrated the robustness of feature selection while mitigating the limitations of single-feature approaches. While the Adversarial Neural Network (ANN) model is simpler and more computationally efficient, it lacks the adaptability and precision of the PSO-GPR approach, which, despite its complexity, provides a more reliable and scalable solution for battery management systems (see scheme in Fig. 10.C).

Another study by Tian et al.¹⁷³ employed a deep learning model named Long Short Term Memory (LSTM) to map ultrasonic features (signal local amplitude and TOF) to SOC with high precision, with TOF decreasing as SOC increased. The study compared various frequencies, finding that higher frequency signals, such as 140 kHz, resulted in significantly lower accuracy (RMSE reaching 10.68 %) and that 60 kHz provided the highest accuracy (lowest RMSE was 3.07 %), making it the optimal detection frequency for the conditions that they explored. This is likely due to the fact that higher frequency waves have shorter wavelengths and thus energy may be distributed in multiple guided wave modes,

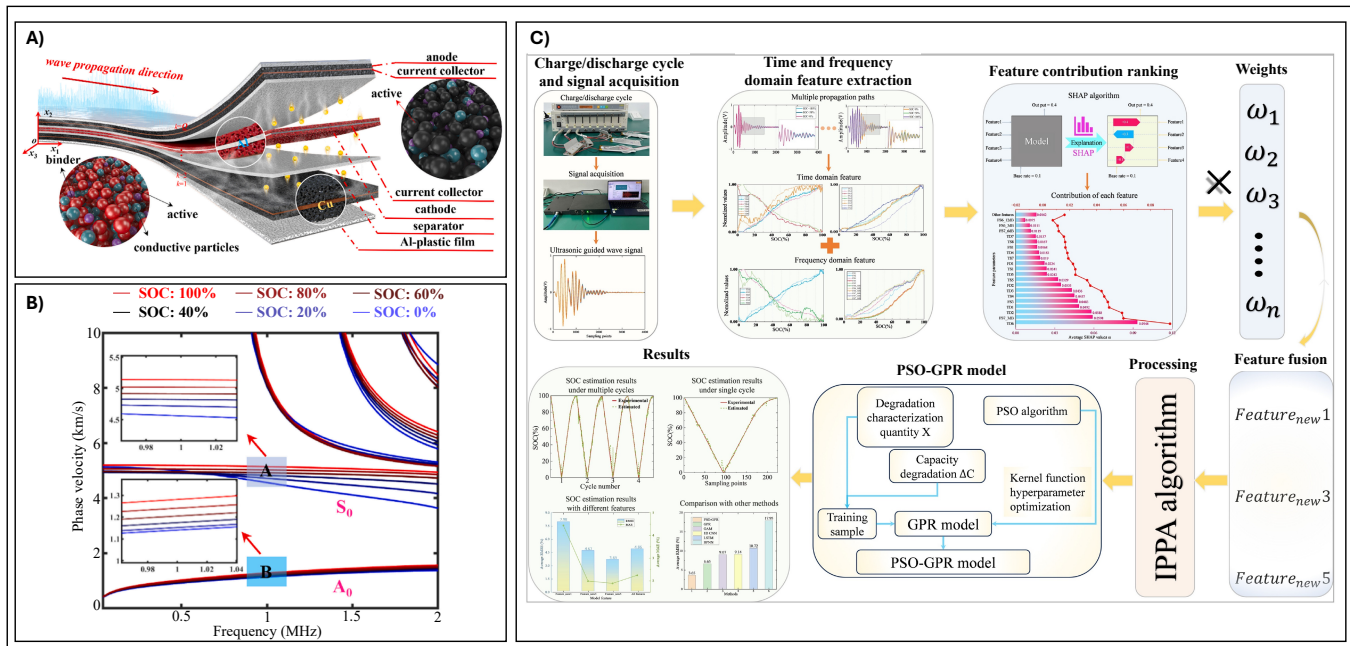


FIG. 10. Guided wave modeling approaches in LIBs. **A)** Geometry used to model guided wave propagation on multilayered LIB, including porous electrode materials. Reproduced with permission from Ref.²⁸ Copyright 2024 Elsevier. **B)** Dispersion curves calculated using simulations at different SOC values of a unit cell of a LIB. Clear changes in phase velocities of the A_0 and S_0 modes as a function of SOC are highlighted in the insets. Reproduced with permission from Ref.²⁸ Copyright 2024 Elsevier. **C)** SOC estimation framework based on PSO-GPR model. Time and frequency domain features from guided waves were used as inputs to the model. Multidimensional features were ranked and weighted with SHAP. The IPPA algorithm merged and developed a new feature sequence to feed the PSO-GPR model, which then estimated the SOC. Reproduced with permission from Ref.¹⁷⁹ Copyright 2025 Elsevier.

whose group velocity and amplitude decay may differ from single-mode propagation.

B. Ultrasonic Techniques for Damage Detection

While most experimental publications employing UT on LIBs have focused on its viability for SOC and SOH estimation, a benefit of ultrasonic inspection is its potential to additionally monitor damage evolution within the cells. Ultrasonic inspection of LIBs has been used to detect gas formation^{86,184}, lithium plating^{80,82,153,185}, overcharge^{104,109,110,136,170}, over-discharge^{32,99,170}, thermal abuse^{26,64,65,81,86,130,140,141,174,186}, and delamination⁹². Since thermal runaway is the most catastrophic and costly failure state of LIBs, damage detection centered on early detection of thermal runaway is the highest priority for the BMS²¹. Since the primary cause of thermal runaway is high-temperature thermal abuse, ultrasonic detection of this damage condition will be discussed first. Overcharge and over-discharge are also common damage conditions which may lead to thermal runaway, so ultrasonic detection of these damage conditions will be discussed next. We conclude this section with a discussion of UT for general defect detection in cells including gas detection.

1. Thermal Abuse and Temperature Effects

Due to the fact that LIB performance degrades at low and elevated temperatures, researchers have conducted many studies on the ability of UT to detect changes in the temperature of cells. Most of the work to date has focused on moderate temperature changes, i.e. temperatures ranging from -10°C to 65°C , though some examples of UT at temperatures leading to thermal runaway have also been reported. Ke et al. heated cells to 39°C in an oven, and found that the TOF increased with temperature while the changes in SA were “small and irregular¹³⁷.” Owen et al. placed cells in a temperature chamber and recorded US data as the cell was heated from -10°C to 60°C finding that TOF increases and SA decreases with increasing temperature within the reported range¹³⁰. Similarly, Popp et al. measured the TOF of guided waves as a cell was thermally cycled from 5°C to 45°C at a rate of $10^{\circ}\text{C h}^{-1}$ ¹⁶⁸ and found a positive cubic relationship between TOF and cell temperature in that range while Chang et al. thermally cycled cells from 0°C to 60°C in a temperature controlled oven and found that the SA decreased rapidly in that temperature range, which they attributed to gas generation⁸¹. Zhang et al. noted that the density and viscosity of a common solvent in electrolyte, dimethyl

carbonate, are affected by increases in the temperature range of 20–50 °C¹⁴⁰. They found that the received waveform arrives earlier in time with increased temperature, which indicates an increase in wave velocity. They attributed this to a decrease in density of the electrolyte with temperature, although in a closed system where the mass is held constant the density can only decrease if the volume increases¹⁴⁰. Fariñas et al. performed non-contact transmission UT on lithium-ion pouch cells using air-coupled transducers and measured the transmission coefficient spectra. Through this, they excited acoustic thickness resonances that could be used to obtain an “acoustic fingerprint” and monitor the shift of these thickness resonances with different SOC and temperatures. They tested cells at 21 °C, 30 °C, 40 °C and 55 °C, and found that the thickness resonance frequencies of the transmitted waves shifted to lower values with increasing temperature¹⁰⁷.

Chang et al. studied the effect of temperature transitions from 0 °C to 60 °C by cycling LCO cells in temperature-controlled incubators⁸¹. Their objective was not only to measure ultrasonic TOFS during temperature cycling, but also to investigate how various charge-discharge profiles at different temperatures would change battery performance. Some of the temperature-cycling profiles resulted in complete failure and extensive gas generation, while others did not. They showed that elevated temperatures (greater than 20 °C) following lithium plating at low temperature (below 10 °C) can induce significant gassing and failure. Acoustic signal attenuation effectively detects gassing, with the rate of drop in SA following an Arrhenius relationship to temperature shifts. Furthermore, the SA decrease was related to the magnitude of the temperature shift, and they attribute the reduction in SA to substantial gassing. During cycling at <60 °C, the TOFS showed a generally decreasing trend with cycle number, while the SA trend varied from cell to cell. For all temperature profiles they reported, the US signal eventually dropped to the noise floor. The larger the temperature changes, the more rapid the reduction of the signal amplitude to the noise floor⁸¹. They also noted that the TOFS tended to increase following the temperature shifts until the signal dropped to the noise floor. The authors hypothesized that the observed changes may result from a combination of lithium plating on the anode surface during the previous low-temperature cycling and enhanced electrolyte decomposition due to the higher temperatures of the following cycling.

Research has been conducted to investigate the effects of high-temperature loading and rapid temperature shifts on damage associated with thermal abuse, which can sometimes lead to failure. Zappen et al. made use of a guided wave transducer configuration by using three transducers: two on the same cell face and one opposing the receiving transducer on the opposite cell face. Although they label the two paths as “In-plane” and “Through-Plane”, both receiving transducers should detect guided waves. They did not specify the exact fre-

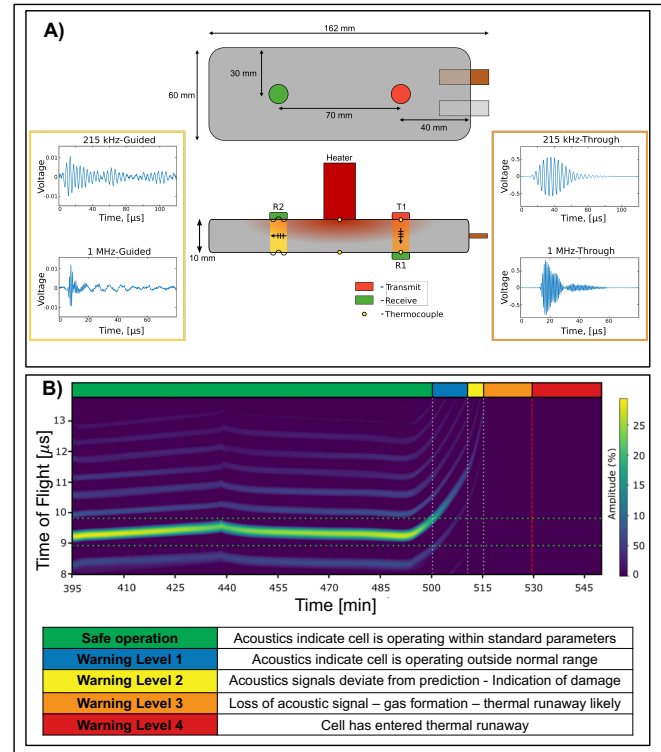


FIG. 11. Examples of UT to detect thermal abuse in LIBs: **A)** schematic illustration of UT performed on a cell exposed to localized thermal abuse, as was performed by McGee et al.^{26,64} **B)** Proposed framework to evaluate the risk of thermal runaway events depending on deviations of the TOF measurements from the expected values. Reproduced with permission from Ref.⁶⁵ Copyright 2024 IOP Publishing.

quency used for the guided wave, which could influence the energy content of the received signals¹⁷⁴. Their work considered the heating of an NMC pouch cell at 100 % SOC from room temperature to 110 °C while continuously acquiring guided wave UT measurements¹⁷⁴. They found that the signal intensity (akin to SA) decreased for both the “In-plane” and the “Through-plane” paths with a sudden decrease at 90 °C, while what they refer to as the “center of gravity” of the signal in the time domain (akin to TOFS) increased slowly with temperature followed by a rapid increase at 90 °C. It is not surprising that they found similar behavior for both observed paths since the transducer placement during these measurements meant that both measured the same guided wave, just at different locations. In a similar study, Pham et al. heated LCO pouch cells charged to 100 % SOC to TR while taking pulse-echo measurements using 2.25 MHz center frequency pulses. They noted that the TOF increased with applied heat and that the ultrasonic signal was lost due to significant gas generation, though they did not report TOF values or temperature explicitly⁸⁶. Furthermore, the authors had mis-attributed each oscillation observed in the received waveform to distinct layers within the cell structure. This is unlikely for wavelengths

of ultrasonic signals at 2.25 MHz ($\approx 670 \mu\text{m}$) which are much larger than typical thicknesses of layers within each cell ($\approx 10 - 100 \mu\text{m}$).

Similar work by Kirchev et al. monitored ultrasonic signals transmitted with a frequency of 150 kHz through model 18650 NMC811 cylindrical cells in an adiabatic Accelerating Rate Calorimeter (ARC) to either 160 °C or TR depending on the cell SOC, and found that the ultrasonic signal strength decreased for all tested SOC with increasing temperature¹⁸⁶. In a related study using ARC techniques but for a pouch cell, Feinauer et al.¹⁸⁷ integrated data from 150 kHz ultrasonic transducers, a strain gauge, a thermocouple, and voltage and resistance measurements to monitor the thermal runaway process with cells heated up to 350 °C. This work found that the transmitted ultrasonic signals can be used as an early detection metric of gas evolution, which leads to cell venting. They also showed that stable exothermic behavior (a key thermal event associated with self-heating during the thermal runaway process) can only be detected by the temperature and the overall disappearance of the ultrasonic signal. Fig. 11.A shows a schematic of the experimental setup of McGee et al. who performed two studies using UT of mechanically-confined NMC532 pouch cells exposed to localized high-temperature thermal abuse using contact ultrasonic transducers that generate 250 kHz guided waves and 1 MHz through-thickness longitudinal waves^{26,64}. When testing for *in situ* detection of thermal abuse, they found that the SA and TOFS of longitudinal bulk waves decreased and increased, respectively. In contrast, the SA increased for guided waves as temperature increased, and both of these indicators could provide an early indicator of failure⁶⁴. The same authors then looked at the ability of UT measurements to detect localized thermal abuse in charge-discharge cycles that follow abuse and found that the SA and TOFS of the longitudinal bulk waves both increased globally in the three charge-discharge cycles following abuse at levels of 100 °C or higher²⁶.

Additional recent work by Owen et al. showed the ability of UT to track averaged internal temperature fluctuations⁶⁵ that can be used to design multi-stage warning systems based on the expected behavior of the TOF of ultrasonic signals during the cell cycling as shown in Fig. 11.B. That work showed how the internal temperature can be estimated knowing the TOFS associated with SOC and temperature changes from previous tests, which can be a better metric compared to temperature measurements made on the surface of the cells, since LIBs are excellent thermal insulators.

2. Overcharge or Over-discharge

While many researchers have broadly demonstrated the ability of UT to detect when a cell is overcharged, it is important to first explain that the term “overcharge” is very general and includes different types of overcharging scenarios. Overcharging can be carried out either through constant-current charging or constant-voltage charging. Constant-current charging delivers a fixed cur-

rent to the terminals of the cell until it reaches a certain cut-off voltage or until the cell exceeds a specified temperature threshold, which, if inadequately defined, may lead to thermal runaway. In contrast, constant-voltage charging maintains the cell voltage at a constant level while applying a gradually decreasing current. For instance, as shown in Fig. 3.A, volume changes in cathode materials can exhibit nonlinear behavior at high SOC approaching overcharge conditions, behavior that may be detected with ultrasonic measurements and motivates further investigation. Additionally, several researchers utilize slight levels of overcharging during testing, both with and without raised temperatures, to hasten aging mechanisms within the cells. Research that employs combined thermo-electrical loading complicates the separation of individual effects on the received ultrasonic signals.

Li et al. conducted an experiment on an LCO pouch cell involving a slight overcharge test to 107% SOC and observed that the received ultrasonic signal using guided waves dropped to the noise floor¹⁷⁰. In a similar work using also LCO pouch cells, Wu et al. repetitively cycled a cell to an overcharge voltage of 4.5 V in a laboratory oven held at a constant 45 °C to accelerate the effects of aging¹⁰⁴. They simultaneously acquired ultrasonic data at 0% SOC for each cycle and found that the TOFS increased with aging from 7.6 μs to 8.4 μs , while the SA decreased with increasing cycle number. Their sample size consisted of two cells, both of which exhibited a decrease in SA as they were subjected to aging caused by overcharging, though the extent of the SA decrease differed between cells¹⁰⁴. They also performed a single overcharge to 5 V on a cell that had previously been cycled 210 times. In this test, they found that the TOFS increased by 0.2 μs when the cell voltage reached 4.5 V, when compared to the TOFS observed at the standard cutoff of 4.2 V. They attributed this increase in TOFS, which is contrary to the normal reduction in TOFS during voltage increases in normal operating ranges, to tiny amounts of gas generation. The TOFS then increased rapidly following cell swelling, at which point the experiment was stopped. Wu et al. noted a steadily decreasing SA as the cell was cycled to normal limits. However, the SA increased dramatically at a voltage of 4.5 V, then decreased, followed by a leveling off before spiking a second time following cell swelling, though the authors did not specify the physical mechanism leading to the increase in SA¹⁰⁴.

Appleberry et al. performed experiments using bulk longitudinal waves across four different combinations of temperature and overcharging. Those authors conducted constant-current (CC) overcharge and constant-voltage (CV) overcharge at 23 °C, and both CC and CV overcharge at 65 °C¹⁰⁹. Separately cells were cycled three times at 18 °C, 20 °C, 22 °C, 34 °C, 40 °C, 45 °C, 50 °C, and 65 °C to understand the temperature effect on US transmission. These authors utilized the root mean square of the time signal (similar to SA), the time of the peak in a Hilbert transform of the time signal (akin

to TOF), and the maximum amplitude derived from a Fast Fourier Transform (FFT) of the time signal, finding that for CC overcharge, the two metrics analogous to SA declined in value as cell voltage increased, while the metric related to TOF remained relatively stable¹⁰⁹.

Shen et al. investigated UT to detect overcharge¹¹⁰. Those authors overcharged pouch cells to 4.8 V and 5.0 V, finding massive reduction in signal energy when overcharged to 5.0 V. These researchers verified through X-ray computed tomography (CT) that at this cell voltage, substantial electrolyte decomposition occurred, which caused the layers to separate¹¹⁰.

Davies et al. performed a “low impedance closed circuit over-discharge event” on a LCO pouch cell that had previously been cycled 106 times to a SOH of >98%⁹⁹. The SA of a bulk wave generated with a 2.25 MHz transducer diminishes quite rapidly as the cell approaches a nearly depleted state, which the authors attribute to the breakdown of the electrolyte and the generation of gas within the cell. In the cycles following this over-discharge event the SA appears to return to normal while the TOFS appears to grow with each cycle⁹⁹. It is also notable to recall that the previously discussed work of McGee et al.²⁶ utilized the rate of change of SA and TOFS in the subsequent cycles following a thermal abuse event as a sign of prior damage in the context of over-charge or over-discharge. Namely, the metric devised in that work might also potentially indicate past over-discharge events.

Kirchev et al. performed longitudinal bulk wave UT on 18650 cylindrical cells as they were overcharged with different constant currents to a voltage exceeding 4.8 V for cells rated to 4.2 V¹³⁶. The cells were fitted with charge interrupting devices (CID) that activated at differing SOC depending on the applied C-rate. They showed that the SA “fluctuates significantly” throughout the overcharging process, complicating the interpretation of results. Furthermore, they carried out constant-voltage overcharging of cells at voltages of 4.6 V, 4.7 V, 4.8 V and 4.9 V and observed variable SA trends for each cell tested, even within normal SOC¹³⁶. To analyze their findings, they employed clustering techniques and mapped the power spectral density of the received waveforms, enabling them to use ultrasound as an early warning signal for overcharging.

3. General Defect Detection including Gas

Defects noticeable by UT can be identified as manufacturing defects (e.g. coating irregularities, contamination, improper electrode assembly) and in-use defects from cycling or abuse conditions (e.g. gas formation, lithium plating, electrolyte depletion, electrode ruffling). While much work for detecting damage within LIBs has focused on detecting thermal abuse or electrical abuse via UT measurements, there is also great need for tools that can identify mechanical defects within LIB cells. Additionally, defects of various sizes can form during normal charge-discharge cycling, or under non-dangerous but still sub-optimal operating conditions¹⁸⁸. The most commonly investigated damage condition for

UT is gas formation^{87,155,189,190}, but other types of ultrasonically detectable damage include metallic particle contaminants within an electrode layer¹⁹¹, lithium plating on the anode surface^{27,82,95,185,190}, electrolyte wetting or dry-out^{87,88,192}, or electrode ruffling where conductive layers may lose contact⁹². Since these types of defects may occur randomly across the planar area of the cells, some groups have designed experiments where they can scan the cell by taking UT measurements across the cell surface^{87,95,101,110,155,190}.

Wang et al. incorporated a layer of lithium metal into their 13-layer COMSOL model to simulate lithium plating, and discovered that for a given frequency, the transmission coefficient through a cell decreases with the presence of lithium plating²⁷. Li and Zhou used air-coupled UT to identify a defect they called “stomata,” which is effectively a gas pocket within a particular layer¹⁵⁵. In order to simulate a near-surface and near-bottom “stomata” they pasted copper “flakes” to the surfaces of the cell. Given the significant impedance mismatch between copper and air, it is unclear if this method of simulating damage is appropriate. Regardless, they found that the amplitude of the transmitted wave was reduced in the presence of a “stomata”¹⁵⁵. In addition, they performed a scan of the entire cell and provided a heat map representation of the transmitted amplitude through the cell.

Bommier et al. used longitudinal bulk UT on LiCoO₂/Graphite pouch cells to detect lithium plating on the graphite anode⁸⁰. They intentionally induced lithium plating by charge cycling cells at low temperatures and elevated C-rates (up to 4C). To determine a baseline TOFS at the end of charge, they used a fixed-capacity charging protocol at a C-rate of C/15, which did not induce lithium plating. They then compared this TOFS endpoint to the TOFS observed at various temperature and C-rate combinations and found that UT indicated lithium plating when the TOFS end point was more positive than baseline at low temperatures and high C-rates⁸⁰.

Bauermann et al. conducted scanning acoustic microscopy (SAM) on coin and pouch cell batteries using immersion transducers with the cell in a tank of distilled water¹⁸⁹. The device they employed was a 500 HD² microscope (PVA TePla Analytical Systems GmbH) and the researchers used two different transducers with resonance frequencies of 15 MHz and 100 MHz in a pulse-echo setup. In order to test the ability of their SAM system to detect defects, they built coin cells with specific defects such as a cut anode or a cracked and poorly processed anode layer. The defects are clearly detectable via SAM compared to a scan of a defect-free coin cell¹⁸⁹. They identified areas of gas inclusions in their scans of a pouch cell, which they verified with a cell tear-down¹⁸⁹. Scanning ultrasonic imaging methods have also been employed in different works by Wasylowski et al.^{82,153,190}. Wasylowski et al.’s first work¹⁹⁰ used scanning US (using a 1 MHz) on cells with different pressure loads to test the effect of pressure on capacity retention. They im-

aged their cells with US and also SEM to confirm lithium plating on the anode as well as gas formation¹⁹⁰. Subsequent research¹⁵³ built on these results by introducing *in-situ* tomography using a higher frequency transducer (25 MHz) and the reflected signal to obtain ultrasound images to achieve depth resolved electrode layer separation, allowing improved analysis of internal structural changes in aging cells. Finally, this research group applied SAM for *in operando* visualization of lithium layer dynamics during fast charging, achieving 75 μm spatial resolution and demonstrating real-time tracking of formation and stripping of lithium plating during cycling⁸² using a focused ultrasonic transducer of 25 MHz at a specific internal layer as shown in the scheme in Fig. 12.A. Key challenges in these studies include accurate deconvolution of overlapping wave reflections, signal attenuation in deeper layers, and optimization of transducer design for improved penetration and resolution. The use of ultrasonic tomography represents a promising technology to gain depth resolution in property and damage maps of LIBs, which potentially will give more insights in terms of defect location and shape¹⁹¹. For example, quality assurance in manufacturing could benefit from further research using this technique. Although it is more accessible and cost-effective than its other techniques like X-ray CT, ultrasound tomography still must overcome resolution challenges due to LIBs' thin-layered structure and their ultrasonic attenuation.

Similar work by Deng et al. employed ultrasonic scanning on NMC532/graphite and NMC622/graphite pouch cells using immersion focused transducers (2 MHz frequency, 30 mm focal length) and a cell situated in a silicone oil bath⁸⁷. They generated scans based on the peak-to-peak voltage of the received signals. The researchers created custom pouch cells without any electrolyte, discovering that a significantly lower amplitude signal is detected in these dry cells. They successfully tracked the electrolyte wetting process over time by analyzing the amplitude of a transmitted acoustic wave. Utilizing the same method, they monitored gas evolution within the cells by identifying regions with low transmission. In a subsequent experiment, cells were cycled 2,500 times at 55 °C to either 4.1 V and 4.2 V or 4.3 V. They observed a phenomenon they termed "un-wetting," where the electrolyte no longer fully wetted the electrodes. To ensure that this was not misidentified as gas formation, they degassed the cells for verification. The same research group later applied ultrasonic mapping, using the same ultrasonic settings, to investigate two scenarios: (1) to track electrolyte distribution in 4.20 V NMC811 cells cycled at 40 °C for one year⁸⁸ and (2) how ultrasonic transmission mapping provides insights into electrolyte depletion caused by increased lithium porosity over cycling¹⁹². The objective of the first study was to determine whether electrolyte uptake and jelly roll "unwetting" had occurred. They found that electrolyte depletion was not a significant issue under these aging conditions for that specific cell, as shown in Fig. 12.B. The second study investigated anode-free NMC532 cells, which clearly showed

electrolyte depletion via reduced ultrasonic transmission, as can be seen in Fig. 12.C.

Robinson et al. performed ultrasonic scanning on both custom-built NMC622 pouch cells and purchased LCO pouch cells. For the custom-built cells, they used a 10 MHz, 1D linear phased array probe in reflection mode to identify added defects such as the removal of one half of a complete electrode layer. They confirmed the presence of these defects through the variation of some peaks in the reflected signal and with X-ray CT⁹⁸. They also performed measurements with a Panametrics pulser-receiver on the commercial cells both pulse-echo (1 MHz) and through-transmission (1 MHz transmit, 5 MHz transducer as the receiver) configurations. The authors claim to have identified a defect in a commercial cell using both UT and X-ray CT that reduced the transmitted ultrasound SA to near zero. However, the defect they claimed to have observed is on the order of microns and, based on diffraction-based resolution limits, it is unlikely that such a small defect would completely block the transmission of an unfocused ultrasonic wave through a transducer with a diameter of 12.7 mm. Although, the defect was small, they suggested that associated changes, such as small gas generation on the surroundings of the defect may explain the significant drop in the SA of the transmitted signal⁹⁸. Other researchers have also explored the use of phased array probes to image in cells. For example, Xu et al.¹⁸⁴ used ultrasonic phased array imaging to non-invasively track the appearance and evolution of gases in lithium-ion batteries using total focusing methods as the beamforming process to obtain ultrasonic images.

C. UT inspection during the LIB life-cycle

UT techniques are gaining increasing attention for use throughout the LIB life cycle, beyond their more explored use in condition and damage detection. This includes its use for electrode fabrication and interface engineering, battery performance enhancement, second-life battery screening, and charging protocol optimization. Overall, ultrasound-based methods offer the ability to monitor and the potential to actively influence battery performance and degradation mechanisms. This section summarizes the various applications of UT to battery manufacturing/conditioning, second-life batteries, recycling, and other applications in the battery life cycle.

1. UT for battery manufacturing and conditioning

Ultrasonic techniques offer valuable capabilities to monitor different processes within the battery manufacturing stage. Various studies have explored the integration of ultrasound in processes such as electrode manufacturing^{193–196} and electrolyte-filling monitoring^{87,88}, which is a critical step to achieve high performance in LIBs^{197,198}. The same techniques discussed in Section III B 3 for defect detection can be adapted to study electrolyte wetting during the filling process. McGovern et al. highlight many such needs during the manufacturing of LIBs where UT could pro-

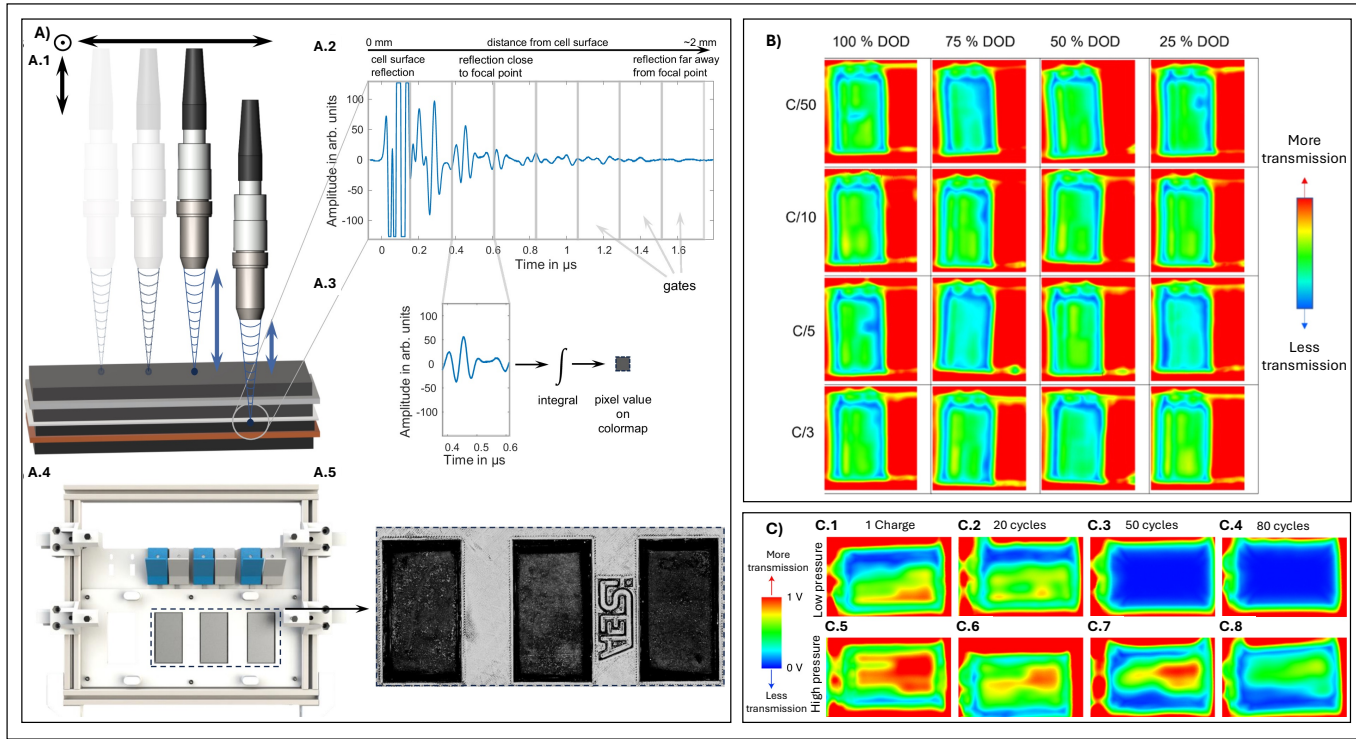


FIG. 12. Ultrasonic imaging as a tool for LIBs inspection. **A)** Example of a workflow and signal processing scheme to obtain images from mechanical scans of a focused ultrasonic transducer. Reproduced with permission from Ref.⁸² Copyright 2024 Springer Nature, under the terms of the CC BY license [<https://creativecommons.org/licenses/by/4.0/>]. Ultrasonic mapping in transmission mode for: **B)** NMC811 pouch cells at different C-rates and discharge depth conditions (reproduced with permission from Ref.⁸⁸ Copyright 2022 IOP Publishing, under the terms of the CC BY license [<https://creativecommons.org/licenses/by/4.0/>]), and **C)** NMC532 pouch cells at different pressures and cycles (reproduced with permission from Ref.¹⁹² Copyright 2020 Springer Nature, under the terms of the CC BY license [<https://creativecommons.org/licenses/by/4.0/>]).

vide insight into the adhesion, porosity, and thickness of electrode coatings on the current collector films⁶¹. For instance, an in situ ultrasound acoustic technique for measuring lithium-ion battery electrode drying dynamics was developed by Zhang et al.¹⁹³. They continuously monitored the drying process, and revealed correlations between acoustic signal attenuation and the three-stage drying mechanism, linking binder distribution and solvent removal to electrochemical performance (as illustrated in Fig. 13.C). The study demonstrated the technique's sensitivity to drying temperature, showing that lower temperatures promote more homogeneous binder distribution and improved electrochemical properties. As a continuation of research, they showed in another study¹⁹⁴ measurements of electrodes with varying coating thicknesses (200, 250, 300, and 350 μm). Analysis of TOF signal shifts revealed three distinct drying stages: an initial stage with significant TOF decrease due to solvent evaporation, a second stage with milder changes, and a final stable stage. This TOF evolution, validated by concurrent gravimetric analysis, demonstrated the technique's potential for real-time process optimization by dynamically adjusting drying rates based on acoustic feedback.

Building on these capabilities, Guk et al.^{195,196} investigated the role of ultrasonic testing in battery manufacturing. They were focused on the impact of calendering parameters on the microstructure of graphite anodes and NMC cathodes, demonstrating that ultrasonic testing could provide real-time insights of the electrode uniformity. The study proposed the potential integration of ultrasound as an in-line quality control method for battery production. For instance, Liminal¹⁹⁹ and Titan AES²⁰⁰ are some examples of industrial efforts to develop commercial ultrasonic inspection facilities for battery manufacturing.

As the final process within the manufacturing stage, LIBs will go through a very critical step of formation cycles, which occur at very low C-rates, where ultrasonic measurements can monitor the gas generated during interface formation of the initial SEI layer of the cells^{125,201}. The ability to monitor the formation process is critical, because it can take as long as three weeks and is estimated to account for 48 % of the battery's total manufacturing cost²².

2. UT for second-life batteries

As described in Secs. III A and III B, UT can be applied to monitor the change of mechanical properties of materials, the growth of gas pockets, and other forms of mechanical degradation like delamination of electrolyte layers. The increasing development of the EV market is generating a significant amount of retired LIBs. While these batteries may no longer meet the power demand of EVs, they normally have enough remaining capacity and functionality to be used in second-life applications that have less demanding usage requirements²⁰². However, in order to evaluate cells for reuse in second-life applications, LIBs retired from high-power applications will need to be graded in terms of electrochemical performance and safety. This evaluation requires efficient and accurate methods for assessing their remaining state of health¹⁷⁶. Ultrasonic inspection techniques are emerging as a promising non-destructive approach for this purpose, offering speed and cost-effectiveness when compared to traditional methods²⁴. In addition, features such as gas pockets and delamination inside cells, which are not easily detected via electrochemical evaluation, may be identified using ultrasonic techniques. These features are key indicators of the potential hazards associated with localized high current densities that could cause local heating and risk of thermal runaway. Since these high-risk features may more easily be captured via UT, the use of ultrasound holds the potential to be cost-effectively scaled to meet the anticipated high throughput of end-of-life assessment of cells in the future.

A few studies have explored the correlation between UT and specific degradation mechanisms in LIBs. This includes the work of Williams et al.¹⁴⁸ who found a strong correlation between SOH reduction, which is attributed to loss of lithium inventory (LLI), and TOFS in ultrasonic signal responses. They observed consistent shifts in TOF, although the degradation rate was not perfectly linear, with fluctuations across charge cycles. Sun et al.¹¹⁶ developed an acoustic framework to diagnose nonlinear aging characteristics under high-rate discharge conditions, proposing an *S*-value metric (defined in terms of the rise time and maximum amplitude of the envelope for a certain wave packet over the frequency of acoustic activity) that represents energy dissipation as the acoustic wave propagates. They argued that this could be a more robust metric compared to conventional TOF and SA metrics and identified cathode material collapse as a dominant factor for capacity fade under these high C-rate discharging conditions. Xie et al.¹⁴⁶ used ultrasonic diagnostics along with spatially-resolved deformation detection, to investigate the effects of lithium plating on inhomogeneous degradation in large-format batteries. They identified lithium plating as a primary mechanism for accelerated degradation, leading to inhomogeneous reactions and reduced performance.

Montoya-Bedoya et al.²⁰³ used an ultrasound array to assess the influence of SOC and SOH on TOF and speed of sound in retired 18650 NMC cylindrical batteries. While clear correlations were not established in

their preliminary study, they observed trends between ultrasound wave properties and the battery state. This work emphasizes the need for further research to improve measurement protocols and refine the understanding of the relationship between US signals and battery health in cylindrical cells. The study also notes the inherent complexity of ultrasound responses in second-life batteries due to the co-existence of multiple degradation mechanisms. Fordham et al.²⁵ employed a combination of NDE techniques — infrared thermography, ultrasonic imaging, X-ray CT, and synchrotron X-ray diffraction — to analyze the aging of large-format pouch cells (with an LMO/NCA cathode blend and graphite anode) retired from an automotive application. They performed experiments on batteries vertically (“rotated”) and horizontally (“flat”) oriented within the EV’s battery pack. Using a TOF window between 26 μ s and 38 μ s, they extracted the maximum SA and derived a percentage metric from the cell area exposed to high attenuation. They showed that “rotated” cells exhibited a higher area of high acoustic attenuation compared to “flat” cells, associated with higher degradation, highlighting the importance of cell orientation and location within a battery pack. This multi-modal approach is likely to yield improved understanding in future work and shows complementary insights into cell degradation, demonstrating the power of integrating different NDE methods.

Another recent study employed a 64-element ultrasonic array to obtain spectral-based quantitative parameters, including mid-band fit (MBf), spectral slope, and intercept, from circumferential waves propagating around cylindrical batteries²⁰⁴. That work demonstrated that the MBf parameter is highly sensitive to both SOC and SOH, and that it could be used to effectively classifying second-life batteries using this frequency-based ultrasonic parameter, even without knowledge of the prior usage history, thereby working to address one of the main challenges exposed by Zhu et al.²⁴ for the use of acoustic monitoring to assess the SOH of used batteries. Notably, their method relied on measurements on pristine batteries of the same chemistry and manufacturer, which are not always available, to compare with the second-life batteries. However, it showcases a possible path to address this limitation.

One critical aspect of UT as currently employed is that they have been shown to be effective in a relative sense, by comparing observables from the same cell over time, rather than in an absolute sense, where one could infer the state or damage condition of a LIB based on measurements in arbitrary conditions and past loading history. However, in the case of second-life applications and recycling, batteries must be evaluated as a “black-box” without monitoring history for comparison. It is therefore of high importance to determine reliable ultrasonic signal signatures that are indicators of LIB state and damage type in the absence of previous history for UT to be a valuable tool for recycling applications and evaluation for second-life use.

The ability to integrate ultrasonic inspection into a comprehensive assessment procedure further enhances its value in optimizing the end-of-life decision-making process for retired cells from EV application²⁴. Further research is needed to address existing limitations and fully extract the potential of ultrasonic inspection in promoting a sustainable circular economy for battery technology. The integration of advanced data analysis techniques and multi-modal NDE approaches will be crucial for achieving more accurate and reliable SOH estimations, facilitating the wider adoption of second-life battery applications²⁰⁵.

3. UT for recycling

Presently, 80% of retired Li-ion batteries have been sent to landfills due to a lack of effective ways to reuse or recycle them²⁰⁶. The increasing volume of toxic heavy metals (e.g., cobalt, nickel, manganese, among others) and flammable electrolytes coming from spent LIBs poses a significant environmental issue^{207,208}. Inappropriate final disposal by land filling or incineration results in soil and water contamination, air pollution, and greenhouse gas emissions²⁰⁹. In addition, the scarcity of critical materials such as cobalt and lithium²¹⁰ highlights the economic need of efficient recycling to ensure resource independence and minimize dependence on potentially unstable geopolitical sources²¹¹. Current battery recycling technologies, while evolving, often involve energy-intensive processes and may not achieve complete material recovery^{211,212}, prompting the search for innovative and sustainable solutions. Here, a distinction must be made between ultrasonication, which has been used for recycling processes for a significant amount of time as a high-intensity source of energy (c.f. Refs. ^{213–215}), and ultrasonic inspection, which is low power and does not damage cells and therefore offers a promising way to improve the inspection efficiency and safety associated with battery recycling processes. In the context of battery recycling, these capabilities translate into the potential to assess battery SOH, detect internal damage, and monitor the efficacy of recycling processes.

For instance, in the recycling sector, UT methods can play a crucial role in the assessment of the state of spent LIBs before processing, helping to prevent thermal runaway incidents. The work of Wu et al.²¹⁶ demonstrates the importance of discharging spent LIBs to a safe voltage (< 1.5 V) before disassembly to mitigate thermal runaway risks. This pre-processing step is critical, as incompletely discharged cells retain significant energy that can lead to explosions or fires during handling and processing. UT can rapidly assess the SOC and voltage of individual cells, enabling efficient sorting and prioritizing for discharge. Furthermore, UT methods can detect internal defects such as cracks, delamination, or swelling, providing valuable information for optimizing the recycling process and ensuring safe handling. In addition, though outside the scope of this review and not covered here, some studies have explored the use of ultrasonic

assisted methods to enhance recycling processes. The reader can find more information in these articles^{217–222}.

While the explicit application of ultrasonic inspection in monitoring battery recycling is not widely documented, the underlying principles and capabilities of ultrasonic techniques strongly suggest their potential utility. The existing literature reveals a clear trend towards the development of advanced NDE methods for LIB characterization, and ultrasonic inspection offers several advantages that could be leveraged in this context. For instance, the work by Bauermann et al. demonstrates the successful application of SAM to visualize internal defects in coin and pouch-type battery cells. SAM, a high-resolution ultrasonic imaging technique, revealed defects such as electrolyte leakage, faulty electrodes, and gas accumulation with high accuracy¹⁸⁹. This capability is directly relevant to battery recycling, as it could enable the rapid and non-destructive sorting of spent batteries based on their condition. Batteries with minor defects might be candidates for second-life applications²²³, while those with significant damage would require different processing strategies²¹¹. Moreover, the ability of ultrasonic techniques to detect internal damage is crucial for enhancing the safety of battery dismantling and pre-treatment processes¹⁸⁹, minimizing the risk of thermal runaway or other hazards²²⁴.

The potential for integrating ultrasonic inspection into various stages of the battery recycling process warrants further investigation. For example, ultrasonic sensors could be incorporated into automated disassembly lines to guide the separation of various battery components²²⁵. Real-time monitoring of the recycling process using ultrasonic techniques could allow process optimization and increase material recovery rates^{211,212}. The ability to monitor material degradation during pyrometallurgical or hydro-metallurgical treatments²¹² could provide valuable feedback for process control and efficiency improvements. In addition, ultrasonic inspection could play a role in quality control of recovered materials to ensure that recycled components meet the required specifications for reuse or re-manufacturing²¹¹. Future research should focus on optimizing process parameters, such as ultrasonic frequency and treatment duration, to maximize efficiency and further explore its integration with emerging green recycling technologies.

4. Other uses of UT in the life-cycle of LIBs

The use of ultrasonic inspection techniques has expanded beyond conventional battery characterization and defect detection, finding innovative applications throughout the lithium-ion battery life-cycle and performance enhancement^{226–230}, demonstrating the versatility of this non-destructive technology.

Some authors have explored the use of ultrasound for battery interface engineering. Jie et al.²³¹ explored the role of ultrasound in modifying the SEI layer of lithium-ion batteries. They exposed coin cells to an ultrasound frequency of 40 kHz through a bath sonicator over the different electrochemical characterizations. They discov-

ered that ultrasound-assisted treatment led to the formation of an inorganic-rich, thinner SEI layer, which enhanced charge transfer kinetics and improved cycling stability (as seen in Fig. 13.A). This study highlights ultrasound's potential for fine-tuning battery interfaces to optimize electrochemical performance. Another work in this area comes from Shpigel et al.²³², who developed an *in situ* acoustic diagnostic technique to monitor particle-binder interactions in battery electrodes. In their study, an electrochemical quartz crystal microbalance with dissipation monitoring (crystal oscillating in the MHz-range frequency) was introduced to assess binder degradation and electrode stability. This method provides valuable insights into electrode integrity, aiding in the development of more durable battery materials.

On the side of battery operation, Li et al.²²⁸ integrated ultrasound with a model predictive control (MPC) approach, and they were able to optimize battery charging protocols, preventing lithium plating and enhancing battery safety. Their research showed that ultrasound can help identify early-stage lithium deposition, a major cause of capacity loss and battery failure. An electrochemistry physics-based model was used to exploit the relationship between having a negative electrode potential of less than 0 V and the generation of lithium plating. Thus, maintaining the negative electrode potential above 0 V was the target for designing a model predictive control strategy for optimal charging. They used an ultrasonic array of 64 elements with a center frequency of 1 MHz to detect gas generated inside the battery, which the authors assumed to be associated with the lithium plating critical point. The voltage at which this critical point occurs for different temperatures was used for the model calibration. Another approach to improving the performance of rapid battery charging was reported by Im et al.²³⁰, where they transmitted ultrasonic waves while charging the cells using a custom-designed multi-stage constant current protocol. This work built on their previous work²²⁹ where they demonstrated that ultrasound waves of 35 kHz can reduce internal impedance by up to 16.9 % at room temperature and increase the usable capacity by 53.4 % at low temperature. Verified by complementary techniques, they showed an increased porosity in the SEI layer due to cavitation-induced disruptions, which facilitates the lithium-ion transport. These works demonstrate that ultrasound is not limited to passive monitoring; it can actively influence battery operation. In this sense, Huang et al.²²⁶ explored using surface acoustic waves (SAW) devices to enable rapid charging in lithium metal batteries. Their study demonstrated that a SAW device, operating at 100 MHz, generates intense localized accelerations, inducing acoustic streaming—a form of electrolyte flow—within the battery's interelectrode gap. This electrolyte flow suppressed dendrite formation and facilitated uniform lithium deposition, allowing for significantly higher charging rates. As a continuation of this work, a more recent study²²⁷ explored the use of a 40 MHz SAW device as a tool to address intrinsic limitations in fast-charging LIBs with NMC532

chemistry, implemented as depicted in Fig. 13.B. This enhanced electrolyte flow significantly improves lithium-ion transport, mitigating the formation of concentration gradients that are detrimental during fast charging. For instance, compared to batteries without SAW integration, the energy density doubled at a 6C charge rate and the batteries maintained at least 72 % of their initial capacity after 2000 cycles. However, further research is needed to fully elucidate the underlying mechanisms and optimize the SAW device design and integration for various battery configurations. Other more recent study²³³ has also explored the use of non-ultrasonic acoustic frequencies (between 6 – 11 kHz) to enhance the performance of lithium metal batteries through stabilizing the SEI layer.

From material synthesis to performance optimization and manufacturing quality control, ultrasound promises advantages as a versatile and powerful tool in lithium-ion battery technology. The studies discussed here illustrate how ultrasound can be used both passively in diagnostics and monitoring, and actively for material processing and electrochemical performance enhancement.

IV. CAPABILITY GAP ANALYSIS FOR UT METHODS IN LIBS

A. Cell-dependent ultrasonic response classification

Ultrasonic wave propagation can differ for different LIB form factors due to evolving mechanical properties as discussed in Sec. II. The presence of soft casings (i.e. pouch cells) versus rigid casings (i.e., prismatic or cylindrical cells) affects wave behavior. In addition, different cell geometries could support distinct types of ultrasonic wave propagation. In this regard, while much of the research has focused on pouch cells, expanding studies to prismatic^{40,160,234} and cylindrical^{66,105,204,235,236} cells is crucial for a comprehensive understanding of how ultrasonic response varies with different cell geometries and internal designs and how this information can be exploited to enable US testing.

Additionally, to realize the full potential of UT of LIBs, the specific relationship between the internal states of cells and their ultrasonic response should be fully categorized. In theory, this would amount to testing under very specific conditions at very well-defined internal states and using well-understood methods of wave propagation. In practice, this is much more difficult. For example, Chang et al. demonstrated that fast changes in cell temperature can induce gas formation⁸¹, which means researchers attempting to isolate thermal effects need to be careful in their experimental design. While isolating specific internal states may be difficult if not impossible, the impact of UT experiments can be amplified if authors report as much information as possible on experimental details such as the cell condition including ambient temperature, extent of calendar aging or cycle aging, exact specifications and compositions of cell components, and explicit statements regarding the type of wave propagation used.

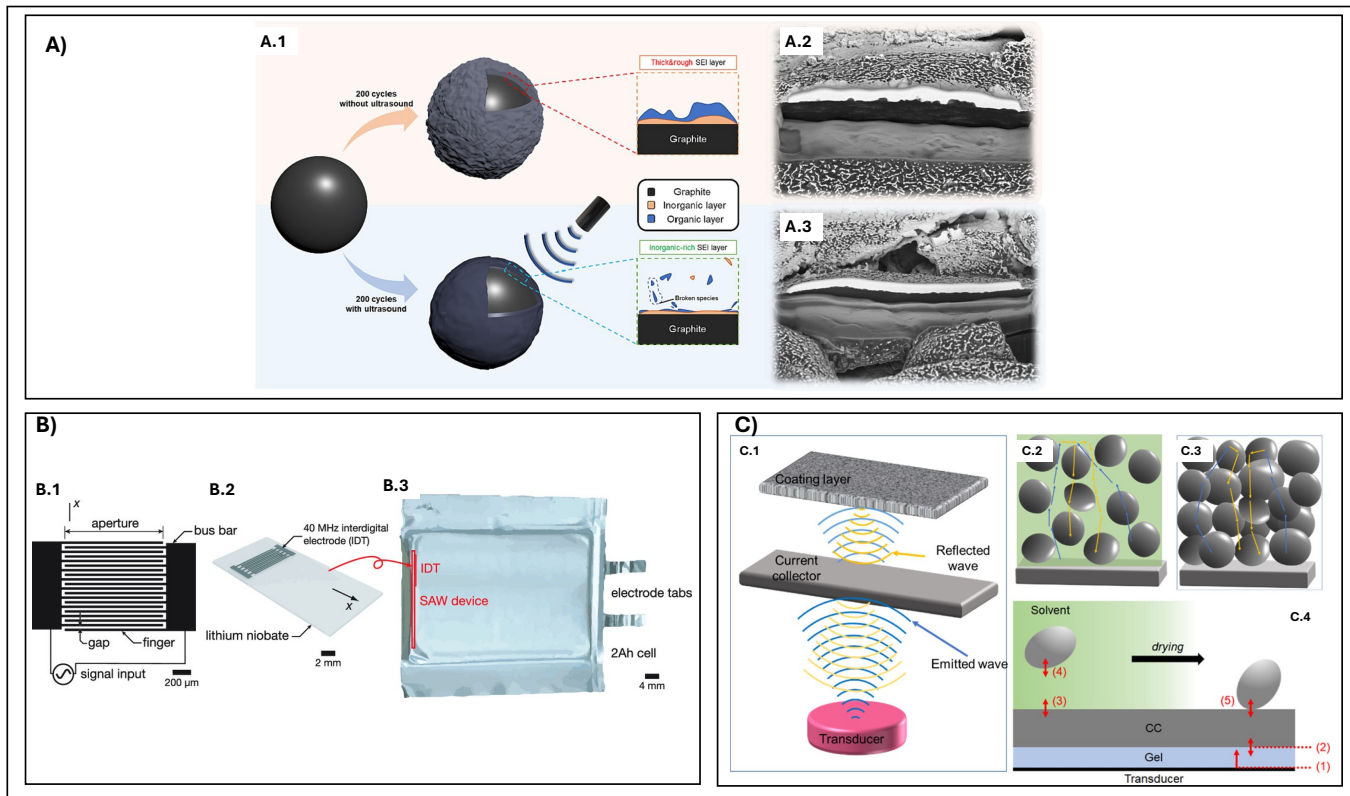


FIG. 13. Non-conventional uses of ultrasonic testing for LIBs. **A)** Influence of high intensity ultrasound exposure during cycling: A.1) Illustrations of the graphite surface with (top) and without UT (bottom) exposure after 200 cycles, and FIB-SEM images of the anode with (A.2) and without (A.3) UT exposure. Reproduced with permission from Ref.²³¹ Copyright 2023 Elsevier. **B)** Integration of a surface acoustic wave device into a pouch cell to enable fast charging through ion transport. Reproduced with permission from Ref.²²⁷ Copyright 2022 Wiley. **C)** Illustration of UT wave reflection in electrode coatings, exemplifying wave paths through wet (solvent-filled) and dried (solid) electrode. Reprinted (adapted) with permission from Ref.¹⁹³ Copyright 2021 American Chemical Society.

Given these challenges, a comprehensive approach - refining the experimental design, standardizing reporting, and applying advanced analysis - is crucial for wider use of UT of LIBs. Here, the use of machine learning techniques trained on well-characterized ultrasonic data could provide insights by identifying patterns and correlations between specific degradation mechanisms and ultrasonic signals¹⁶². Additionally, researchers should validate their hypotheses of internal cell states with advanced imaging techniques such as XRD or SEM, as was shown in Refs.^{82,190}. With better reporting on cell condition, cell composition, and wave propagation researchers should be able to better understand the lack of complete agreement surrounding ultrasonic signal characteristics and various cell states.

B. Model improvement with better parameterization of material properties

Obtaining accurate measurements of the mechanical properties of cell components is challenging for a number of reasons. The material properties of cell components are

dependent on temperature^{237–239}, pressure²⁴⁰, presence and type of electrolyte environment^{237,241,242}, degree of lithiation^{55,58,243,244}, electrodes chemistry⁵⁹, and orientation relative to manufacturing direction^{237,242,245}. These effects are further complicated by spatial variability along the plane of each component, meaning that individual measurements may not provide a complete picture of the material properties of each constituent. Because material properties of components are affected by the presence of the electrolyte environment²⁴⁶ and many cell components may react in an air environment²⁴⁷, measurements need to either be taken *in situ* or in an inert environment. Future modeling efforts will benefit from multi-scale material characterization approaches, where both macro and microscale effects are mechanically considered. As interest in this research field grows, accurate measurements of cell component material properties will also become more important. As component material properties become more fully documented, cell models will become more reliable. Additionally, understanding the microstructural variability of internal battery materials, which currently leads to a significant number of free variables that are es-

timated or approximated, should contribute to reducing the number of unknown parameters and, therefore, improve the quality and reliability of wave physics models.

To improve the reliability of these ultrasonic wave propagation models, open-access databases containing experimentally-validated material property datasets for different operating conditions should be developed. These open-access resources would aid in the improvement of the accuracy of comparisons across different research works, thereby advancing the research of the entire community. Another key aspect is the dynamic nature of all material properties in LIBs, which evolve due to aging, mechanical stress, and continuous electrochemical cycling. Thus, future studies should aim to integrate these changes into modeling frameworks to improve their effectiveness in evaluating battery performance and degradation.

C. Solving engineering challenges associated with adopting UT in field applications

For ultrasonic testing to pass the barrier from the research stage to real-world applications, several engineering challenges must be addressed. So far, most work involving UT of LIBs has focused on single cells. For this NDE methodology to be practical, it must be demonstrated in systems containing higher numbers of cells. Experiments should be expanded to test the practicality of UT of modules of cells or even full packs if possible. As the community evaluates the potential challenges, there will be two main scenarios for the usage of UT: (i) cases where batteries can be extracted from the application to do an ultrasonic measurement. An example of this scenario is for rapid screening of batteries for second-life applications using UT or manufacturing monitoring, where virtually every individual cell can be tested due to the speed and ease of use of UT. (ii) The second case is for continuous monitoring of battery performance. Depending on the scale of the application and with the current state of the technology, ultrasonic sensors will need to be located at each individual cell. Placing the transducer at each cell raises questions about economic feasibility and technical considerations, such as the size and specific location of the transducers. For small-scale form factors, such as cylindrical cells or small pouch cells, challenges might arise regarding miniaturization of current transducer sizes used at the lab scale (characteristic size of 10–25 mm). On the other hand, large pouch or prismatic format factors might benefit from ultrasonic guided wave approaches, since these waves can cover a larger surface area of the cells. In addition, integrating ultrasonic monitoring into commercial BMS requires robust, cost-effective transducer designs and real-time ultrasonic data processing capabilities.

For instance, validating UT for EVs requires testing under real driving conditions that emulate load profiles, such as those being explored by some research^{130,168,204}. By testing under these conditions, researchers will gain important insights into the behavior of ultrasonic signals

under real driving conditions. In addition, practical implementation will also depend on robust coupling methods for long-term operation since the most obvious approach, direct-contact or embedded piezoelectric transducers, require consistent adhesion over their lifetime.

Another engineering choice will be whether one employs single-element transducers or transducer arrays for different applications and desired outcomes. Single-element transducers remain simple and affordable, yet arrays can deliver beam steering capabilities along with dynamic focusing and better spatial accuracy. Assessing these approaches through comparative studies will be necessary to optimize their use in large-scale LIB systems.

Additionally, groups should demonstrate the ability of ultrasonic inspection systems to be miniaturized and for the decision devices to be produced on a circuit board or chip-level, as was explored in Refs. ^{168,175}. These research efforts will represent a critical step towards the commercialization of ultrasound-based solutions, through reducing cost and power requirements, facilitating the integration into the LIBs value chain.

As noted by Galiounas et al. ¹⁴⁹, ultrasonic inspection has been shown to be a tool for identifying battery states within known cells, but it has not been demonstrated to generalize across a wider cell population. Further development is required to create ultrasonic features that work across all cell populations and maintain accurate correlation with battery state indicators (SOC/SOH) for different cells. The capability of ultrasonic-based techniques to transition from academic research into industrial applications relies heavily on their adaptability to various cell types.

D. Application of UT to next-generation cells and electrochemical systems

Ultrasonic inspection provides insights into electrode morphology, interfacial stability, and tracking battery state over operation at different conditions. One direction for future work on UT of electrochemical systems is to expand the work to the so-called next-generation cells, including fully solid-state cells^{126,127,248,249}, cells incorporating lithium metal anodes^{95,125,127,249}, silicon anodes^{76,126}, other novel nanoengineered electrodes¹⁷², redox flow batteries^{250,251}, sulfur electrodes testing for lithium-sulfur technology²⁵², sodium-ion batteries²⁵³, and lithium-ion capacitors²⁵⁴. UT is a promising method for state detection for these next-generation cells for many reasons. For example, silicon anodes experience a volume increase of 300 % when fully lithiated, which should result in an obvious change in the received ultrasonic signals. For instance, Sun et al. used ultrasound to investigate the chemo-mechanical dynamics of silicon anodes in solid-state batteries, showing how metastable Li_xSi phases lead to significant and irreversible porosity changes during cycling¹²⁶.

In addition, the recent work by Chang et al. ¹²⁵ explored the use of acoustic transmission measurements

to track the effective stiffness of anode-free cells, which are cells that are produced without an anode, but a lithium metal anode is formed after the first time it is charged²⁵⁵. The study found that a faster formation rate (C/3) yielded comparable cycling performance and cell stiffness changes to a slower rate (C/10), suggesting that the traditionally slower formation processes may be unnecessary for anode-free cells. This contrasts with previous studies using *in situ* volume and pressure measurements that found only linear relationships with SOC, highlighting the superior sensitivity of ultrasonic inspection to detect subtle, nonlinear changes associated with complex internal processes. Related to this work, Webster et al.²⁵⁶ explored local ultrasound resonance spectroscopy on lithium metal cells. They tracked the performance with this technique during aging for 0.1C, 0.2C, and 0.5C and observed shifts to lower resonance frequencies as the battery ages with an inhomogeneous shift for different regions of the battery. These resonances are detected through tracking a minimum in the reflected spectrum associated with through-thickness resonances of the LIBs. They demonstrated the potential to quantitatively track shifts in the acoustic resonances of batteries and assess changes in average bulk properties due to aging and reported resonance maps obtained by scanning the samples. Future research should focus on the complex task of mapping the shift in resonance location to quantitative values of effective elastic moduli. Ultrasonic resonance spectroscopy is a well-known technique in UT, which has been used to compute all components of the elastic modulus tensor in other applications²⁵⁷. These techniques have strong potential to provide additional information on changes in LIBs.

Beyond LIBs, Sun et al. applied operando acoustic transmission to sulfur electrodes in lithium-sulfur batteries and found that wave damping correlates with sulfur phase transitions, enabling real-time detection of structural evolution and demonstrated how ultrasonic wave damping is highly sensitive to solid-liquid-solid transformations in sulfur cathodes²⁵². Another work by Laufen et al.²⁵³, has recently implemented ultrasonic diagnostics for sodium-ion batteries, which compared to lithium-ion technology may suffer more particle cracking and volumetric changes due to the bigger size of sodium ions in compared to lithium-ions. However, that work only showed the ability of the technique to detect gas generation after aging in this new battery technology.

Despite its advantages, ultrasonic inspection faces technical challenges on next-gen batteries. Signal interpretation remains complex, particularly in differentiating lithium plating from gas evolution, as both induce similar acoustic signatures^{95,127}. Spatial and temporal resolution limitations prevent nanometer-scale imaging of solid-electrolyte interphases, making it difficult to precisely characterize early-stage degradation in next-generation chemistries¹²⁶.

V. SUMMARY AND OUTLOOK

UT for LIBs is a developing field at the intersection between materials science, electrochemistry, and acoustics. The field is still in its infancy, despite notable advancements in showcasing the potential of UT techniques for battery assessment. The physical sources of observed acoustic signatures, the generalizability of results across cell chemistries, and wave propagation in operational cells are just a few of the many fundamental questions that still need to be answered. This review presented a comprehensive summary of the research done on ultrasonic inspection for different sections of the LIB life-cycle. It also provided a broad overview of the fundamentals of ultrasonic wave propagation in LIBs as multilayer structures and presented the challenges and opportunities for this technique as a non-destructive tool that provides information on LIB behavior unique from traditional measurements.

UT methods have emerged as powerful diagnostic tools for energy storage devices, which can provide rapid and cost-effective insight into material changes within LIB cells. UT has been shown to accurately determine the SOC/SOH of cells and identify various unfavorable phenomena within cells that may pose risks or cause accelerated capacity degradation, such as gas formation.

However, quantitatively linking the ultrasonic signals to internal physical properties remains a fundamental challenge and requires more extensive material characterization and validation of the sources of the changes in ultrasonic signals using multi-modal diagnostics. If a higher level of confidence can be achieved, UT methods will open further opportunities for rapid identification of important degradation mechanisms in cells, more accurate lifetime predictions, and a tool for estimating the risk of cells undergoing hazardous failure. Modeling is a key enabler to achieving higher confidence, where ultrasonic signal responses can be modeled for known internal physical changes that are anticipated to occur. This requires a significant effort to link existing electrochemical and system models with elastic and poroelastic wave modeling, which is a topic that is still in its infancy.

In this sense, notable challenges and opportunities exist for the application of ultrasound monitoring and characterization of LIBs, which we summarize below:

1. The effect of different cell form factors (e.g., pouch or prismatic vs. cylindrical) on ultrasound wave propagation requires further investigation.
2. The development of reliable ultrasonic signal signatures that indicate LIB state and damage type in the absence of previous history in order to compare cells with different histories is a challenge that must be addressed in order for UT to be a valuable tool for recycling applications and evaluation for second-life use.
3. Temperature and C-rate variations during operation introduce changes in signal interpretation, re-

quiring robust compensation models or guaranteeing very stable operating conditions.

4. Further research is needed to parametrize the mechanical properties of LIB constituent materials and create models to relate ultrasonic signals to physical phenomena within the cells.
5. Ultrasonic testing represents a path to understand the coupling between electrochemical, mechanical, and thermal domains in LIBs, which could lead to significant insights for better batteries for the future.
6. Machine learning approaches have shown promise in correlating ultrasound signals with LIB state metrics. However, their generalization across cell chemistries and even across batches of the same cell remains an open question.

SUPPLEMENTARY MATERIAL

See Supplementary Material at [*URL will be inserted by AIP*] for a mathematical description and additional context regarding ultrasonic wave propagation in LIBs.

ACKNOWLEDGMENTS

The authors acknowledge support from grant AR0001723 under the ARPA-E Jumpstart Opportunities to Unleash Leadership in Energy Storage (JOULES) program, managed by Halle Cheeseman. J. S. Lee acknowledges support from Chungnam University for sabbatical research visit. S. Montoya-Bedoya acknowledges support from the Foreign Fulbright Colombia Minciencias program.

AUTHOR DECLARATIONS

Conflict of interest

The authors have no conflicts to disclose.

DATA AVAILABILITY

The data that support the findings of this study are available within the review article and supplementary material.

¹J. J. Yun, J. Jeon, K. Park, and X. Zhao, “Benefits and costs of closed innovation strategy: Analysis of Samsung’s Galaxy Note 7 explosion and withdrawal scandal,” *Journal of Open Innovation: Technology, Market, and Complexity*, vol. 4, no. 3, p. 20, 2018.

²T. Placke, R. Kloepsch, S. Dühnen, and M. Winter, “Lithium ion, lithium metal, and alternative rechargeable battery technologies: the odyssey for high energy density,” *Journal of Solid State Electrochemistry*, vol. 21, pp. 1939–1964, 2017.

³M. H. Lipu, M. Hannan, T. F. Karim, A. Hussain, M. H. M. Saad, A. Ayob, M. S. Miah, and T. I. Mahlia, “Intelligent algorithms and control strategies for battery management system in electric vehicles: Progress, challenges and future outlook,” *Journal of Cleaner Production*, vol. 292, p. 126044, 2021.

⁴L. Mauler, F. Duffner, W. G. Zeier, and J. Leker, “Battery cost forecasting: a review of methods and results with an outlook to 2050,” *Energy & Environmental Science*, vol. 14, no. 9, pp. 4712–4739, 2021.

⁵International Energy Agency, “Global EV outlook 2025: Expanding sales in diverse markets,” report, International Energy Agency (IEA), Paris, France, 2025. [Accessed 28-12-2025].

⁶O. Catsaros, “Lithium-ion battery pack prices fall to 108 usd per kilowatt-hour, despite rising metal prices: BloombergNEF — BloombergNEF — about.bnef.com.” <https://about.bnef.com/insights/clean-transport/lithium-ion-battery-pack-prices-fall-to-108-per-kilowatt-hour-despite-rising-metal-prices-bloombergnef/>. [Accessed 28-12-2025].

⁷Department of Energy (DOE), “FOTW 1234, April 18, 2022: Volumetric energy density of lithium-ion batteries increased by more than eight times between 2008 and 2020.” <https://www.energy.gov/eere/vehicles/articles/fotw-1234-april-18-2022-volumetric-energy-density-lithium-ion-batteries>. [Accessed 28-12-2025].

⁸“COP26 Declaration on accelerating the transition to 100 [Accessed 28-12-2025].

⁹R. Dorenkamp, “Ford joins appeal to the EU for 100% all-electric vehicle sales by 2035,” 2022. [Accessed 28-12-2025].

¹⁰D. Shepardson, “GM still planning to end gas-powered vehicle sales by 2035 – CEO,” 2023. [Accessed 28-12-2025].

¹¹EY, “China, Sweden and Germany lead the way on the EY Electric Vehicle Country Readiness Index,” 2021. [Accessed 28-12-2025].

¹²P. Sun, R. Bisschop, H. Niu, and X. Huang, “A review of battery fires in electric vehicles,” *Fire technology*, vol. 56, pp. 1361–1410, 2020.

¹³H. Maleki and J. N. Howard, “Internal short circuit in li-ion cells,” *Journal of Power Sources*, vol. 191, p. 568–574, June 2009.

¹⁴D. P. Finegan, E. Darcy, M. Keyser, B. Tjaden, T. M. M. Heenan, R. Jervis, J. J. Bailey, R. Malik, N. T. Vo, O. V. Magdysyuk, R. Atwood, M. Drakopoulos, M. DiMichiel, A. Rack, G. Hinds, D. J. L. Brett, and P. R. Shearing, “Characterising thermal runaway within lithium-ion cells by inducing and monitoring internal short circuits,” *Energy & Environmental Science*, vol. 10, no. 6, p. 1377–1388, 2017.

¹⁵M. Yang, Y. Ye, A. Yang, Z. Jiang, X. Wang, H. Yuan, and M. Rong, “Comparative study on aging and thermal runaway of commercial lifepo4/graphite battery undergoing slight overcharge cycling,” *Journal of Energy Storage*, vol. 50, p. 104691, June 2022.

¹⁶W. Zuo, R. Liu, J. Cai, Y. Hu, M. Almazrouei, X. Liu, T. Cui, X. Jia, E. Apodaca, J. Alami, Z. Chen, T. Li, W. Xu, X. Xiao, D. Parkinson, Y. Yang, G.-L. Xu, and K. Amine, “Nondestructive analysis of commercial batteries,” *Chemical Reviews*, Dec. 2024.

¹⁷X. C. A. Chacón, S. Laureti, M. Ricci, and G. Cappuccino, “A review of non-destructive techniques for lithium-ion battery performance analysis,” *World Electric Vehicle Journal*, vol. 14, p. 305, Nov. 2023.

¹⁸J. Gao, S. Wang, and F. Hao, “A review of non-destructive testing for lithium batteries,” *Energies*, vol. 17, p. 4030, Aug. 2024.

¹⁹H. Popp, M. Koller, M. Jahn, and A. Bergmann, “Mechanical methods for state determination of lithium-ion secondary batteries: A review,” *Journal of Energy Storage*, vol. 32, p. 101859, Dec. 2020.

²⁰Y. Wang, X. Lai, Q. Chen, X. Han, L. Lu, M. Ouyang, and Y. Zheng, “Progress and challenges in ultrasonic technology for state estimation and defect detection of lithium-ion batteries,” *Energy Storage Materials*, p. 103430, 2024.

²¹D. Williams, R. Copley, P. Bugryniec, R. Dwyer-Joyce, and S. Brown, “A review of ultrasonic monitoring: Assessing current approaches to li-ion battery monitoring and their relevance to thermal runaway,” *Journal of Power Sources*, vol. 590,

p. 233777, Jan. 2024.

²²C. Gervillié-Mouravieff, W. Bao, D. A. Steingart, and Y. S. Meng, "Non-destructive characterization techniques for battery performance and life-cycle assessment," *Nature Reviews Electrical Engineering*, vol. 1, p. 547–558, July 2024.

²³K. A. Severson, P. Attia, N. Jin, N. Perkins, B. Jiang, Z. Yang, M. Chen, M. Aykol, P. Herring, D. Fragedakis, M. Bazant, S. Harris, W. Chueh, and R. Braatz, "Data-driven prediction of battery cycle life before capacity degradation," *Nature Energy*, vol. 4, no. 5, pp. 383–391, 2019.

²⁴J. Zhu, I. Mathews, D. Ren, W. Li, D. Cogswell, B. Xing, T. Sedlatschek, S. N. R. Kantareddy, M. Yi, T. Gao, Y. Xia, Q. Zhou, T. Wierzbicki, and M. Z. Bazant, "End-of-life or second-life options for retired electric vehicle batteries," *Cell Reports Physical Science*, vol. 2, p. 100537, Aug. 2021.

²⁵A. Fordham, Z. Milojevic, E. Giles, W. Du, R. E. Owen, S. Michalik, P. A. Chater, P. K. Das, P. S. Attidekou, S. M. Lambert, P. K. Allan, P. R. Slater, P. A. Anderson, R. Jervis, P. R. Shearing, and D. J. Brett, "Correlative non-destructive techniques to investigate aging and orientation effects in automotive li-ion pouch cells," *Joule*, vol. 7, p. 2622–2652, Nov. 2023.

²⁶T. M. McGee, B. Neath, S. Matthews, O. A. Ezekoye, and M. R. Haberman, "Ultrasonic detection of pre-existing thermal abuse in lithium-ion pouch cells," *Journal of Power Sources*, vol. 595, p. 234035, 2024.

²⁷X.-l. Wang, Y. Lyu, G.-r. Song, L.-h. Zhang, and C.-f. He, "Theoretical analysis of ultrasonic reflection/transmission characteristics of lithium-ion battery," in *2020 15th Symposium on Piezoelectricity, Acoustic Waves and Device Applications (SPAUDA)*, pp. 292–296, IEEE, 2021.

²⁸J. Gao, Y. Lyu, H. Chen, W. Song, H. Liu, B. Wu, and C. He, "Guided waves propagation in lithium-ion batteries: Theoretical modeling and experimental analysis," *NDT & E International*, vol. 145, p. 103102, July 2024.

²⁹M. A. Biot, "Theory of Propagation of Elastic Waves in a Fluid-Saturated Porous Solid. I. Low-Frequency Range," *The Journal of the Acoustical Society of America*, vol. 28, no. 2, pp. 168–178, 1956.

³⁰M. A. Biot, "Theory of Propagation of Elastic Waves in a Fluid-Saturated Porous Solid. I. Low-Frequency Range," *The Journal of the Acoustical Society of America*, vol. 28, no. 2, pp. 168–178, 1956.

³¹L. Gold, T. Bach, W. Virsik, A. Schmitt, J. Müller, T. E. Staab, and G. Sextl, "Probing lithium-ion batteries' state-of-charge using ultrasonic transmission—concept and laboratory testing," *Journal of Power Sources*, vol. 343, pp. 536–544, 2017.

³²J.-J. Chang, X.-F. Zeng, and T.-L. Wan, "Real-time measurement of lithium-ion batteries' state-of-charge based on air-coupled ultrasound," *AIP Advances*, vol. 9, no. 8, 2019.

³³G. Jie, L. Yan, Z. Mingfang, L. Mingkun, L. Hongye, W. Bin, and H. Cunfu, "Guided waves propagation in multi-layered porous materials by the global matrix method and biot theory," *Applied Acoustics*, vol. 184, p. 108356, 2021.

³⁴M. Huang, N. Kirkaldy, Y. Zhao, Y. Patel, F. Cegla, and B. Lan, "Quantitative characterisation of the layered structure within lithium-ion batteries using ultrasonic resonance," *Journal of Energy Storage*, vol. 50, p. 104585, 2022.

³⁵L. Gold, T. Herzog, F. Schubert, H. Heuer, and G. A. Giffin, "Ultrasound propagation in lithium-ion battery cell materials: Basis for developing monitoring and imaging methods," *Energy Technology*, vol. 11, no. 5, p. 2200861, 2023.

³⁶M. Huang, F. Cegla, and B. Lan, "Stiffness matrix method for modelling wave propagation in arbitrary multilayers," *International Journal of Engineering Science*, vol. 190, p. 103888, 2023.

³⁷B. Zhang, Y. Lyu, J. Gao, G. Song, Y. Zheng, Y. chun Lee, and C. He, "Ultrasonic characterization of multi-layered porous lithium-ion battery structure for state of charge," *Ultrasonics*, p. 107060, 2023.

³⁸B. Zhang, Y. Lyu, J. Gao, G. Song, Y. chun Lee, C. He, W. Song, and H. Chen, "Ultrasonic reflection/transmission characteristics for state of charge of li-ion battery," *Applied Acoustics*, vol. 214, p. 109687, 2023.

³⁹G. Jie, Z. Liangheng, L. Yan, S. Fan, W. Bin, and H. Cunfu, "Ultrasonic guided wave measurement and modeling analysis of the state of charge for lithium-ion battery," *Journal of Energy Storage*, vol. 72, p. 108384, 2023.

⁴⁰S. Zhang, P. Zuo, X. Yin, and Z. Fan, "Exploring the correlation between ultrasound time of flight and the state of health of lifepo4 prismatic cells," *Journal of Energy Storage*, vol. 83, p. 110715, 2024.

⁴¹D. Chimenti, "Guided waves in plates and their use in materials characterization," *Applied Mechanics Reviews*, vol. 50, no. 5, pp. 247–284, 1997.

⁴²D. Chimenti, "Review of air-coupled ultrasonic materials characterization," *Ultrasonics*, vol. 54, no. 7, pp. 1804–1816, 2014.

⁴³B. Reichmann and Z. Sharif-Khodaei, "Ultrasonic guided waves as an indicator for the state-of-charge of li-ion batteries," *Journal of Power Sources*, vol. 576, p. 233189, Aug. 2023.

⁴⁴D. L. Johnson and T. J. Plona, "Acoustic slow waves and the consolidation transition," *The Journal of the Acoustical Society of America*, vol. 72, no. 2, pp. 556–565, 1982.

⁴⁵D. L. Johnson, "Impact of t. j. plona's observation and quantification of the biot fast and slow waves," in *Poromechanics VI*, p. 1587–1603, American Society of Civil Engineers, July 2017.

⁴⁶P. Zhu, D. Gastol, J. Marshall, R. Sommerville, V. Goodship, and E. Kendrick, "A review of current collectors for lithium-ion batteries," *Journal of Power Sources*, vol. 485, p. 229321, Feb. 2021.

⁴⁷A. M. Boyce, D. J. Cumming, C. Huang, S. P. Zankowski, P. S. Grant, D. J. L. Brett, and P. R. Shearing, "Design of scalable, next-generation thick electrodes: Opportunities and challenges," *ACS Nano*, vol. 15, p. 18624–18632, Dec. 2021.

⁴⁸H. Lee, M. Yilmaz, O. Toprakci, K. Fu, and X. Zhang, "A review of recent developments in membrane separators for rechargeable lithium-ion batteries," *Energy Environ. Sci.*, vol. 7, no. 12, p. 3857–3886, 2014.

⁴⁹D. Larcher and J.-M. Tarascon, "Towards greener and more sustainable batteries for electrical energy storage," *Nature Chemistry*, vol. 7, p. 19–29, Nov. 2014.

⁵⁰A. Manthiram, "An Outlook on Lithium Ion Battery Technology," *ACS Central Science*, vol. 3, p. 1063–1069, Sept. 2017.

⁵¹A. Manthiram, "A reflection on lithium-ion battery cathode chemistry," *Nature communications*, vol. 11, no. 1, p. 1550, 2020.

⁵²E. Feyzi, A. K. M R, X. Li, S. Deng, J. Nanda, and K. Zaghrib, "A comprehensive review of silicon anodes for high-energy lithium-ion batteries: Challenges, latest developments, and perspectives," *Next Energy*, vol. 5, p. 100176, Oct. 2024.

⁵³X. Li, A. M. Colclasure, D. P. Finegan, D. Ren, Y. Shi, X. Feng, L. Cao, Y. Yang, and K. Smith, "Degradation mechanisms of high capacity 18650 cells containing si-graphite anode and nickel-rich nmc cathode," *Electrochimica Acta*, vol. 297, pp. 1109–1120, 2019.

⁵⁴S. Schweißler, L. de Biasi, A. Schiele, P. Hartmann, T. Brezesinski, and J. Janek, "Volume changes of graphite anodes revisited: A combined operando x-ray diffraction and in situ pressure analysis study," *The Journal of Physical Chemistry C*, vol. 122, p. 8829–8835, Apr. 2018.

⁵⁵Y. Qi, H. Guo, L. G. Hector, and A. Timmons, "Threefold increase in the young's modulus of graphite negative electrode during lithium intercalation," *Journal of The Electrochemical Society*, vol. 157, no. 5, p. A558, 2010.

⁵⁶V. A. Sethuraman, L. J. Hardwick, V. Srinivasan, and R. Kostecki, "Surface structural disordering in graphite upon lithium intercalation/deintercalation," *Journal of Power Sources*, vol. 195, no. 11, pp. 3655–3660, 2010.

⁵⁷J. R. Dahn, "Phase diagram of Li_xC_6 ," *Physical Review B*, vol. 44, p. 9170–9177, Nov. 1991.

⁵⁸R. Koerver, W. Zhang, L. de Biasi, S. Schweieler, A. O. Kondrakov, S. Kolling, T. Brezesinski, P. Hartmann, W. G. Zeier, and J. Janek, "Chemo-mechanical expansion of lithium electrode materials—on the route to mechanically optimized all-solid-state batteries," *Energy & Environmental Science*, vol. 11, no. 8, pp. 2142–2158, 2018.

⁵⁹J. C. Stallard, L. Wheatcroft, S. G. Booth, R. Boston, S. A. Corr, M. F. De Volder, B. J. Inkson, and N. A. Fleck, "Mechanical properties of cathode materials for lithium-ion batteries," *Joule*, vol. 6, p. 984–1007, May 2022.

⁶⁰R. Schröder, M. Aydemir, and G. Seliger, "Comparatively assessing different shapes of lithium-ion battery cells," *Procedia Manufacturing*, vol. 8, pp. 104–111, 2017.

⁶¹M. E. McGovern, D. D. Bruder, E. D. Huemiller, T. J. Rinker, J. T. Bracey, R. C. Sekol, and J. A. Abell, "A review of research needs in nondestructive evaluation for quality verification in electric vehicle lithium-ion battery cell manufacturing," *Journal of Power Sources*, vol. 561, p. 232742, 2023.

⁶²R. Wagner, N. Preschitschek, S. Passerini, J. Leker, and M. Winter, "Current research trends and prospects among the various materials and designs used in lithium-based batteries," *Journal of Applied Electrochemistry*, vol. 43, p. 481–496, Feb. 2013.

⁶³B. Gulsoy, H. Chen, C. Briggs, T. Vincent, J. Sansom, and J. Marco, "Real-time simultaneous monitoring of internal temperature and gas pressure in cylindrical cells during thermal runaway," *Journal of Power Sources*, vol. 617, p. 235147, Oct. 2024.

⁶⁴T. M. McGee, B. Neath, S. Matthews, O. A. Ezekoye, and M. R. Haberman, "Ultrasonic inspection of lithium-ion pouch cells subjected to localized thermal abuse," *Journal of Power Sources*, vol. 583, p. 233542, 2023.

⁶⁵R. E. Owen, E. Wiśniewska, M. Braglia, R. Stocker, P. R. Shearing, D. J. L. Brett, and J. B. Robinson, "Operando ultrasonic monitoring of the internal temperature of lithium-ion batteries for the detection and prevention of thermal runaway," *Journal of The Electrochemical Society*, vol. 171, p. 040525, Apr. 2024.

⁶⁶A. Hsieh, S. Bhadra, B. Hertzberg, P. Gjeltema, A. Goy, J. W. Fleischer, and D. A. Steingart, "Electrochemical-acoustic time of flight: in operando correlation of physical dynamics with battery charge and health," *Energy & environmental science*, vol. 8, no. 5, pp. 1569–1577, 2015.

⁶⁷B. Zhang, Y. Zheng, J. Gao, Y. Lyu, L. Cao, and C. He, "Ultrasonic estimation of lithium-ion battery state parameters using hybrid sparrow search algorithm and relevance vector machine," *Journal of Power Sources*, vol. 633, p. 236469, Mar. 2025.

⁶⁸T. J. Plona, "Observation of a second bulk compressional wave in a porous medium at ultrasonic frequencies," *Applied Physics Letters*, vol. 36, no. 4, pp. 259–261, 1980.

⁶⁹S. Feiler, L. Gold, S. Hartmann, and G. A. Giffin, "Modeling acoustic attenuation, sound velocity and wave propagation in lithium-ion batteries via a transfer matrix," *Batteries & Supercaps*, Nov. 2024.

⁷⁰P.-S. Ma, H. Lee, and Y.-H. Seo, "Identifying ultrasonic scattering from multi-layered lithium-ion battery cells: Mechanical modeling and experimental validation," *Journal of Energy Storage*, vol. 92, p. 112077, July 2024.

⁷¹J. S. Edge, S. O'Kane, R. Prosser, N. D. Kirkaldy, A. N. Patel, A. Hales, A. Ghosh, W. Ai, J. Chen, J. Yang, S. Li, M.-C. Pang, L. Bravo Diaz, A. Tomaszevska, M. W. Marzook, K. N. Radhakrishnan, H. Wang, Y. Patel, B. Wu, and G. J. Offer, "Lithium ion battery degradation: what you need to know," *Physical Chemistry Chemical Physics*, vol. 23, no. 14, p. 8200–8221, 2021.

⁷²L. S. de Vasconcelos, R. Xu, Z. Xu, J. Zhang, N. Sharma, S. R. Shah, J. Han, X. He, X. Wu, H. Sun, S. Hu, M. Perrin, X. Wang, Y. Liu, F. Lin, Y. Cui, and K. Zhao, "Chemomechanics of rechargeable batteries: Status, theories, and perspectives," *Chemical Reviews*, vol. 122, p. 13043–13107, July 2022.

⁷³R. Li, N. D. Kirkaldy, F. F. Oehler, M. Marinescu, G. J. Offer, and S. E. J. O'Kane, "The importance of degradation mode analysis in parameterising lifetime prediction models of lithium-ion battery degradation," *Nature Communications*, vol. 16, Mar. 2025.

⁷⁴K. Rah, B. Choi, and C. Kim, "Effective measures of thickness evolution of the solid electrolyte interphase of graphite anodes for li-ion batteries," *Langmuir*, vol. 40, p. 7550–7559, Mar. 2024.

⁷⁵S. T. Oyakhire and S. F. Bent, "Interfacial engineering of lithium metal anodes: what is left to uncover?," *Energy Advances*, vol. 3, no. 1, p. 108–122, 2024.

⁷⁶C. Bommier, W. Chang, J. Li, S. Biswas, G. Davies, J. Nanda, and D. Steingart, "Operando acoustic monitoring of SEI formation and long-term cycling in NMC/SiGr composite pouch cells," *Journal of The Electrochemical Society*, vol. 167, no. 2, p. 020517, 2020.

⁷⁷Y. Chai, W. Jia, Z. Hu, S. Jin, H. Jin, H. Ju, X. Yan, H. Ji, and L.-J. Wan, "Monitoring the mechanical properties of the solid electrolyte interphase (sei) using electrochemical quartz crystal microbalance with dissipation," *Chinese Chemical Letters*, vol. 32, p. 1139–1143, Mar. 2021.

⁷⁸G. Rong, X. Zhang, W. Zhao, Y. Qiu, M. Liu, F. Ye, Y. Xu, J. Chen, Y. Hou, W. Li, W. Duan, and Y. Zhang, "Liquid-phase electrochemical scanning electron microscopy for in situ investigation of lithium dendrite growth and dissolution," *Advanced Materials*, vol. 29, Jan. 2017.

⁷⁹A. Aghili Mehrizi, F. Yeganehdoust, A. K. Madikere Raghunatha Reddy, and K. Zaghib, "Challenges and issues facing ultrafast-charging lithium-ion batteries," *Batteries*, vol. 11, p. 209, May 2025.

⁸⁰C. Bommier, W. Chang, Y. Lu, J. Yeung, G. Davies, R. Mohr, M. Williams, and D. Steingart, "In operando acoustic detection of lithium metal plating in commercial $LiCoO_2$ /graphite pouch cells," *Cell Reports Physical Science*, vol. 1, no. 4, 2020.

⁸¹W. Chang, C. Bommier, T. Fair, J. Yeung, S. Patil, and D. Steingart, "Understanding adverse effects of temperature shifts on li-ion batteries: An operando acoustic study," *Journal of The Electrochemical Society*, vol. 167, no. 9, p. 090503, 2020.

⁸²D. Wasylowski, H. Ditler, M. Sonnet, T. Falkenstein, L. Leogrande, E. Ronge, A. Blömeke, A. Würsig, F. Ringbeck, and D. U. Sauer, "Operando visualisation of lithium plating by ultrasound imaging of battery cells," *Nature Communications*, vol. 15, Nov. 2024.

⁸³J. Meyer, A. Dietz, M. Zhan, A. Fill, and K. P. Birke, "Spatially resolved, in operando detection of reversible lithium plating using ultrasonic waves," *Journal of Power Sources*, vol. 653, p. 237723, Oct. 2025.

⁸⁴W. Xu, L. Li, F. Shi, and Q. Chen, "Ultrasonic spectroscopy for in situ early detection and dynamic monitoring of lithium plating in lithium-ion batteries," *Cell Reports Physical Science*, vol. 6, p. 102507, Apr. 2025.

⁸⁵F. Pistorio, D. Clerici, F. Mocera, and A. Somà, "Review on the experimental characterization of fracture in active material for lithium-ion batteries," *Energies*, vol. 15, p. 9168, Dec. 2022.

⁸⁶M. T. Pham, J. J. Darst, D. P. Finegan, J. B. Robinson, T. M. Heenan, M. D. Kok, F. Iacoviello, R. Owen, W. Q. Walker, O. V. Magdysyuk, *et al.*, "Correlative acoustic time-of-flight spectroscopy and x-ray imaging to investigate gas-induced delamination in lithium-ion pouch cells during thermal runaway," *Journal of Power Sources*, vol. 470, p. 228039, 2020.

⁸⁷Z. Deng, Z. Huang, Y. Shen, Y. Huang, H. Ding, A. Luscombe, M. Johnson, J. E. Harlow, R. Gauthier, and J. R. Dahn, "Ultrasonic scanning to observe wetting and "unwetting" in li-ion pouch cells," *Joule*, vol. 4, no. 9, pp. 2017–2029, 2020.

⁸⁸A. Eldesoky, M. Bauer, T. Bond, N. Kowalski, J. Corsten, D. Rathore, R. Dressler, and J. R. Dahn, "Long-term study on the impact of depth of discharge, c-rate, voltage, and temperature on the lifetime of single-crystal nmc811/artificial graphite

pouch cells," *Journal of The Electrochemical Society*, vol. 169, p. 100531, Oct. 2022.

⁸⁹X. Liu, Y. Lyu, J. Gao, M. Geng, M. Fan, Z. Han, and C. Zhang, "Non-destructive estimation of internal state for lithium-ion batteries by ultrasonic phased array scanning and imaging technologies," *Journal of Energy Storage*, vol. 117, p. 116155, May 2025.

⁹⁰M. Morra, "An ultrasonic meter to characterize degree of fouling and cleaning in reverse osmosis filters," in *AIP Conference Proceedings*, vol. 657, p. 1673–1680, AIP, 2003.

⁹¹W. Araki, H. Azuma, T. Yota, Y. Arai, and J. Malzbender, "Mechanical characteristics of electrolytes assessed with resonant ultrasound spectroscopy," *Fuel Cells*, vol. 13, p. 542–548, Mar. 2013.

⁹²B. Sood, M. Osterman, and M. Pecht, "Health monitoring of lithium-ion batteries," in *2013 IEEE Symposium on Product Compliance Engineering (ISPCE)*, pp. 1–6, IEEE, 2013.

⁹³H. Sun, N. Muralidharan, R. Amin, V. Rathod, P. Ramuhalli, and I. Belharouak, "Ultrasonic nondestructive diagnosis of lithium-ion batteries with multiple frequencies," *Journal of Power Sources*, vol. 549, p. 232091, 2022.

⁹⁴M. G. O. Ajaereh, O. J. Cook, H. N. Jones, N. Kizer, L. Katch, C. S. Wheatley, C. Vagg, C. Courtney, C. M. Kube, and A. P. Argüelles, "Assessing spatial non-uniformities in lithium-ion battery state of charge using ultrasound immersion testing," in *186th Meeting of the Acoustical Society of America and the Canadian Acoustical Association*, vol. 54, p. 045004, ASA, 2024.

⁹⁵W. Chang and D. Steingart, "Operando 2D acoustic characterization of lithium-ion battery spatial dynamics," *ACS Energy Letters*, vol. 6, no. 8, pp. 2960–2968, 2021.

⁹⁶K. Meng, X. Chen, W. Zhang, W. Chang, and J. Xu, "A robust ultrasonic characterization methodology for lithium-ion batteries on frequency-domain damping analysis," *Journal of Power Sources*, vol. 547, p. 232003, 2022.

⁹⁷J. O. Majasan, J. B. Robinson, R. E. Owen, M. Maier, A. N. P. Radhakrishnan, M. Pham, T. G. Tranter, Y. Zhang, P. R. Shearing, and D. J. L. Brett, "Recent advances in acoustic diagnostics for electrochemical power systems," *Journal of Physics: Energy*, vol. 3, p. 032011, June 2021.

⁹⁸J. B. Robinson, R. E. Owen, M. D. Kok, M. Maier, J. Majasan, M. Braglia, R. Stocker, T. Amietszajew, A. J. Roberts, R. Bhagat, *et al.*, "Identifying defects in li-ion cells using ultrasound acoustic measurements," *Journal of The Electrochemical Society*, vol. 167, no. 12, p. 120530, 2020.

⁹⁹G. Davies, K. W. Knehr, B. Van Tassell, T. Hodson, S. Biswas, A. G. Hsieh, and D. A. Steingart, "State of charge and state of health estimation using electrochemical acoustic time of flight analysis," *Journal of The Electrochemical Society*, vol. 164, no. 12, p. A2746, 2017.

¹⁰⁰J. B. Robinson, M. Pham, M. D. Kok, T. M. Heenan, D. J. Brett, and P. R. Shearing, "Examining the cycling behaviour of li-ion batteries using ultrasonic time-of-flight measurements," *Journal of Power Sources*, vol. 444, p. 227318, 2019.

¹⁰¹J. B. Robinson, M. Maier, G. Alster, T. Compton, D. J. Brett, and P. R. Shearing, "Spatially resolved ultrasound diagnostics of li-ion battery electrodes," *Physical Chemistry Chemical Physics*, vol. 21, no. 12, pp. 6354–6361, 2019.

¹⁰²C. Qin, Z. Cai, and J. Shen, "Construction of a lithium-ion battery degradation model based on ultrasonic detection," in *Fourth International Conference on Artificial Intelligence and Electromechanical Automation (AIEA 2023)*, vol. 12709, pp. 659–665, SPIE, 2023.

¹⁰³E. Galiounas, F. Iacoviello, M. Mirza, L. Rasha, R. E. Owen, J. B. Robinson, and R. Jervis, "Investigations into the dynamic acoustic response of lithium-ion batteries during life-time testing," *Journal of The Electrochemical Society*, vol. 171, p. 070514, July 2024.

¹⁰⁴Y. Wu, Y. Wang, W. K. Yung, and M. Pecht, "Ultrasonic health monitoring of lithium-ion batteries," *Electronics*, vol. 8, no. 7, p. 751, 2019.

¹⁰⁵D. Rohrbach, E. Garcia-Tamayo, J. Potter, V. Martinez, and M. Bernal, "Nondestructive state-of-charge assessment of lithium-ion batteries using quantitative ultrasound spectroscopy," in *2021 IEEE International Ultrasonics Symposium (IUS)*, pp. 1–4, IEEE, 2021.

¹⁰⁶Z. Huang, Y. Zhou, Z. Deng, K. Huang, M. Xu, Y. Shen, and Y. Huang, "Precise state-of-charge mapping via deep learning on ultrasonic transmission signals for lithium-ion batteries," *ACS Applied Materials & Interfaces*, vol. 15, no. 6, pp. 8217–8223, 2023.

¹⁰⁷L. Fariñas, M. M. Sánchez, and T. G. Álvarez-Arenas, "Lithium-ion batteries' state-of-charge and health assessment by non-contact ultrasound spectroscopy," in *2023 IEEE International Ultrasonics Symposium (IUS)*, pp. 1–4, IEEE, 2023.

¹⁰⁸L. Fariñas, M. Muñoz, and T. E. Gómez Álvarez Arenas, "Contactless ultrasound spectroscopy for testing state-of-charge and integrity in lithium-ion batteries," *iScience*, vol. 27, p. 111046, Oct. 2024.

¹⁰⁹M. C. Appleberry, J. A. Kowalski, S. A. Africk, J. Mitchell, T. C. Ferree, V. Chang, V. Parekh, Z. Xu, Z. Ye, J. F. Whitacre, *et al.*, "Avoiding thermal runaway in lithium-ion batteries using ultrasound detection of early failure mechanisms," *Journal of Power Sources*, vol. 535, p. 231423, 2022.

¹¹⁰Y. Shen, B. Zou, Z. Zhang, M. Xu, S. Wang, Q. Li, H. Li, M. Zhou, K. Jiang, and K. Wang, "In situ detection of lithium-ion batteries by ultrasonic technologies," *Energy Storage Materials*, vol. 62, p. 102915, 2023.

¹¹¹Y. Wei, Y. Yan, C. Zhang, K. Meng, and C. Xu, "State estimation of lithium-ion batteries based on the initial rise time feature of ultrasonic signals," *Journal of Power Sources*, vol. 581, p. 233497, Oct. 2023.

¹¹²B. Sun, C. Zhang, S. Liu, L. Jin, and Q. Yang, "Acoustic response characteristics of lithium cobaltate/graphite battery during cycling," *Journal of The Electrochemical Society*, vol. 169, p. 030511, Mar. 2022.

¹¹³S. Feiler, L. Gold, S. Hartmann, and G. A. Giffin, "Investigation of acoustic attenuation and resonances in lithium-ion batteries using ultrasound spectroscopy," *Batteries & Supercaps*, July 2024.

¹¹⁴G. Zhao, Y. Liu, G. Liu, S. Jiang, and W. Hao, "State-of-charge and state-of-health estimation for lithium-ion battery using the direct wave signals of guided wave," *Journal of Energy Storage*, vol. 39, p. 102657, 2021.

¹¹⁵T. Hamann, A. Knight, Y. Sha, and J. S. Ko, "Multi-modal assessment of battery aging by coupling ultrasound and impedance signatures," *ACS Applied Energy Materials*, vol. 8, p. 15051–15058, Oct. 2025.

¹¹⁶B. Sun, C. Zhang, Z. Xu, S. Liu, and Q. Yang, "Ultrasonic diagnosis of the nonlinear aging characteristics of lithium-ion battery under high-rate discharge conditions," *Journal of Power Sources*, vol. 567, p. 232921, 2023.

¹¹⁷X. Lin, X. Li, M. Deng, and W. Li, "Mapping of state of charge and cathode material in ncm li-ion batteries: an in-situ study based on the quasi-static component of nonlinear guided wave," *Energy Storage Materials*, vol. 79, p. 104298, June 2025.

¹¹⁸X. Lin, X. Li, M. Deng, and W. Li, "Real-time soc monitoring in ncm li-ion batteries via quasi-static component of nonlinear guided wave," *Applied Physics Letters*, vol. 127, Nov. 2025.

¹¹⁹X. Yuan, Y. Wang, W. Li, and M. Deng, "A novel approach for state-of-charge estimation of lithium-ion batteries by quasi-static component generation of ultrasonic waves," *Measurement Science and Technology*, vol. 35, p. 096003, June 2024.

¹²⁰H. Sun, P. Ramuhalli, R. Amin, and I. Belharouak, "Second harmonic generation for estimating state of charge of lithium-ion batteries," *Applied Physics Letters*, vol. 124, Feb. 2024.

¹²¹S. Sampath, X. Yin, Z. W. Tham, Y. F. Chen, and L. Zhang, "Real-time and non-contact estimation of state of charge for lithium-ion battery using laser ultrasonics," *Journal of Power Sources*, vol. 605, p. 234544, June 2024.

¹²²A. Siegl, B. Schweighofer, A. Bergmann, and H. Wegleiter, “An electromagnetic acoustic transducer for generating acoustic waves in lithium-ion pouch cells,” in *2022 IEEE International Instrumentation and Measurement Technology Conference (I2MTC)*, pp. 1–6, IEEE, 2022.

¹²³X. Li, X. Yu, Y. Tian, J. Tian, and R. Xiong, “Battery state characterization based on a contactless electromagnetic ultrasound testing method,” *Journal of Energy Storage*, vol. 100, p. 113499, Oct. 2024.

¹²⁴B. Hosten, D. A. Hutchins, and D. W. Schindel, “Measurement of elastic constants in composite materials using air-coupled ultrasonic bulk waves,” *The Journal of the Acoustical Society of America*, vol. 99, no. 4, pp. 2116–2123, 1996.

¹²⁵W. Chang, G. Thorsteinsson, U. Janakiraman, R. R. Chowdhury, Z. Herman, L. Katzman, and D. A. Steingart, “Relating chemo-mechanical hysteresis and formation protocols for anode-free lithium metal batteries,” *Journal of The Electrochemical Society*, vol. 171, p. 040506, Apr. 2024.

¹²⁶K. Sun, G. Thorsteinsson, D. Zhao, C. Owen, A. Ponnekanti, Z. Herman, B. Parris, I. Kothari, and D. A. Steingart, “Chemomechanics and morphological dynamics of si electrodes in all-solid-state li-ion batteries,” *ACS Energy Letters*, p. 1229–1234, Feb. 2025.

¹²⁷H. Huo, K. Huang, W. Luo, J. Meng, L. Zhou, Z. Deng, J. Wen, Y. Dai, Z. Huang, Y. Shen, et al., “Evaluating interfacial stability in solid-state pouch cells via ultrasonic imaging,” *ACS Energy Letters*, vol. 7, no. 2, pp. 650–658, 2022.

¹²⁸J.-Y. Kim, J.-H. Jo, and J.-W. Byeon, “Ultrasonic monitoring performance degradation of lithium ion battery,” *Microelectronics Reliability*, vol. 114, p. 113859, 2020.

¹²⁹R. Copley, D. Cumming, Y. Wu, and R. Dwyer-Joyce, “Measurements and modelling of the response of an ultrasonic pulse to a lithium-ion battery as a precursor for state of charge estimation,” *Journal of Energy Storage*, vol. 36, p. 102406, 2021.

¹³⁰R. E. Owen, J. B. Robinson, J. S. Weaving, M. T. Pham, T. G. Tranter, T. P. Neville, D. Billson, M. Braglia, R. Stocker, A. A. Tidblad, et al., “Operando ultrasonic monitoring of lithium-ion battery temperature and behaviour at different cycling rates and under drive cycle conditions,” *Journal of The Electrochemical Society*, vol. 169, no. 4, p. 040563, 2022.

¹³¹K. W. Knehr, T. Hodson, C. Bommier, G. Davies, A. Kim, and D. A. Steingart, “Understanding full-cell evolution and non-chemical electrode crosstalk of li-ion batteries,” *Joule*, vol. 2, no. 6, pp. 1146–1159, 2018.

¹³²E. Galionas, T. G. Tranter, R. E. Owen, J. B. Robinson, P. R. Shearing, and D. J. Brett, “Battery state-of-charge estimation using machine learning analysis of ultrasonic signatures,” *Energy and AI*, vol. 10, p. 100188, 2022.

¹³³S. Feiler, P. Daubinger, L. Gold, S. Hartmann, and G. A. Giffin, “Interplay between elastic and electrochemical properties during active material transitions and aging of a lithium-ion battery,” *Batteries & Supercaps*, vol. 6, no. 4, p. e202200518, 2023.

¹³⁴X. Liu, Z. Deng, Y. Liao, J. Du, J. Tian, Z. Liu, Y. Shen, and Y. Huang, “Decoupling of the anode and cathode ultrasonic responses to the state of charge of a lithium-ion battery,” *Physical Chemistry Chemical Physics*, vol. 25, no. 32, pp. 21730–21735, 2023.

¹³⁵L. Fu, Z. Wang, X. Zhao, Y. Xu, F. Gu, and A. D. Ball, *An Overview of Ultrasonic Signature-Based Lithium-Ion Battery Health Monitoring*, p. 563–576. Springer Nature Switzerland, 2024.

¹³⁶A. Kirchev, N. Guillet, L. Lonardoni, and S. Dumenil, “Li-ion cell safety monitoring using mechanical parameters, part 3: Battery behaviour during abusive overcharge,” *Batteries*, vol. 9, no. 7, p. 338, 2023.

¹³⁷Q. Ke, S. Jiang, W. Li, W. Lin, X. Li, and H. Huang, “Potential of ultrasonic time-of-flight and amplitude as the measurement for state of charge and physical changings of lithium-ion batteries,” *Journal of Power Sources*, vol. 549, p. 232031, 2022.

¹³⁸M. Xu, B. Zou, Y. Shen, K. Wang, and K. Jiang, “Feature extraction of ultrasonic monitoring during lithium-ion battery cycling,” in *2022 7th International Conference on Power and Renewable Energy (ICPRE)*, pp. 1000–1003, IEEE, 2022.

¹³⁹M. Xu, E. Zhang, S. Wang, Y. Shen, B. Zou, H. Li, Y. Wan, K. Wang, and K. Jiang, “Dynamic ultrasonic response modeling and accurate state of charge estimation for lithium ion batteries under various load profiles and temperatures,” *Applied Energy*, vol. 355, p. 122210, Feb. 2024.

¹⁴⁰R. Zhang, X. Li, C. Sun, S. Yang, Y. Tian, and J. Tian, “State of charge and temperature joint estimation based on ultrasonic reflection waves for lithium-ion battery applications,” *Batteries*, vol. 9, no. 6, p. 335, 2023.

¹⁴¹A. Kirchev, N. Guillet, D. Brun-Buission, and V. Gau, “Li-ion cell safety monitoring using mechanical parameters: Part i. normal battery operation,” *Journal of The Electrochemical Society*, vol. 169, no. 1, p. 010515, 2022.

¹⁴²J. Gao, X. Liu, Y. Lyu, X. Qiao, and C. He, “Soc detection of multi-regional lithium-ion battery based on ultrasonic flexible sensing technology,” in *2024 IEEE International Instrumentation and Measurement Technology Conference (I2MTC)*, p. 1–5, IEEE, May 2024.

¹⁴³J. Tian, J. Du, K. Huang, X. Liu, Y. Zhou, and Y. Shen, *Artificial Intelligence Analysis of State of Charge Distribution in Lithium-Ion Battery Based on Ultrasonic Scanning Data*, p. 87–93. Springer Nature Singapore, 2024.

¹⁴⁴T. Tang, Q. Xia, M. Xu, Z. Deng, F. Jiang, Z. Wu, Y. Ren, D. Yang, and C. Qian, “Uneven internal soc distribution estimation of lithium-ion batteries using ultrasonic transmission signals: A new data screening technique and an improved deep residual network,” *eTransportation*, p. 100406, Feb. 2025.

¹⁴⁵P. Liu, R. Xu, Y. Liu, F. Lin, and K. Zhao, “Computational modeling of heterogeneity of stress, charge, and cyclic damage in composite electrodes of li-ion batteries,” *Journal of The Electrochemical Society*, vol. 167, p. 040527, Jan. 2020.

¹⁴⁶Y. Xie, S. Wang, R. Li, D. Ren, M. Yi, C. Xu, X. Han, L. Lu, B. Friess, G. Offer, and M. Ouyang, “Inhomogeneous degradation induced by lithium plating in a large-format lithium-ion battery,” *Journal of Power Sources*, vol. 542, p. 231753, Sept. 2022.

¹⁴⁷Z. Cai, H. Jiang, T. Pan, C. Qin, J. Xu, and Y. Wang, “Remaining capacity prediction of li-ion batteries based on ultrasonic signals,” *Journal of the Chinese Institute of Engineers*, pp. 1–11, 2024.

¹⁴⁸D. Williams, J. Green, P. Bugryniec, S. Brown, and R. Dwyer-Joyce, “Battery age monitoring: Ultrasonic monitoring of ageing and degradation in lithium-ion batteries,” *Journal of Power Sources*, vol. 631, p. 236174, Mar. 2025.

¹⁴⁹E. Galionas, R. E. Owen, J. B. Robinson, and R. Jervis, “The generalisation challenge: Assessment of the efficacy of acoustic signals for state estimation of lithium-ion batteries via machine learning,” *Journal of Power Sources*, vol. 630, p. 236047, Feb. 2025.

¹⁵⁰O. Furat, D. P. Finegan, Z. Yang, T. R. Tanim, K. Smith, and V. Schmidt, “Quantifying the impact of charge rate and number of cycles on structural degeneration of li-ion battery electrodes,” *Journal of The Electrochemical Society*, vol. 169, p. 100541, Oct. 2022.

¹⁵¹A. Wade, A. V. Llewellyn, T. M. M. Heenan, C. Tan, D. J. L. Brett, R. Jervis, and P. R. Shearing, “First cycle cracking behaviour within ni-rich cathodes during high-voltage charging,” *Journal of The Electrochemical Society*, vol. 170, p. 070513, July 2023.

¹⁵²A. Soleimani Borujerdi, C. Jin, and J. Zhu, “Ultrasonic monitoring of lithium-ion batteries with in-situ self-temperature correction,” *Journal of Power Sources*, vol. 597, p. 234103, Mar. 2024.

¹⁵³D. Wasylowski, S. Neubauer, M. Faber, H. Ditler, M. Sonnet, A. Blömeke, P. Dechent, A. Gitis, and D. U. Sauer, “In situ tomography of lithium-ion battery cells enabled by scan-

ning acoustic imaging," *Journal of Power Sources*, vol. 580, p. 233295, 2023.

¹⁵⁴P. M. Attia, A. Bills, F. Brosa Planella, P. Dechent, G. dos Reis, M. Dubarry, P. Gasper, R. Gilchrist, S. Greenbank, D. Howey, O. Liu, E. Khoo, Y. Preger, A. Soni, S. Sripad, A. G. Stefanopoulou, and V. Sulzer, "Review—"knees" in lithium-ion battery aging trajectories," *Journal of The Electrochemical Society*, vol. 169, p. 060517, June 2022.

¹⁵⁵H. Li and Z. Zhou, "Numerical simulation and experimental study of fluid-solid coupling-based air-coupled ultrasonic detection of stomata defect of lithium-ion battery," *Sensors*, vol. 19, no. 10, p. 2391, 2019.

¹⁵⁶S. Guorong, L. Mingkun, L. Yan, L. Yungchun, W. Bin, and H. Cunfu, "Application of legendre orthogonal polynomial method in calculating reflection and transmission coefficients of multilayer plates," *Wave Motion*, vol. 84, pp. 32–45, 2019.

¹⁵⁷G. Song, Y. Li, Y. Lyu, H. Chen, W. Song, J. Gao, and C. He, "Ultrasonic reflection characteristics of lithium-ion battery based on legendre orthogonal polynomial method," *Ultrasonics*, vol. 124, p. 106736, 2022.

¹⁵⁸R. Copley and R. Dwyer-Joyce, "Prediction of the internal structure of a lithium-ion battery using a single ultrasound wave response," *Journal of Energy Storage*, vol. 72, p. 108778, 2023.

¹⁵⁹F. Yang, Q. Mao, J. Zhang, G. Bao, K. W. E. Cheng, and K.-H. Lam, "Novel joint algorithm for state-of-charge estimation of rechargeable batteries based on the back propagation neural network combining ultrasonic inspection method," *Journal of Energy Storage*, vol. 99, p. 113391, Oct. 2024.

¹⁶⁰Q. Wang, D. Song, X. Lin, H. Wu, and H. Shen, "Application of machine learning in ultrasonic diagnostics for prismatic lithium-ion battery degradation evaluation," *Frontiers in Energy Research*, vol. 12, Mar. 2024.

¹⁶¹K. Liu, Y. Liu, S. Zhao, X. Li, and Q. Peng, "An ultrasonic wave-based method for efficient state-of-health estimation of li-ion batteries," *IEEE Transactions on Industrial Electronics*, p. 1–11, 2024.

¹⁶²K. Liu, J. Fang, S. Zhao, Y. Liu, H. Dai, L. Ye, and Q. Peng, "Battery state-of-health estimation: An ultrasonic detection method with explainable ai," *Energy*, p. 134923, Feb. 2025.

¹⁶³K. E. Willcox, O. Ghattas, and P. Heimbach, "The imperative of physics-based modeling and inverse theory in computational science," *Nature Computational Science*, vol. 1, no. 3, pp. 166–168, 2021.

¹⁶⁴P. Ladpli, F. Kopsaftopoulos, and F.-K. Chang, "Estimating state of charge and health of lithium-ion batteries with guided waves using built-in piezoelectric sensors/actuators," *Journal of Power Sources*, vol. 384, pp. 342–354, 2018.

¹⁶⁵X. Li, C. Wu, C. Fu, S. Zheng, and J. Tian, "State characterization of lithium-ion battery based on ultrasonic guided wave scanning," *Energies*, vol. 15, p. 6027, Aug. 2022.

¹⁶⁶M. Koller, G. Glanz, A. Bergmann, and H. Popp, "Determination of Lamb wave modes on lithium-ion batteries using piezoelectric transducers," *Sensors*, vol. 22, no. 13, p. 4748, 2022.

¹⁶⁷B. Liu, W. Tong, Y. Cao, and J. Li, "Soc estimation method based on the ultrasonic guided waves considering the significant effect of charge/discharge rate," *Journal of Energy Storage*, vol. 87, p. 111434, May 2024.

¹⁶⁸H. Popp, M. Koller, S. Keller, G. Glanz, R. Klambauer, and A. Bergmann, "State estimation approach of lithium-ion batteries by simplified ultrasonic time-of-flight measurement," *IEEE Access*, vol. 7, pp. 170992–171000, 2019.

¹⁶⁹S. Zheng, S. Jiang, Y. Luo, B. Xu, and W. Hao, "Guided wave imaging of thin lithium-ion pouch cell using scanning laser doppler vibrometer," *Ionics*, vol. 27, pp. 643–650, 2021.

¹⁷⁰X. Li, W. Hua, C. Wu, S. Zheng, Y. Tian, and J. Tian, "State estimation of a lithium-ion battery based on multi-feature indicators of ultrasonic guided waves," *Journal of Energy Storage*, vol. 56, p. 106113, 2022.

¹⁷¹A. Siegl, B. Schweighofer, and H. Wegleiter, "A sensor model to simulate the excitation and propagation of lamb waves in lithium-ion pouch cells," *IEEE Sensors Letters*, 2023.

¹⁷²C. An, S. Wang, L. Lin, X. Ding, Q. Deng, and N. Hu, "Construction and ultrasonic inspection of the high-capacity li-ion battery based on the mno2 decorated by au nanoparticles anode," *Microstructures*, vol. 4, Jan. 2024.

¹⁷³Y. Tian, S. Yang, R. Zhang, J. Tian, and X. Li, "State of charge estimation of lithium-ion batteries based on ultrasonic guided waves by chirped signal excitation," *Journal of Energy Storage*, vol. 84, p. 110897, Apr. 2024.

¹⁷⁴H. Zappen, G. Fuchs, A. Gitis, and D. U. Sauer, "In-operando impedance spectroscopy and ultrasonic measurements during high-temperature abuse experiments on lithium-ion batteries," *Batteries*, vol. 6, no. 2, p. 25, 2020.

¹⁷⁵M. Koller, G. Glanz, R. Jaber, and A. Bergmann, "Ultrasonic battery management system for Lamb wave mode tracking on lithium-ion pouch cells," *Journal of Energy Storage*, vol. 74, p. 109347, 2023.

¹⁷⁶V. S. H. S. Che, J. Selvaraj, K. S. Tey, J. W. Lee, H. Shareef, and R. Errouissi, "State of health (soh) estimation methods for second life lithium-ion battery—review and challenges," *Applied Energy*, vol. 369, p. 123542, Sept. 2024.

¹⁷⁷Y. Gou, Y. Yan, J. Li, S. Chen, Z. Zeng, and Y. Liu, "Study on guided wave propagation characteristics in multilayered porous lithium batteries based on the wave finite element method," in *2024 IEEE Ultrasonics, Ferroelectrics, and Frequency Control Joint Symposium (UFFC-JS)*, p. 1–4, IEEE, Sept. 2024.

¹⁷⁸Y. Liu, R. Zhang, and W. Hao, "Evaluation of the state of charge of lithium-ion batteries using ultrasonic guided waves and artificial neural network," *Ionics*, vol. 28, p. 3277–3288, Apr. 2022.

¹⁷⁹X. Ji, Y. Liao, J. Tu, Q. Liu, and X. Qing, "Pso-gpr model for state estimation of lithium-ion battery using ultrasonic guided waves with multi-feature fusion technique," *Journal of Energy Storage*, vol. 112, p. 115580, Mar. 2025.

¹⁸⁰J. Gao, Y. Lyu, and C. He, "Estimating state of charge of lithium-ion batteries by using ultrasonic guided waves detection technology," *Journal of Physics: Conference Series*, vol. 2198, p. 012015, May 2022.

¹⁸¹X. Lin, Y. Lyu, J. Gao, Y. Zheng, and C. He, "Dispersion of thermoelastic guided waves in multi-layered porous media," *Mechanics of Advanced Materials and Structures*, p. 1–19, Aug. 2024.

¹⁸²X. Lin, Y. Lyu, J. Gao, F. Shi, B. Wu, and C. He, "Thermoelastic guided wave behavior modeling and distributed experimental analysis of the inhomogeneous state of charge for silicon carbon lithium-ion batteries," *Journal of Energy Storage*, vol. 114, p. 115896, Apr. 2025.

¹⁸³H. Zhang, L. Wang, X. Chen, J. Li, Y. Liu, H. Liu, and Y. Liu, "On propagation characteristics of ultrasonic guided waves in layered fluid-saturated porous media using spectral method," *The Journal of the Acoustical Society of America*, vol. 156, p. 3021–3032, Nov. 2024.

¹⁸⁴W. Xu, Y. Yang, F. Shi, L. Li, F. Wen, and Q. Chen, "Ultrasonic phased array imaging of gas evolution in a lithium-ion battery," *Cell Reports Physical Science*, vol. 4, p. 101579, Sept. 2023.

¹⁸⁵G. Jie, Z. Yifan, L. Yan, W. Xiangling, L. Yang, W. Bin, and H. Cunfu, "A novel ultrasonic transmission coefficient spectrums approach to detecting lithium deposition of lithium-ion batteries," *Journal of Power Sources*, vol. 636, p. 236555, Apr. 2025.

¹⁸⁶A. Kirchev, N. Guillet, L. Lonardoni, S. Dumenil, and V. Gau, "Li-ion cell safety monitoring using mechanical parameters: Part ii. battery behavior during thermal abuse tests," *Journal of The Electrochemical Society*, vol. 170, no. 1, p. 010503, 2023.

¹⁸⁷M. Feinauer, A. A. Abd-El-Latif, P. Sichler, A. Aracil Regalado, M. Wohlfahrt-Mehrens, and T. Waldmann, "Change of safety by main aging mechanism – a multi-sensor accelerating rate calorimetry study with commercial li-ion pouch cells," *Journal of Power Sources*, vol. 570, p. 233046, June 2023.

¹⁸⁸G. Qian, F. Monaco, D. Meng, S.-J. Lee, G. Zan, J. Li, D. Kar-pov, S. Gul, D. Vine, B. Stripe, J. Zhang, J.-S. Lee, Z.-F. Ma, W. Yun, P. Pianetta, X. Yu, L. Li, P. Cloeten, and Y. Liu, "The role of structural defects in commercial lithium-ion batteries," *Cell Reports Physical Science*, vol. 2, p. 100554, Sept. 2021.

¹⁸⁹L. P. Bauermann, L. Mesquita, C. Bischoff, M. Drews, O. Fitz, A. Heuer, and D. Biro, "Scanning acoustic microscopy as a non-destructive imaging tool to localize defects inside battery cells," *Journal of Power Sources Advances*, vol. 6, p. 100035, 2020.

¹⁹⁰D. Wasylowski, N. Kisseler, H. Ditler, M. Sonnet, G. Fuchs, F. Ringbeck, and D. U. Sauer, "Spatially resolving lithium-ion battery aging by open-hardware scanning acoustic imaging," *Journal of Power Sources*, vol. 521, p. 230825, 2022.

¹⁹¹M. Yi, F. Jiang, L. Lu, S. Hou, J. Ren, X. Han, and L. Huang, "Ultrasonic tomography study of metal defect detection in lithium-ion battery," *Frontiers in Energy Research*, vol. 9, Dec. 2021.

¹⁹²A. J. Louli, A. Eldesoky, R. Weber, M. Genovese, M. Coon, J. deGooyer, Z. Deng, R. T. White, J. Lee, T. Rodgers, R. Petibon, S. Hy, S. J. H. Cheng, and J. R. Dahn, "Diagnosing and correcting anode-free cell failure via electrolyte and morphological analysis," *Nature Energy*, vol. 5, p. 693–702, Aug. 2020.

¹⁹³Y. S. Zhang, A. N. Pallipurath Radhakrishnan, J. B. Robinson, R. E. Owen, T. G. Tranter, E. Kendrick, P. R. Shearing, and D. J. L. Brett, "In situ ultrasound acoustic measurement of the lithium-ion battery electrode drying process," *ACS Applied Materials & Interfaces*, vol. 13, p. 36605–36620, July 2021.

¹⁹⁴Y. S. Zhang, J. B. Robinson, R. E. Owen, A. N. P. Radhakrishnan, J. Li, J. O. Majasan, P. R. Shearing, E. Kendrick, and D. J. L. Brett, "Effective ultrasound acoustic measurement to monitor the lithium-ion battery electrode drying process with various coating thicknesses," *ACS Applied Materials & Interfaces*, vol. 14, p. 2092–2101, Dec. 2021.

¹⁹⁵E. Guk, M. F. Niri, T. A. Vincent, G. Apachitei, C. Briggs, B. Gulsoy, S. Chao, Z. Guo, J. E. Sansom, and J. Marco, "Investigation of calendering parameters on the microstructure of graphite anodes within lithium-ion batteries: Insights from ultrasonic testing," *Journal of Power Sources*, vol. 614, p. 235063, Sept. 2024.

¹⁹⁶E. Guk, M. Faraji Niri, H. F. Tolie, M. Capener, P. Bellchambers, and J. Marco, "Exploring the influence of calendering and coating line conditions on the microstructure of cathode electrode in lithium-ion batteries: Ultrasonic testing insights," *Journal of Power Sources*, vol. 645, p. 237111, July 2025.

¹⁹⁷G. Qian, S. Kuppan, A. Gallo, J. Zhou, Z. Liu, and Y. Liu, "From in-situ experimentation to in-line metrology: Advanced imaging characterization for battery research and manufacturing," *Energy Storage Materials*, vol. 73, p. 103819, Nov. 2024.

¹⁹⁸W. Li, Z. Zhao, A. Yanyachi, S. Kuppan, Z. Liu, J. Zhou, O. Ezekoye, H. Khani, and Y. Liu, "Sponge-inspired pressing approach to facilitate electrolyte wetting in li-ion pouch cells," *Journal of The Electrochemical Society*, vol. 172, p. 090528, Sept. 2025.

¹⁹⁹"Liminal insights." <https://www.liminalinsights.com/>. [Accessed 28-12-2025].

²⁰⁰"Titan advanced energy solutions." <https://www.titanaes.com/>. [Accessed 28-12-2025].

²⁰¹A. Ponnekanti, G. Thorsteinsson, D. Wasylowski, K. Sun, R. May, B. Schumacher, B. Schwartz, Z. Herman, L. Katzman, T. Olushina, D. U. Sauer, and D. A. Steingart, "Operando acoustic analysis of formation parameter coupling in lithium metal batteries," *Journal of The Electrochemical Society*, vol. 172, p. 030524, Mar. 2025.

²⁰²X. Hu, X. Deng, F. Wang, Z. Deng, X. Lin, R. Teodorescu, and M. G. Pecht, "A review of second-life lithium-ion batteries for stationary energy storage applications," *Proceedings of the IEEE*, vol. 110, p. 735–753, June 2022.

²⁰³S. Montoya-Bedoya, M. Bernal, L. A. Sabogal-Moncada, H. V. Martinez-Tejada, and E. Garcia-Tamayo, "Noninvasive ultrasound for lithium-ion batteries state estimation," in *2021 IEEE UFFC Latin America Ultrasonics Symposium (LAUS)*, p. 1–4, IEEE, Oct. 2021.

²⁰⁴S. Montoya-Bedoya, E. Garcia-Tamayo, D. Rohrbach, J. P. Gaviria-Cardona, H. V. Martinez-Tejada, B. Planden, D. A. Howey, W. F. Florez, R. A. Valencia, and M. Bernal, "Quantitative ultrasound spectroscopy for screening cylindrical lithium-ion batteries for second-life applications," *Batteries & Supercaps*, vol. 7, Apr. 2024.

²⁰⁵P. M. Attia, E. Moch, and P. K. Herring, "Challenges and opportunities for high-quality battery production at scale," *Nature Communications*, vol. 16, Jan. 2025.

²⁰⁶M. Rasheed, R. Hassan, M. Kamel, H. Wang, R. Zane, S. Tong, and K. Smith, "Active reconditioning of retired lithium-ion battery packs from electric vehicles for second-life applications," *IEEE Journal of Emerging and Selected Topics in Power Electronics*, vol. 12, p. 388–404, Feb. 2024.

²⁰⁷X. Zheng, Z. Zhu, X. Lin, Y. Zhang, Y. He, H. Cao, and Z. Sun, "A mini-review on metal recycling from spent lithium ion batteries," *Engineering*, vol. 4, p. 361–370, June 2018.

²⁰⁸X. Wang, Z. Gu, E. H. Ang, X. Zhao, X. Wu, and Y. Liu, "Prospects for managing end-of-life lithium-ion batteries: Present and future," *Interdisciplinary Materials*, vol. 1, p. 417–433, June 2022.

²⁰⁹W. Mrozik, M. A. Rajaeifar, O. Heidrich, and P. Christensen, "Environmental impacts, pollution sources and pathways of spent lithium-ion batteries," *Energy & Environmental Science*, vol. 14, no. 12, p. 6099–6121, 2021.

²¹⁰D. Bauer, D. Diamond, J. Li, D. Sandalow, P. Telleen, and B. Wanner, "U.S. department of energy critical materials strategy," Dec. 2010.

²¹¹E. Mossali, N. Picone, L. Gentilini, O. Rodriguez, J. M. Perez, and M. Colledani, "Lithium-ion batteries towards circular economy: A literature review of opportunities and issues of recycling treatments," *Journal of Environmental Management*, vol. 264, p. 110500, June 2020.

²¹²F. Larouche, F. Tedjar, K. Amouzegar, G. Houlachi, P. Bouchard, G. P. Demopoulos, and K. Zaghib, "Progress and status of hydrometallurgical and direct recycling of li-ion batteries and beyond," *Materials*, vol. 13, p. 801, Feb. 2020.

²¹³C. Lei, I. Aldous, J. M. Hartley, D. L. Thompson, S. Scott, R. Hanson, P. A. Anderson, E. Kendrick, R. Sommerville, K. S. Ryder, and A. P. Abbott, "Lithium ion battery recycling using high-intensity ultrasonication," *Green Chemistry*, vol. 23, no. 13, p. 4710–4715, 2021.

²¹⁴Z. Tong, X. Ren, M. Ni, X. Bu, and L. Dong, "Review of ultrasound-assisted recycling and utilization of cathode materials from spent lithium-ion batteries: State-of-the-art and outlook," *Energy & Fuels*, vol. 37, p. 14574–14588, Sept. 2023.

²¹⁵X. Song, Y. Xu, L. Cheng, T. Ren, B. Cai, D. Yang, J. Chen, T. Liang, R. Huang, E. H. Ang, X. Liao, B. Ge, and H. Xiang, "Exploring a sustainable and eco-friendly high-power ultrasonic method for direct regeneration of lithium iron phosphate," *Journal of Energy Storage*, vol. 82, p. 110578, Mar. 2024.

²¹⁶L. Wu, F.-S. Zhang, K. He, Z.-Y. Zhang, and C.-C. Zhang, "Avoiding thermal runaway during spent lithium-ion battery recycling: A comprehensive assessment and a new approach for battery discharge," *Journal of Cleaner Production*, vol. 380, p. 135045, Dec. 2022.

²¹⁷T. Nshizirungu, M. Rana, Y. T. Jo, E. Uwiragiye, J. Kim, and J.-H. Park, "Ultrasound-assisted sustainable recycling of valuable metals from spent li-ion batteries via optimisation using response surface methodology," *Journal of Environmental Chemical Engineering*, vol. 12, p. 112371, Apr. 2024.

²¹⁸L. Kong, F. Liu, X. Hu, Z. Shi, A. Liu, and X. Wang, "An improved pretreatment method for recovering cathode materials from lithium-ion battery: ultrasonic-assisted naoh-enhanced dissolving," *Energy Sources, Part A: Recovery, Utilization, and Environmental Effects*, vol. 45, p. 877–887, Feb. 2023.

²¹⁹Q. Chen, Y. Guo, X. Lai, X. Han, X. Liu, L. Lu, M. Ouyang, and Y. Zheng, "Chemical-free recycling of cathode material and

aluminum foil from waste lithium-ion batteries by combining plasma and ultrasonic technology," *ACS Applied Materials & Interfaces*, vol. 16, p. 31076–31084, June 2024.

²²⁰S. Yan, Y. Jiang, X. Chen, and T. Zhou, "Improved advanced oxidation process for in situ recycling of al foils and cathode materials from spent lithium-ion batteries," *Industrial & Engineering Chemistry Research*, vol. 61, p. 12728–12738, Aug. 2022.

²²¹S. Zhao, W. Zhang, G. Li, H. Zhu, J. Huang, and W. He, "Ultrasonic renovation mechanism of spent lco batteries: A mild condition for cathode materials recycling," *Resources, Conservation and Recycling*, vol. 162, p. 105019, Nov. 2020.

²²²Y. Huang, M. Sun, C. Xu, H. Hu, S. Zhu, and W. He, "Degradation of organic pollutants accompanied by the ultrasonic separation of the spent lithium-ion battery cathode materials," *Waste Management & Research: The Journal for a Sustainable Circular Economy*, vol. 42, p. 74–80, Apr. 2023.

²²³H. Iqbal, S. Sarwar, D. Kirli, J. K. H. Shek, and A. E. Kiprakis, "A survey of second-life batteries based on techno-economic perspective and applications-based analysis," *Carbon Neutrality*, vol. 2, Apr. 2023.

²²⁴L. Bravo Diaz, X. He, Z. Hu, F. Restuccia, M. Marinescu, J. V. Barreras, Y. Patel, G. Offer, and G. Rein, "Review—meta-review of fire safety of lithium-ion batteries: Industry challenges and research contributions," *Journal of The Electrochemical Society*, vol. 167, p. 090559, Jan. 2020.

²²⁵L. Lander, C. Tagnon, V. Nguyen-Tien, E. Kendrick, R. J. Elliott, A. P. Abbott, J. S. Edge, and G. J. Offer, "Breaking it down: A techno-economic assessment of the impact of battery pack design on disassembly costs," *Applied Energy*, vol. 331, p. 120437, Feb. 2023.

²²⁶A. Huang, H. Liu, O. Manor, P. Liu, and J. Friend, "Enabling rapid charging lithium metal batteries via surface acoustic wave-driven electrolyte flow," *Advanced Materials*, vol. 32, Feb. 2020.

²²⁷A. Huang, H. Liu, P. Liu, and J. Friend, "Overcoming the intrinsic limitations of fast charging lithium-ion batteries using integrated acoustic streaming," *Advanced Energy and Sustainability Research*, vol. 4, Dec. 2022.

²²⁸X. Li, L. Chen, W. Hua, X. Yang, Y. Tian, J. Tian, and R. Xiong, "Optimal charging for lithium-ion batteries to avoid lithium plating based on ultrasound-assisted diagnosis and model predictive control," *Applied Energy*, vol. 367, p. 123396, Aug. 2024.

²²⁹G. Im, D. Barnes, W. Lu, B.-I. Popa, and B. I. Epureanu, "Ultrasound-induced impedance reduction in lithium ion batteries," *Journal of The Electrochemical Society*, vol. 170, p. 100519, Oct. 2023.

²³⁰G. Im, W. Lu, B. I. Popa, and B. I. Epureanu, "Ultrasound-enabled adaptive protocol for fast charging of lithium-ion batteries," *Journal of Electrochemical Energy Conversion and Storage*, vol. 22, Oct. 2024.

²³¹S. Jie, J. Kang, S. Baek, and B. Lee, "Enhanced electrochemical performance of li-ion battery via ultrasonic-assisted inorganic-rich and thin sei layer," *Ultrasonics Sonochemistry*, vol. 100, p. 106620, Nov. 2023.

²³²N. Shpigel, S. Sigalov, M. D. Levi, T. Mathis, L. Daikhin, A. Janes, E. Lust, Y. Gogotsi, and D. Aurbach, "In situ acoustic diagnostics of particle-binder interactions in battery electrodes," *Joule*, vol. 2, p. 988–1003, May 2018.

²³³Q. Zhang, L. Bo, H. Li, J. Li, T. Li, Z. Tian, and R. Qiao, "Enhancing performance of lithium metal batteries through acoustic field application," *Journal of Materials Chemistry A*, vol. 13, no. 3, p. 2047–2055, 2025.

²³⁴Z. Zhu, L. Zhang, H. Wu, S. Chen, X. Wei, and H. Dai, "Wavelet packet energy proportion-based early warning for the failure of lithium-ion batteries," *IEEE Transactions on Transportation Electrification*, vol. 11, p. 2219–2229, Feb. 2025.

²³⁵J. Chen, T. Hannan, Y. Yao, and G. Song, "Estimating state of charge of cylindrical lithium-ion cells using multiple random convolutional kernel transform and low-frequency stress waves," *Energy Storage Materials*, vol. 72, p. 103730, Sept. 2024.

²³⁶T. D. Nguyen, H. Sun, R. Amin, P. Ramuhalli, C.-B. M. Kwon, and I. Belharouak, "Ultrasonic nondestructive diagnosis of cylindrical batteries under various charging rates," *Journal of The Electrochemical Society*, vol. 171, p. 020522, Feb. 2024.

²³⁷J. Xu, L. Wang, J. Guan, and S. Yin, "Coupled effect of strain rate and solvent on dynamic mechanical behaviors of separators in lithium ion batteries," *Materials & Design*, vol. 95, pp. 319–328, 2016.

²³⁸C. T. Love, "Thermomechanical analysis and durability of commercial micro-porous polymer li-ion battery separators," *Journal of Power Sources*, vol. 196, no. 5, pp. 2905–2912, 2011.

²³⁹C. T. Love, "Perspective on the mechanical interaction between lithium dendrites and polymer separators at low temperature," *Journal of Electrochemical Energy Conversion and Storage*, vol. 13, no. 3, p. 031004, 2016.

²⁴⁰R. Li, W. Li, A. Singh, D. Ren, Z. Hou, and M. Ouyang, "Effect of external pressure and internal stress on battery performance and lifespan," *Energy Storage Materials*, vol. 52, p. 395–429, Nov. 2022.

²⁴¹J. Chen, H. Hu, S. Li, and Y. He, "Evolution of mechanical properties of polypropylene separator in liquid electrolytes for lithium-ion batteries," *Journal of Applied Polymer Science*, vol. 135, no. 27, p. 46441, 2018.

²⁴²A. Sheidaei, X. Xiao, X. Huang, and J. Hitt, "Mechanical behavior of a battery separator in electrolyte solutions," *Journal of Power Sources*, vol. 196, no. 20, pp. 8728–8734, 2011.

²⁴³Y. Qi, L. G. Hector, C. James, and K. J. Kim, "Lithium Concentration Dependent Elastic Properties of Battery Electrode Materials from First Principles Calculations," *Journal of The Electrochemical Society*, vol. 161, no. 11, pp. F3010–F3018, 2014.

²⁴⁴R. Xu, H. Sun, L. S. de Vasconcelos, and K. Zhao, "Mechanical and structural degradation of linixmnyco₂ cathode in li-ion batteries: an experimental study," *Journal of The Electrochemical Society*, vol. 164, no. 13, p. A3333, 2017.

²⁴⁵Y. Wang, Q. Li, and Y. Xing, "Porosity variation of lithium-ion battery separators under uniaxial tension," *International Journal of Mechanical Sciences*, vol. 174, p. 105496, 2020.

²⁴⁶L. De Vasconcelos, N. Sharma, R. Xu, and K. Zhao, "In-situ nanoindentation measurement of local mechanical behavior of a li-ion battery cathode in liquid electrolyte," *Experimental Mechanics*, vol. 59, pp. 337–347, 2019.

²⁴⁷Z. Pan, T. Sedlatschek, and Y. Xia, "Effect of state-of-charge and air exposure on tensile mechanical properties of lithium-ion battery electrodes," *Journal of The Electrochemical Society*, vol. 167, no. 9, p. 090517, 2020.

²⁴⁸R. D. Schmidt and J. Sakamoto, "In-situ, non-destructive acoustic characterization of solid state electrolyte cells," *Journal of Power Sources*, vol. 324, pp. 126–133, 2016.

²⁴⁹M. Musiak and Z. S. Li, "Real time ultrasonic monitoring of solid-state lithium-ion cells in the frequency domain," in *2021 IEEE International Conference on Prognostics and Health Management (ICPHM)*, pp. 1–5, IEEE, 2021.

²⁵⁰Y.-S. Chou, N.-Y. Hsu, K.-T. Jeng, K.-H. Chen, and S.-C. Yen, "A novel ultrasonic velocity sensing approach to monitoring state of charge of vanadium redox flow battery," *Applied Energy*, vol. 182, pp. 253–259, 2016.

²⁵¹L. Yan, X. Zang, Z. Nie, L. Zhong, Z. D. Deng, and W. Wang, "Online and noninvasive monitoring of battery health at negative-half cell in all-vanadium redox flow batteries using ultrasound," *Journal of Power Sources*, vol. 580, p. 233417, 2023.

²⁵²K. Sun, G. Thorsteinsson, A. Stiber, L. Katzman, W. Chang, R. May, and D. A. Steingart, "Chemo-mechanical hysteresis of sulfur conversion electrodes via operando acoustic transmission," *Journal of The Electrochemical Society*, vol. 171, p. 100504, Oct. 2024.

²⁵³H. Laufen, S. Klick, H. Ditler, K. L. Quade, A. Mikitisin, A. Blömeke, M. Schütte, D. Wasylowski, M. Sonnet, L. Hen-

rich, A. Schwedt, G. Stahl, F. Ringbeck, J. Mayer, and D. U. Sauer, "Multi-method characterization of a commercial 1.2 ah sodium-ion battery cell indicates drop-in potential," *Cell Reports Physical Science*, vol. 5, p. 101945, May 2024.

²⁵⁴L. Oca, N. Guillet, R. Tessard, and U. Iraola, "Lithium-ion capacitor safety assessment under electrical abuse tests based on ultrasound characterization and cell opening," *Journal of Energy Storage*, vol. 23, pp. 29–36, 2019.

²⁵⁵W. Huang, C. Zhao, P. Wu, H. Yuan, W. Feng, Z. Liu, Y. Lu, S. Sun, Z. Fu, J. Hu, S. Yang, J. Huang, and Q. Zhang, "Anode-free solid-state lithium batteries: A review," *Advanced Energy Materials*, vol. 12, May 2022.

²⁵⁶M. Webster, E. Frankforter, A. Zuercher, S. Deshpande, W.-C. A. Lam, D. Caicedo, B. DeMatta, Y. Lin, and D. Perey, "Ultrasonic assessment of aging in lithium metal pouch cells," *Journal of Power Sources*, vol. 606, p. 234552, June 2024.

²⁵⁷F. F. Balakirev, S. M. Ennaceur, R. J. Migliori, B. Maiorov, and A. Migliori, "Resonant ultrasound spectroscopy: The essential toolbox," *Review of Scientific Instruments*, vol. 90, Dec. 2019.